TRANSFER-PRINTED PHOTONIC CRYSTAL NANOMEMBRANE FANO RESONANCE FILTERS AND MODULATORS

by

YI-CHEN SHUAI

Presented to the Faculty of the Graduate School of

The University of Texas at Arlington in Partial Fulfillment

of the Requirements

for the Degree of

DOCTOR OF PHILOSOPHY

THE UNIVERSITY OF TEXAS AT ARLINGTON

December 2013

Acknowledgements

First and foremost I would like to express my greatest thanks to my advisor Professor Weidong Zhou for his instruction and direction during my pursuit of Ph.D. at UTA. His stringent scientific methods and diligent research attitude taught me so much from research to life. I would like to express my appreciations to my committee members, Professor Michael Vasilyev, Professor Yuze (Alice) Sun, Professor Donald Butler, and Professor Seong Jin Koh.

Thank to our collaborators Professor Ma and Jung-Hun Seo at University of Wisconsin Madison on nanomembrane transfer printing. Thank to Professor Li and her students at University of Illinois at Urbana-Chanpaign for their work on MacEtch process. Thank Dr. Richard Soref, et al for the MIR-MR device characterization. Thank Professor Robert Peale and his student at University of Center Florida for the FIR-MR device characterization.

I would like to express my special thanks to my group members for their great help on my study: Dr. Hongjun Yang on fabrication, Dr. Deyin Zhao on design/simulation. I would like to thank Dr. Li Chen, Dr. Zexuan Qiang, Dr. Yuehui Wang and Rajesh Tummala for their help, teaching and collaboration during the first a few years of my study in UTA. Thank to Dr. Santhad Chuwongin, Dr. Wenjuan, Fan, Dr. Tapas Saha, Dr. Rui Li for their collaboration and helpful discussion. Many thanks to my current group members Arvinder Singh Chadha, Laxmy Menon, Shih-Chia Liu, Yonghao, Liu, Zhaoqiang, Peng, Nandan Vempati for their helpful discussion, support and cooperation.

I thank E.E. Department, UTA (special thanks to Janice Moore, Gail Paniuski, Ann Lewiston, Terri Earle and Pauline Mason for their help). I thank to UTA NanoFAB facilities, travel grant and our staffs. (Dennis Bueno, Richard K. Chambers, Richard E. Wells, Paul C. Logan for their help on the NanoFAB cleanroom tools. Miss. Thanh Bui for

her help on my Austin travels paper works) I thank UT Austin MRC facilities, staffs and my friends there for their kind helps and supports during the past four years. Thanks to Rice Contact traveling Grant, AFOSR MURI, ARO, and AFOSR STTR Phase I/II and other research funding that support our research work.

November 21, 2013

Abstract

TRANSFER-PRINTED PHOTONIC CRYSTAL NANOMEMBRANE FANO RESONANCE FILTERS AND MODULATORS

YI-CHEN SHUAI, PhD

The University of Texas at Arlington, 2013

Supervising Professor: WEIDONG ZHOU

This dissertation presents the research work on photonic crystal nanomembrane Fano resonance devices based on transfer printing techniques. Ultra-compact high quality (Q) factor optical filters have been design, fabricated, and characterized based on single-layer and coupled double-layer photonic crystal slabs (PCS). Optical filters have also been designed and investigated for potentially high speed spatial lighting modulations. Fano resonance membrane reflectors with operation wavelength bands cover from near-infrared to mid and far-infrared have also been fabricated based on both reaction ion-etching and magnetic field guided metal-assisted chemical etching processes.

Based on crystalline semiconductor nanomembrane transfer printing technique, we designed and experimentally demonstrated coupled double-layer PCS high-Q filters with or without lattice displacement. A Q factor of 10,000 was obtained experimentally from coupled double-layer PCS filters without lattice offset. On the other hand, a Q factor of 80,000 was obtained experimentally from a coupled double-layer PCS filters with lattice displacement. Simulated optical Q factors in these double-layer PCS Fano filters can approach 220,000,000 or higher, with optimized designs in lattice displacement and in buffer layer selection. These high Q modes arise from coupled bright or dark

resonance modes in these coupled double-layer PCS cavities. Note that when one assume no material absorption, these coupled PCSs resonator structures can offer an opportunity for infinite Q-factor with optimized design and buffer layer thickness selection.

For a single-layer Si-PCS based filter design, we have experimentally obtained Q factor of 1,700 with 23dB extinction ratio (ER). A unique single-layer PCS Fano resonance modulator was demonstrated by transfer-printing photonic-crystal nanomembrane on glass. Base on the ultra high-Q resonance we have recently achieved in the bi-layers PCSs structure, we also proposed and designed an ultra-compact double-layer photonic-crystal Fano resonance modulator.

Table of Contents

List of Illustrations

List of Tables

Chapter 1

Introduction

Fano resonance, known from atomic physics, has been employed for a wide variety of nanophotonic structures, such as quantum dots, photonic crystals (PCs), plasmonics, and metamaterials, and so on [1]. As well known, the Fano resonance can provide an efficient way to channel light from within the slab to the external environment, and vice versa. The two-dimensional (2D) photonic-crystal slabs (PCSs) as one of the most promising artificial platforms with in-plane periodic modulation of dielectric constant on a wavelength scale, can be transferred onto various foreign substrates, such as glass and flexible polyethylene terephthalate (PET) plastics, based on low temperature transfer and stacking processes. For 2-D PCS membrane based devices, surface-normal ultra-compact narrowband optical filters and broadband reflectors are essential components for their optical applications. They have been demonstrated with unique angle and polarization properties. [2] Design, fabrication and characterization of these unique photonic devices have been reported and reviewed, with focus on the spectral, angular, and polarization properties, based on dispersion engineering. [3] They can be used in optical switches, modulators, lasers, sensors, and beam steering devices.

We firstly introduce one kind of the PCS based devices---Fano resonance membrane reflectors. Experimental demonstration of PCS silicon membrane reflectors of 1.5 μm, 2.3 μm, 8~10 μm, 76 μm operation wavelength bands have been targeted. [4] A new approach of metal-assisted chemical etching (MacEtch) process was introduced for the PCS patterning. [5] With modal dispersion engineering, Fano filters and reflectors can all be realized in single layer dielectric PC structures [6-8]. We experimentally demonstrated single-layer Fano filter with measured Q-factor of 1,700. However, the

double-layer coupled PCSs filters can provide us more engineering design opportunity and flexibility. Sue and Liu et al. [9] reported earlier the optical Q-factors and the optomechanical interactions can be controlled by precisely tuning the lattice displacement between two coupled PC slabs (PCS). We further demonstrated double-layer Fano filters with measured Q-factor of 10,000, based on double-layer PCS with perfectly aligned lattices. [10] Ultra-high Q resonance was observed in two coupled PCSs with lattice displacement. A double-layer high Q filters with 80,000 Q-factor was also demonstrated. [11] Electro-optic modulation was observed on a transfer-printed single-layer PCS silicon nanomembrane on glass substrate. Issues have been discussed. We proposed engineering solutions and a new design of a double-layer stacking structure for the high-speed Fano resonance novel modulator device.

In this dissertation, we demonstrated a few Fano resonance PCS membrane based devices for optical interconnections, such as membrane reflectors, nanomenbrane based high-Q filters and optical modulators. These novel devices can offer great opportunities in optical interconnections and have extraordinary potentials in silicon photonics applications.

1.1 Background

After dominating the electronics industry for decades, silicon is on the verge of becoming the material of choice for the photonic industry. [12] Silicon photonics (known more generally as group IV photonics), which is CMOS compatible, is now the most active and wide-ranging discipline within the field of integrated optics. The long list of applications includes high-speed optical communications, optical interconnects, microwave photonics, ultrafast signal processing, optoelectronic integration, ultralow-power nanophotonics, photonic crystals, slow-light devices, mid-wave and long-wave

infrared devices-and-systems, quantum information, energy conversion, imaging display, conformal-and-flexible membrane photonics and etc. [13]

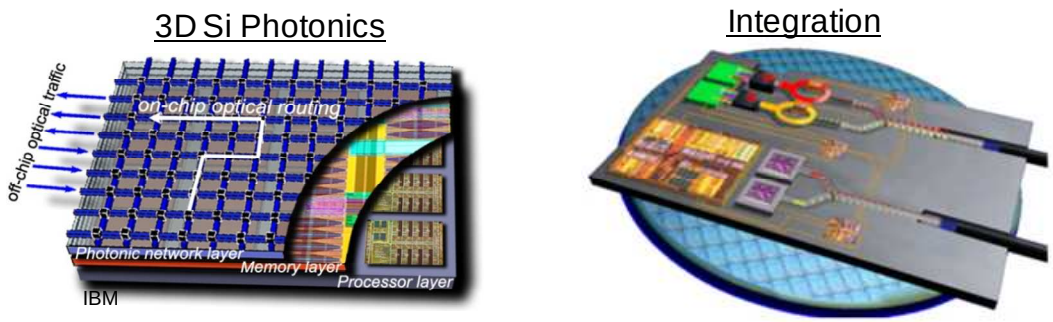

(a) (b)

Figure 1-1 3D Si photonics and integration: (a) IBM silicon nanophotonics speeds servers with 25Gbps light: This future 3D-integated chip consists of several layers connected with each other with very dense and small pitch interlayer vias. The lower layer is a processor itself with many hundreds of individual cores. Memory layer(or layers) are bonded on top to provide fast access to local caches. On top of the stack is the Photonic layer with many thousands of individual optical devices (modulators, detectors, switches) as well as analogue electrical circuits (amplifiers, drivers, latches, etc.). The key role of a photonic layer is not only to provide point-to-point broad bandwidth optical link between different cores and/or the off-chip traffic, but also to route this traffic with an array of nanophotonic switches. Hence it is named Intra-chip optical network (ICON)" IBM.[14] (b) Silicon Photonics Future Vision. Silicon photonics can be used as chip-to-chip interconnects; backplane/display interconnects, in data center fabrics, chemical analysis and even medical lasers. Photocredit: http://www.intel.com/go/sp/ [15-18]

The dominance of silicon as the semiconductor of choice for electronics applications eventually led to the investigation of silicon photonic circuits, primarily because of the potential attraction of integration with electronics in a cost effective manner. Such research began in the mid 1980's and has continued ever since. [19] Stimulated by series of breakthroughs and propelled by increasing investments by industry and governments, the pace of the development of silicon photonics has quickened since 2004. [12, 20] 10~100 Gb/s electro-optic modulators, ultra-fast Ge-on Si photodetectors, efficient fiber to waveguide couplers, and Si Raman lasers have been developed, though Si lasers are still under investigation. The new paradigm for the Si-based photonic and optoelectric integrated circuits is that these chip-scale networks, when suitably designed, will operate at a wavelength anywhere within the broad spectral range of 1.2–100 μm, with cryocooling needed in some cases. [20]

Time runs into 2013, the idea of using light beams to replace wires now dominates all long-distance communications and takes over in networks over shorter distances. And this idea keeps attracting great attention since this new century. [23] In the past ten years, much shorter distances inside digital computers and connecting directly to the silicon chips or even for 3D inter-connections on chips have been intensively investigated. [24-34] Due to their compatibility to CMOS, the most successful technology developed since the last century, Si photonics ultra-compact devices, such as Si based high performance modulators, filters, reflectors, couplers, waveguides, high resonances nanostructures, detectors and possible light sources become the most potential attractions.

In this Ph. D dissertation, we focus on several interesting ultra-compact Si photonic devices through PCS based Fano resonance broadband membrane reflectors (operation wavelength bands cover Near-infrared, Mid-infrared and Far infrared), single

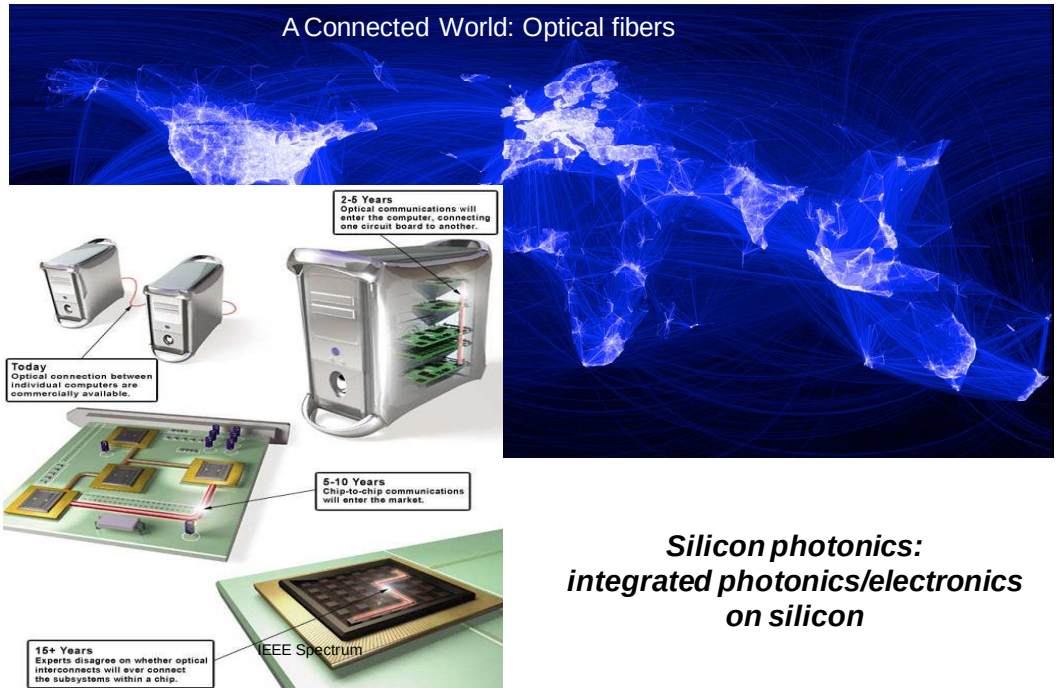

Figure 1-2 Silicon Photonics: integrated photonics/electronics on silicon. Today: all long distance communication connections have been replaced with optical fiber; Optical connections between individual computers are commercially available. In 2~5 years, Optical communications will enter the computer, connecting one circuit board to another. In 5-10 years, Chip-to-chip communications will enter the market. Another 15+ years optical interconnects may connect the subsystems within a chip, though this idea still under debate between experts. [21, 22]

layer Si nanomembrane narrow band filters, coupled PCSs ultra-high Q resonator, to ultra-high Q Si nanomembrane filters and Si nanomembrane based Fano resonance modulators. And these experimental exploring and studies could be important to future Si photonic research and development.

1.2 An over view: photonic crystal membrane based optical devices

As well known, the guided resonances can provide an efficient way to channel light from within the slab to the external environment, and vice versa. It was investigated in one-dimensional grating structures, known as guided mode resonances (GMRs) [35, 36], or high index contrast gratings (HCGs) [37, 38]. The investigation of guided resonance has resulted in using various one dimensional (1D) and two dimensional (2D) dielectric structures in applications, such as filters [39-43], modulators [44, 45], sensors [46, 47], as well as broadband reflectors, lasers, and beam shaping structures, etc [48-57]. One-dimensional subwavelength grating (SWG) structures have long been recognized for these purposes. Both narrowband filters and broadband mirrors [58-61] based on SWG have been demonstrated. On the other hand, two-dimensional photonic crystal slab (2D PCS) structures hold great promises in realizing more compact photonic devices and they can be used for both in-plane and vertically coupled light guiding and manipulating.

Demonstrations of single layer PCS device and application were made intensively during the past decade. In the photonic crystal slab, the index mismatch between the slab and the surrounding medium (usually air) gives rise to the necessary conditions for confining the electric field in all three dimensions. The in-plane confinement is the result of the guided modes that make up the in-plane band structure, while the out-of-plane confinement results from the discontinuity in index at the slab faces. As for one example highlighted here, an air-bridged photonic crystal slabs were demonstrated at visible and near-infrared wavelengths. [41] Both experimental and theoretical studies of the transmission spectra of air-bridged photonic crystal slabs with free space illumination using collimated and focused beams. It showed that the resonances of an air-bridged

photonic crystal slab exhibit considerable differences in their sensitivity to the angle of illumination.

Nevertheless, guided resonances persist and are readily observable in transmission spectra in spite of the increased radiative coupling when consider an asymmetrical situation in which the photonic crystal slab is in contact with a substrate. The substrate does have a noticeable influence on the lineshapes and positions of these modes, but high-Q features are readily apparent in the transmission spectra. [49] Patterned GaN films on sapphire substrates were investigated by A. Rosenberg et al in 2005. It is quite different from the case of the symmetrical (free-standing) membranes studied in the past, [60, 62-66] which can show band gaps in the guided modes even for membranes with moderate values of refractive index.

It was also pointed out that the guided resonance phenomenon can be exiting in a much larger scale and different material system. A guided resonance filter in millimeter wave (MMW), using a material with permittivity of 20 was demonstrated. [67] This is an experimental proof that the guided resonances filter using a single layer PCS can be an efficient method of wavelength selection in communication systems.

The two-dimensional (2D) photonic-crystal slabs (PCSs) as one of the most promising artificial platforms with in-plane periodic modulation of dielectric constant on a wavelength scale, can be transferred onto various foreign substrates, such as glass and flexible polyethylene terephthalate (PET) plastics, based on low temperature transfer and stacking processes, developed by various groups. [68-73] In the last few years, significant progress has been made by Ma's group on record high-speed flexible electronics, and high performance flexible Ge photodetectors, based on transferable Si/SiGe NMs. [71, 74, 75] Many excellent results have also been reported by Lagally et al [72, 76, 77] and Rogers et al [78-81] on the unique electronic, photonic and

thermoelectric and mechanical properties associated with this new class of inorganic flexible semiconductor membrane material system. For these 2-D PCS membrane based devices, surface-normal ultra-compact narrowband optical filters and broadband reflectors are essential components for their optical applications. They have been demonstrated with unique angle and polarization properties. [2] Design, fabrication and characterization of these unique photonic devices have been reported and reviewed, with focus on the spectral, angular, and polarization properties, based on dispersion engineering. [3] They can be used in optical switches, modulators, lasers, sensors, and beam steering devices.

1.3 Nanomembrane based optical high-Q filters and its applications

Most recently, in 2012, with the single layer PCS, a unique high-Q resonance near zero wave vector in macroscopic photonic crystal slabs was firstly observed. [82] Later on in 2013, Hsu et al claimed the tripped light within the radiation continuum where an extremely high-Q was demonstrated experimentally with an angled incidence. [83] In spite of different experimental approaches of high-Q modes in the Fano resonance photonic crystal slabs, with different material systems, symmetric or asymmetric structures with different incidence cases, the major work included in this dissertation will focus on PCSs single and double-layer structures with normal incidence. We will begin with our recent experimental demonstrations on a single layer PCS high-Q filters, which have a record Q factor to the date in a similar structure and material system with normal incidence, then start exploring for those extremely high-Q resonance in the photonic crystal slab based optical systems in Chapter 3.

In the Chapter 4 we will focus on the applications of these recently achieved single or double-layer photonic crystal slabs Fano resonance optical high-Q filters.

Several novel devices were designed and fabricated, including surface normal optical modulators based on single layer PCS or double-layer PCSs structures with high-Q resonances. Issues have been discussed and engineering solutions and new design were suggested. An investigation of optical force research background was reviewed and a few double-layer PCSs related optomechanical applications were also discussed in Chapter 5.

1.4 Overview of dissertation

This dissertation includes five Chapters:

In Chapter 1, we give an introduction of our research focus area---Si photonics and related perspectives. In this dissertation, our target will be on photonic crystal slab (PCS) nanomembrane based Fano resonance photonic devices through reflectors to narrow band high-Q filters and ultra-high Q filters. Applications of these devices were explored and suggested.

In Chapter 2, we introduce one kind of the PCS based devices--- Fano resonance membrane reflectors. Material system analysis and simulation show that high performance PCS membrane reflectors with operation wavelength bands covering through Near-Infrared, Mid-Infrared to Far-Infrared could be achievable. Experimental demonstration of PCS silicon membrane reflectors of 1.5μm, 2.3μm, 8~10μm, 76μm operation wavelength bands have been targeted. Other than reactive ion etching (RIE) process that generally used for PCS fabrication, a new approach of MacEtch process was introduced for the PCS patterning. One most recent achievement on near-infrared membrane reflector (NIR-MR) devices by MacEtch process was discussed.

In Chapter 3, we focus on the most important achievement in this dissertation, the 2D PCS nanomembrane based optical high-Q filters and Ultra-high Q filters at near

1.5μm wavelength band. Surface normal single layer PCS and double-layer PCSs filters were discussed. A record of 23dB extinction ratio with 2000 Q factor was observed on a single layer PCS nanomembrane filter with surface normal incidence. Ultra-high Q resonance between two coupled PCSs was high-lighted. Experimental demonstrations Q factors of 10k and 80k have been made on those coupled double-layer PCSs Fano resonance filters with lattice aligned or misaligned structures respectively. In this Chapter 3, systematic studies and simulations of the PCS based single or double-layer high-Q filters have been given. Optimized design parameters were suggested. Further studies are looking towards extremely high-Q demonstration with even higher experimental Q factors and their possible applications. Moreover, by applying similar coupled symmetric or Asymmetric double-layer PCSs structures, we also expect high-Q resonances appearing at other wavelength region, such as Mid-Infrared or even Far-infrared.

In Chapter 4, we present a few applications based on these Si nanomemrbane Fano resonance high-Q filters, either with single-layer or double-layer design. Single-layer nanomembrane modulator and double-layer nanomembanes modulator novel devices were fabricated. EO modulation on a single layer Fano resonance PCS nanomembrane device was demonstrated. Issues have been discussed. We proposed engineering solutions and a new design of a double-layer stacking structure for the high-speed Fano resonance novel modulator device. The chances for demonstration of these high-speed Si photonics novel modulator devices are still open, as well as the engineering challenges also exist.

In Chapter 5, summary and conclusions were made for this dissertation in four sections. In Section 1, we summarized our work on membrane based photonic crystal Fano reflectors. Conclusion was made based on the material system study and experimental demonstrations. In Section 2, we summarized on the single and double-

layer Fano filters' work. Ultra-high Q demonstration through the coupled PCSs double-layer approach was high-lighted. Conclusion was made. In Section 3, the experimental results of the nanomembrane based Fano modulators were discussed. Issues were analyzed. Solution and new design were also proposed. In Section 4, an investigation of the optomechanics research during past decade was reviewed and a few double-layer PCSs related optomechanical applications were focused. Future work was proposed.

Chapter 2

Photonic Crystal Silicon Membrane Optical Devices

2.1 Background on Fano resonance membrane devices

Broadband reflectors (BBRs) based on Fano resonance, [58] or guided mode resonance, [59, 60] have attracted great attention [84-91] in the past twenty years, where high reflections can be obtained with a single-layer one-dimensional (1-D) grating, or a two-dimensional photonic crystal slab (2-D PCS) structure. Owning to the strong interactions between in-plane guided modes and vertical radiation modes, Fano resonances occur with extremely high reflections. By properly controlling the design parameters, very broadband reflectors can be obtained. Various approaches have been reported to control the spectra performance of Fano BBRs, including stacked thin films [84], [85], [90], and binary grating [89], etc. We also reported narrowband Fano filters and broadband membrane reflectors with patterned silicon nanomembranes (Si-NM) transferred onto glass and flexible polyethylene terephthalate substrates, [3, 92] as well as the resonance control for the practical applications of these Fano resonance optical devices. [91] The angular and polarization properties of Fano filters can also be tailored with the dispersion engineering, which is highly desirable for photonic integration. [3, 93]

2.1.1 Si nanomembrane reflectors at near infrared

Surface-normal ultra-compact broadband reflectors (BBRs) are essential components for numerous optoelectronic device applications, such as microcavities, lasers, photodetectors, solar cells, sensors, and reconfigurable photonics, etc [94]. As an alternative to the conventional multi-layer distributed Bragg reflectors (DBRs), single layer, high index contrast sub-wavelength grating (HCG or SWG) structures that can be

used as ultra-compact broadband reflectors hold great promises for a wide range of device applications. [36, 38, 95, 96] Two-dimensional photonic crystal slab (2D PCS) structures can be used to realize both polarization dependent and independent operations, with proper dispersion engineering and structural optimizations. We previously demonstrated 2D PCS based broadband reflectors on silicon-on-insulator (SOI) substrates, and reported a post-process technique for spectral-trimming of reflection band [91]. With the control of design parameters, broadband reflectors with various spectral bandwidths and different peak reflections can all be realized. The PCS structure was fabricated on silicon-on-insulator (SOI) wafers, using e-beam lithography and plasma dry-etching processes. The target wavelength is around 1550 nm. Single-layer broadband membrane reflectors on glass substrates, based on transferred crystalline silicon nanomembranes (Si NM) [2] also have been reported.

Other than the near infrared MR devices fabricated by e-beam lithography and RIE dry etching processes. We also discussed here the most recently demonstrated the high performance Si nanomembrane reflectors at near infrared by a simple and scalable technique for the fabrication of nanohole arrays in silicon-on-insulator (SOI) wafers using magnetic field-guided metal-assisted chemical etching (*h*-MacEtch). By systematically varying the etch condition, hole diameter, and magnetic field strength, the *h*-MacEtch parameters that affect the morphology of the drilled nanoholes are examined. Using this approach, periodic nanohole array-based photonic crystal membrane reflectors are demonstrated with good agreement between measured and simulated reflectance spectra. This study confirms that MacEtch can be used to produce high quality holes arrays and other more complicated nanostructures in silicon, especially with the assistance of magnetic field.

In recent years, several research groups have demonstrated the use of metal-assisted chemical etching (MacEtch) for the fabrication of micro/nanostructures of various aspect ratios and surface morphologies using both Si and compound semiconductors. [97-103] As the technique relies on patterning of a thin noble metallic catalyst layer, which sink down and engrave into the semiconductor during etching, the semiconductor structures formed using MacEtch are exactly complementary to the metal patterns. Therefore, metal mesh patterns produce vertical pillars [98], [102-104] and discrete metal disks yield cylindrical holes. [105] While vertical nanopillar arrays fabricated using MacEtch have been shown for energy harvesting [106], [99] and light emitting diode (LED) [103] applications, devices relying on MacEtched nanohole arrays have been more elusive. The fabrication of periodic arrays of nanoholes using MacEtch can extend the use of this simple and low-cost technique to the field of optics and nanophotonics for the formation of nanoscale patterned structures and cavities, such as photonic crystals (PhCs) and functional semiconductor metamaterials, currently being made largely by plasma-assisted dry etching process. [4, 57]

A few groups have reported the MacEtch of randomly distributed holes in bulk Si using metal nanoparticles formed by electroless deposition, [107-109] which limits the use of this approach only to applications where a periodic arrangement of holes is not required. However, for the formation of PhCs and metamaterials, uniform etching of an array of holes of sub-micron scale dimensions with precisely defined lattice configurations is critical. Unlike the formation of vertical pillars using a metal mesh layer as the catalyst, drilling an array of holes using isolated catalysts is more challenging due to the absence of connectivity and, thus, coherence while descending between neighboring metal disks. This necessitates the modification of conventional MacEtch methods reported to date to

be used for the drilling of holes in Si and other semiconductor materials with controlled lattice configurations.

In 2012, Oh *et al.* reported the direction-guided, nano / micro shaping of Si using an applied magnetic field for intentionally changing the direction of motion of the catalyst during MacEtch, resulting in the formation of sheets, needles, and zigzag wires. [110] This work motivated us to explore magnetic field-guided MacEtch (*h*-MacEtch) to overcome the challenges in using isolated metal catalysts for the formation of periodic arrays of holes. Such a field-guided MacEtch process can lead to the formation of straight air hole arrays with high aspect ratios, and curved air holes with controlled chirality, a process that is otherwise unachievable with conventional dry etching. we present here a systematic study of the etch parameters required for the fabrication of periodic nanohole arrays of sub-micron dimensions on silicon-on-insulator (SOI) wafers using MacEtch under the influence of an external magnetic field. We then demonstrate, for the first time, the fabrication of high performance two-dimensional (2D) air hole array PhC Si membrane reflectors (Si-MRs) using this approach.

As shown schematically in Fig.2-1(a), a square-lattice air hole PhC structure on an SOI substrate was used for our design. The key lattice parameters are shown in Fig. 2-1(b), where r, a, and t represent air hole radius, lattice constant (period), and Si-MR thickness, respectively. The design was based on rigorous coupled-wave analysis (RCWA) techniques. [57, 111] For the PhC Si-MR design considered here, with target reflection spectral band around 1500 nm, the design parameters are a = 980 nm, r/a = 0.28, and t = 340 nm.

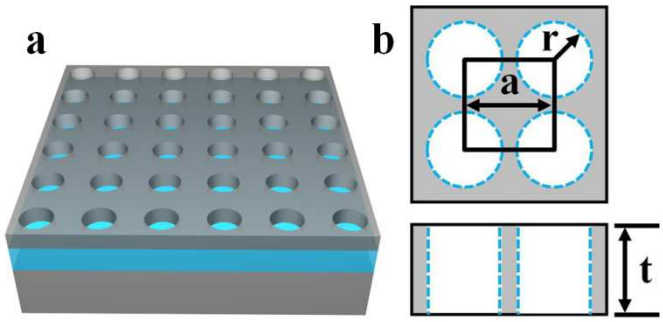

Figure 2-1 (a) 3D sketch of a Si-MR with a patterned 2D air hole square-lattice PC structure on an SOI substrate. (b) Key lattice parameters for the square-lattice air hole PC structures are air hole radius “r”, lattice constant or period “a”, and Si-MR thickness “t”. [5]

After defining the patterns using electron-beam lithography (EBL), we deposited a trilayer stack of metals (Au (20 nm)/Ni (10 nm)/Au (5 nm)) on an SOI wafer (2 µm buried oxide (BOX) and 340 nm top Si) using electron-beam evaporation followed by subsequent liftoff to form metal disc patterns. We then introduced the SOI wafer with metal disc patterns into a Teflon beaker with 49% hydrofluoric acid (HF, 5 mL), 30% hydrogen peroxide (H_2O_2, 1.25 mL) and deionized water (DI, 8 mL) for different etch periods (specified below). A stack of circular neodymium magnetic disks (Applied Magnets), with maximum measured magnetic field strength of 0.2 T, were placed underneath the beaker containing the MacEtch solution to ensure uniform and vertical drilling of holes in the active device area, by avoiding the detouring of metal catalyst disks during etching. The process steps have been shown in Fig. 2-2. Following MacEtch, the SOI wafers were submerged into a commercial gold etchant (Transene Co.) to completely remove the metal stack. Imaging and general inspection of post-MacEtch samples were carried out using a Hitachi S-4800 scanning electron microscope (SEM).

For optical reflectivity measurements, a white light source (covering 1100-1700 nm spectral range) and an optical spectrum analyzer were used to measure the reflection spectra over a wide spectral bandwidth.

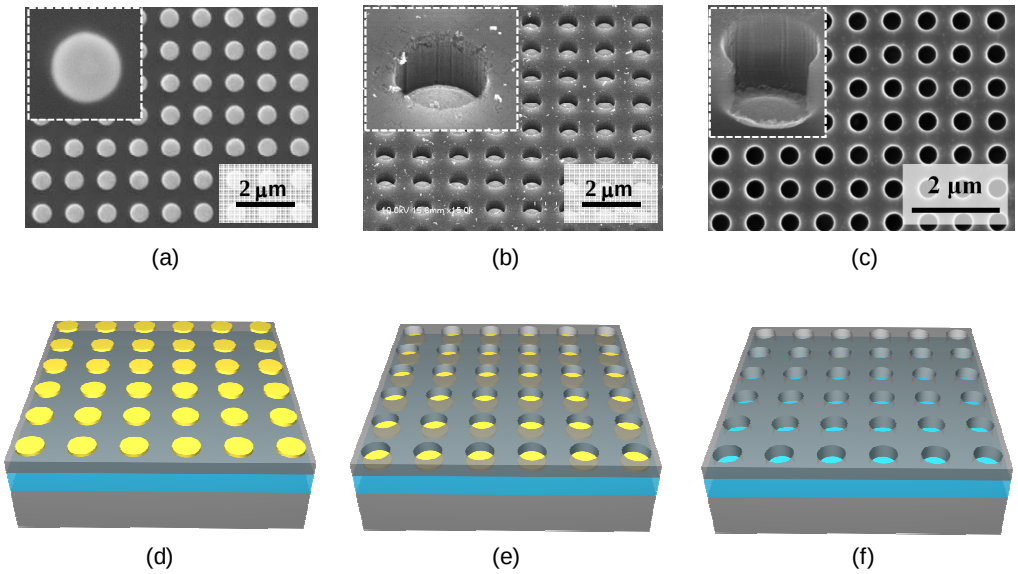

Figure 2-2 (a) topview SEM images of trilayer metal disc on top of SOI (b) 45°tilted-view SEM images of nanohole arrays after MacEtch for 60 s with 0.2 T external magnetic field guidance (c) Top-view SEM image of nanoholes array formed by MacEtch. Inset shows a tilted-view image of a single drilled nanohole and the catalyst disk after MacEtch. Following by the 3D sketches illustration of each step (d), (e), and (f). ((b), (c)and (f) refer to [5])

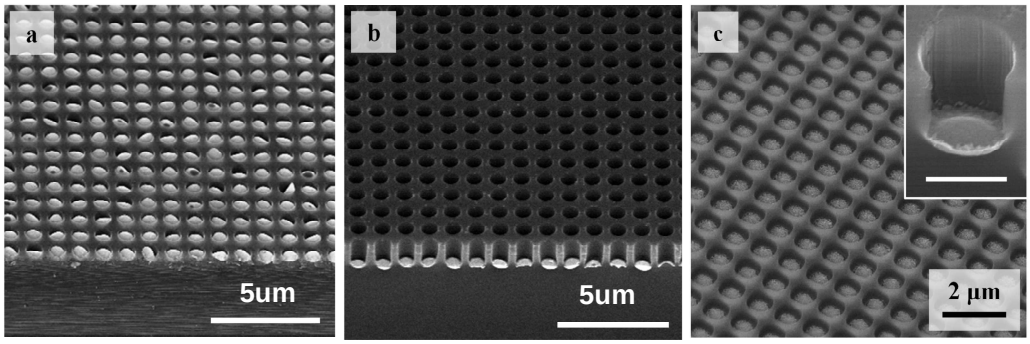

Figure 2-3 45°tilted-view SEM images of nanohole a rrays after MacEtch for 60 s with (a) zero and (b) 0.2 T external magnetic field guidance. The scale bars represent 5 µm. (c) 45°tilted-view SEM image of a nanohole array after a 60 s magnet-guided MacEtch process showing trilayer metal stacks displaced to the bottom of the etched Si air holes. Inset shows a tilted-view image of a single drilled nanohole and the catalyst disk after MacEtch. Inset scale bar represents 500 nm. [5]

Fig. 2-3(c) shows a tilted-view SEM image of a nanohole array (diameter = 550 nm and pitch = 1 µm) fabricated on a p-type (ρ = 5-10 Ω·cm) Si wafer using a 60 s MacEtch process under the influence of an externally applied magnetic field. During the course of etching, the trilayer metal disks sink vertically into the substrate (as shown in the inset) due to the influence of the applied magnetic field attracting the central Ni layer of the trilayer metal stack in a downward direction. By varying the duration of etching, this approach allows for the drilling of vertical holes of any aspect ratio, so long as a perfect interface between the catalyst disk and the underlying semiconductor substrate is preserved. In addition, by switching the polarity and duration of the applied external magnetic field, this technique may, in principle, be extended to drilling helical or spiral-shaped pits for 3D photonic device applications, [112] which cannot be achieved by other anisotropic etching processes. It should be noted that the edge roughness of the metal

disk controls the smoothness of the nanohole sidewalls, due to the inherent nature of the MacEtch process. [103]

For the SOI wafer used for our optical reflectivity measurements, we set the etch duration as 75 seconds in order to ensure full penetration of the catalyst disks through the top Si layer (t=340 nm). In Fig. 2-4 (a), (b) the top view SEM image of a Si-MR formed on top of the BOX layer is shown. We observed that when the metal catalyst reaches the underlying BOX layer, MacEtch no longer continues, as etching of this segment proceeds isotropically in HF (no Si layers are present in the BOX to be oxidized). The patterned MRs formed using MacEtch can be released from the SOI substrate by selectively etching the BOX layer in HF, and can be directly transferred to any other substrates based on the transfer printing technique. [113] We give a comparison of MacEtched MR device and RIE MR device. SEM top-view images were given in Fig. 2-4 along with their measured reflection spectral respectively. A MR device fabricated by RIE process also was shown for comparison as Fig. 2-4 (d) (e) (f).

Fig. 2-4 (c) show the measured (solid, red curve) and simulated (dashed, blue curve) optical reflectivity spectra from a MR with a MacEtch-patterned 2D air hole square-lattice PhC structure. The parameters used for simulation to fit the experimental results are a = 980 nm, r/a = 0.313, and t = 340 nm. Notice that the fitted r/a value is slightly larger than the original design parameter, due to enlarged air hole sizes in the actual etched structures. Clearly, the key features in the broad high-reflection band region between the experimental and simulated optical reflectivity results match very well. The measured peak value of reflectivity is approximately 90% of simulated value at the desired wavelength of 1500 nm. Further improvement of reflectivity can be achieved by minimizing the sidewall roughness of the etched nanoholes caused by the edge roughness of metal disks, resulting from the patterning approach. The results

demonstrated here confirmed experimentally for the first time that MacEtch, a simple, low-cost, and damage-free technique, can be used for the fabrication of Si-MRs without

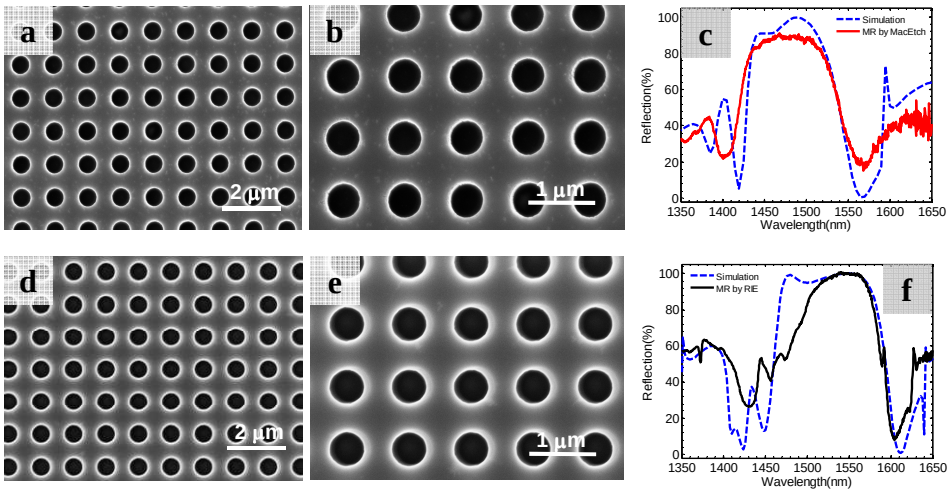

Figure 2-4 (a),(b) SEM top-view of MR device by MacEtch. (c) Simulated and measured reflection spectral of MacEtch MR device. (d),(e) SEM top-view of MR device by RIE process. (f) Simulated and measured reflection spectral of RIE MR device. [5]

the need for high vacuum conditions or a high thermal budget, as required for conventional plasma-assisted etching. Most importantly, the work reported here demonstrates the feasibility of the MacEtch process for high quality photonic structure fabrications, where more complicated 3D structures may be used.

In this work, we report the fabrication of discrete nanohole arrays in Si using magnetic field-guided MacEtch. We have performed a systematic study of the factors affecting the structural morphology of the holes made using this approach, including the strength of the external magnetic field, etch period, and lateral dimensions of the nanohole features. Furthermore, we have fabricated and characterized the optical reflectivity of Si-MRs using this technique. Our results show that the optical device

performance of the Si-MRs made using this simple and low-cost method matches very well with theoretical models, based on RCWA simulations. Our future efforts will focus on the demonstration of spectral tunability using various dimensions of nanohole arrays. Also, we aim to apply the magnetic field-guided MacEtch approach to the fabrication of discrete, non-linear 3D features in Si as well as compound semiconductors.

2.1.2 Long wave membrane reflectors: scaling from near infrared to mid and far infrared.

It was pointed out that [114] ingenious techniques are needed to extend group IV photonics from near-infrared to mid-infrared wavelengths. If achieved, the reward could be on-chip CMOS optoelectronic systems for use in spectroscopy, chemical and biological sensing, and free-space communications. After twenty years being used as a platform for near-infrared photonics, SOI turns to be problematic due to higher absorption loss in silicon oxide for longer wavelengths. However, important to know that 0.6-0.7 dB/cm propagation losses measured for silicon on porous silicon(SiPSi) waveguides at wavelength of 3.39 μm, which is longest wavelength used so far on SOI platform [115]. Preliminary work on group IV photonic waveguides was presented from fabrication to experimental results. [116] It is necessary to dig into the mid and long wave region as well as their applications by more experimental studies. In this section, we will focus on the mid and far infrared wavelength region and explore this interested topic by several experimental demonstrations.

Compact broadband reflectors are of great importance for optoelectronic devices and photonic integrated circuits like lasers, photodetectors, solar cells, and sensors, etc. Traditionally, they can be realized by using metal, or stacked dielectric thin films. Metal films offer larger reflection bandwidth but are limited by their intrinsic absorption losses. Stacked dielectric distributed Bragg reflectors (DBRs) can achieve very low losses, but

they typically require many individual layers with stringent refractive index and thickness tolerances for each layer. It becomes a difficult engineering challenge to realize extremely high reflection DBRs at mid-IR, far-IR, and THz frequencies, due to the scaling of the dielectric quarter-wavelength stack.

Recently, broadband reflectors based on Fano resonance, or guided mode resonance [35, 57, 60, 95, 117], have attracted great attention, where high reflectivity can be obtained with a single layer, one-dimensional (1D) high contrast grating (HCG) [38], or a two-dimensional photonic crystal slab (2D PCS) structure. [57] By properly controlling the design parameters, very broadband reflectors can be obtained. Based on crystalline membrane transfer, high performance membrane reflectors (MRs) and lasers at near-IR (1550nm) have been reported recently fabricated on crystalline Si, SOI and on glass substrates. [57, 118, 119]

We demonstrated here single layer ultra-compact Si-MRs at mid-infrared and far-infrared bands, based on a suspended membrane structure. High performance reflectors were designed for surface-normal incidence with center operation wavelengths of 1.5 μm, ~ 9 μm, 32 μm and 75 μm, respectively. Large area patterned membrane reflectors were also fabricated and transferred onto glass substrates using a PDMS stamp assisted membrane transfer printing process. Close to 100% reflectivity was obtained at the 76 μm spectral band, with a single layer Si membrane thickness of 18 μm.

As shown schematically in Fig. 2-5(a), a square lattice air hole photonic crystal structures on SOI substrate is used for our design. The key lattice parameters are shown in Fig. 2-5(b), where r, a, and t represent air hole radius, lattice constant (period), and Si-MR thickness, respectively. The complex index parameters for Si and SiO2 used in the design are shown in Fig. 2-5(c), and Fig. 2-5(d), respectively. [120] The chosen design parameters were based on finite difference time-domain (FDTD) simulations and rigorous

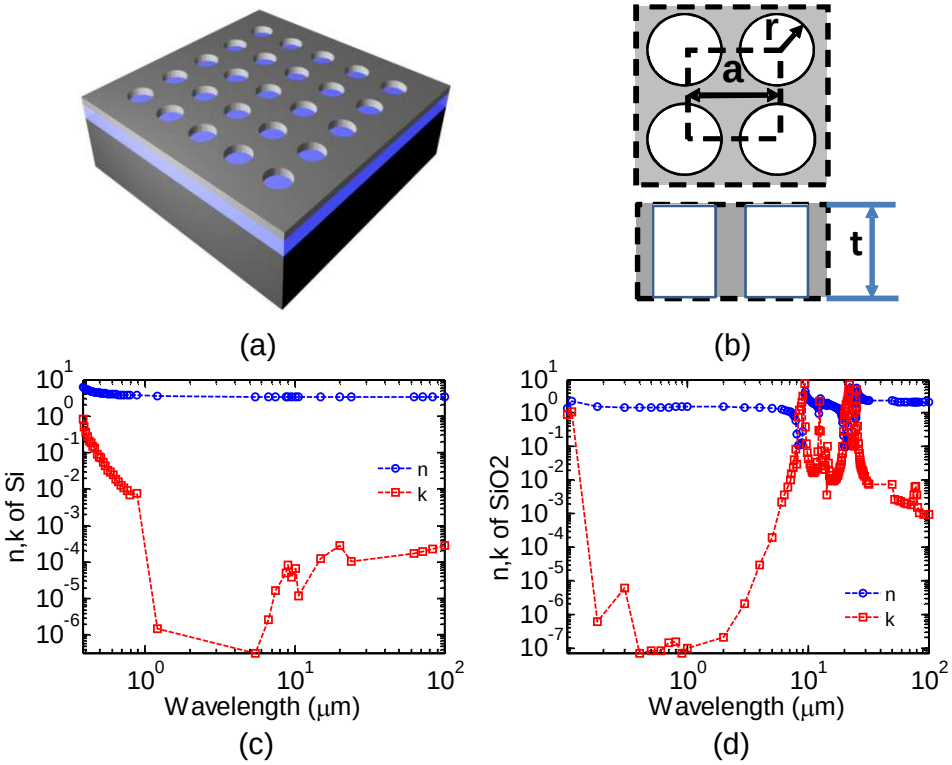

Figure 2-5 (a) 3D sketch of a Si membrane reflector with a patterned 2D air hole square lattice photonic crystal structure on SOI substrate; (b) Key lattice parameters for the square lattice air hole photonic crystal structures are air hole radius (r), lattice constant (period a), and Si-MR thickness (t); (c, d) Complex index parameters for Si and SiO2 used in the simulation.[4]

coupled-wave analysis (RCWA) techniques. [121] Shown in Fig. 2-6 are the simulated reflector performances for designs at four different wavelength bands. All designs are based on suspended (in air) Si-MR configurations. Broadband reflection with 100% peak reflection is achieved for all designed wavelength bands, with the optimal selection of lattice parameters and Si thicknesses. Based on scaling principles, it was found that the

optimal Si-MR thickness (t) is ~0.75-0.85 (λ/n), and the optimal lattice constant (a) is ~1.9-2.1 (λ/n), where λ is the wavelength and n is the refractive index of Si.

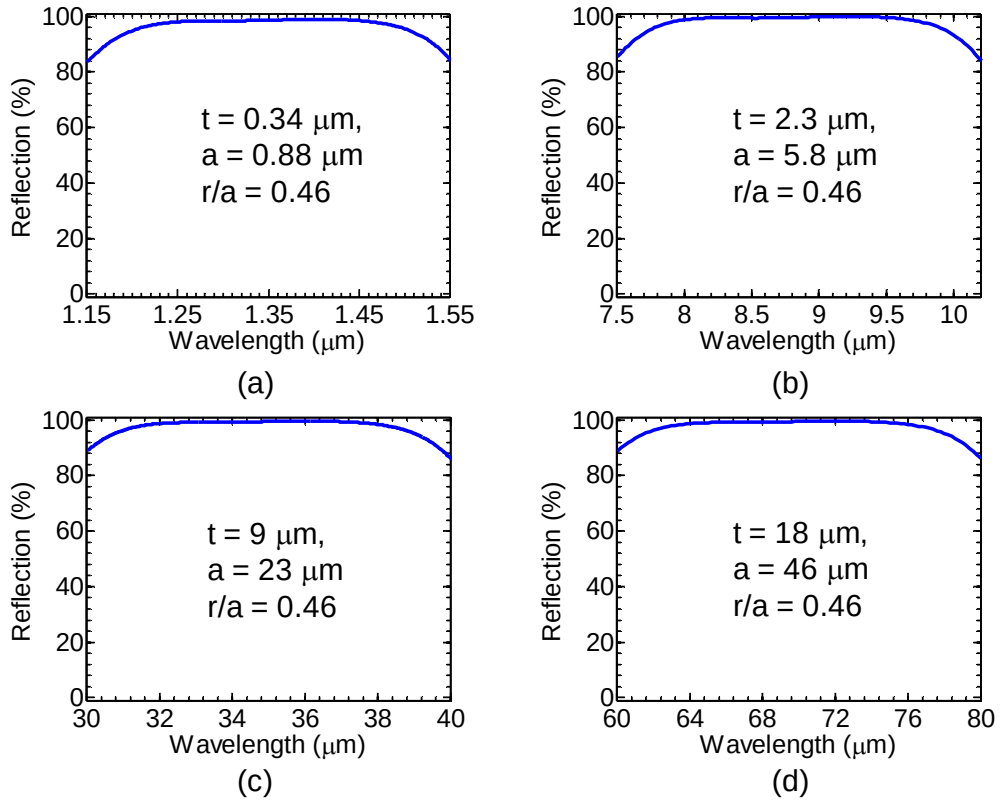

Figure 2-6 Simulated reflector performances for designs at four different wavelength bands.[122]

The Si-MR fabrication process flow is shown schematically in Fig. 2-7. Patterns were first formed in photo-resist on SOI substrates using either e-beam lithography or optical lithography, depending on the feature size required for the different spectral bands. This was followed by a reactive-ion etching (RIE) process to transfer the pattern into the host material. The patterned Si membrane structures were then released by a

selective buffered oxide etchant (BOE) etching of the buried oxide (BOX) layer. Finally the patterned, single layer Si membrane was transferred onto a transparent foreign substrate, such as glass. In order to avoid the strong absorptions in the SiO2 material for wavelengths greater than 5 μm (Fig. 2-7(d)), an open hole was formed on the transparent glass substrate to produce a suspended Si-MR. [123]

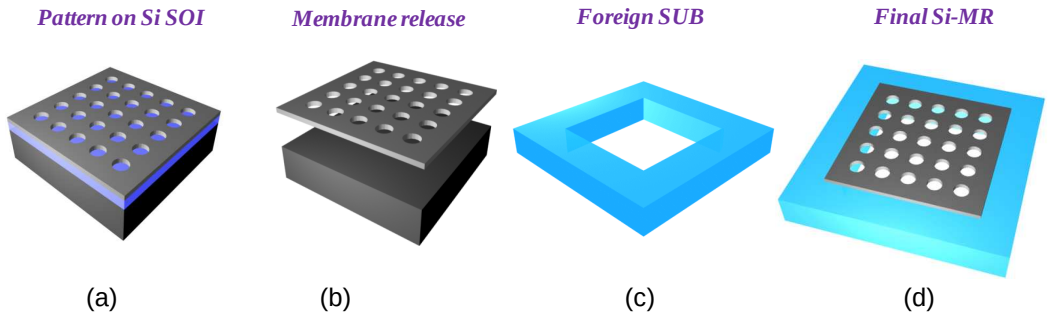

Figure 2-7 Si-MR schematic fabrication process flow: (a) Photonic crystal structure patterned on SOI substrate; (b) Release of patterned top Si-MR layer from Si substrate by selective wet-etching; (c) Preparation of host substrates with center openings; and (d) Final suspended Si-MR on host substrate.[4]

Shown in Fig. 2-8 are images of the fabricated Si-MR patterned on SOI using optical lithography. As shown in Fig. 2-8(a), up to a 1" square, high quality patterned area was formed, with excellent uniformity (Fig. 2-8(b)). The patterned Si membrane 18 μm thickness was released and transferred onto a piece of glass substrate to form a suspended membrane Si-MR as shown in Fig. 2-8(c). Photonic crystal 2D holes arrays patterning have been made with different dimensions (as shown in Fig. 2-9) and patterning approaches.

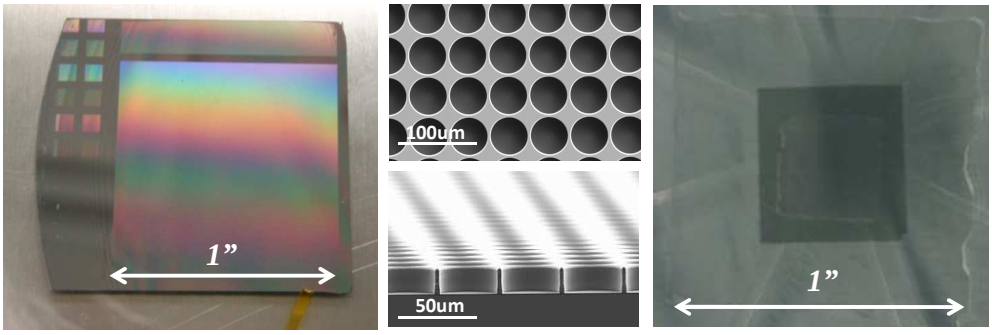

(a) (b) (c)

Figure 2-8 (a) A micrograph of a fabricated Si-MR on SOI with 1 inch by 1 inch uniform patterned size; (b) Scanning-electron micrographs (SEMs) of a fabricated Si-MR at the 76 µm spectral band, top and 3D views; and (c) a micrograph of a transferred Si-MR at the 76 µm spectral band on a glass substrate with a center opening to form a suspended Si-MR.[4]

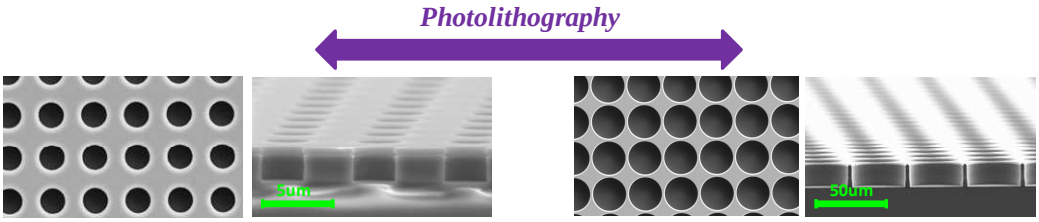

r = 1.66µm; t = 2.3µm **r = 21.5µm; t = 18µm**

(a) (b)

Figure 2-9 (a) A SEM top-view image of the fabricated Si-MR at mid-infrared, with a cross-sectional SEM image; AZ5214 as patterning mask (b) A SEM top-view image of the fabricated Si-MR at far-infrared, with a cross-sectional SEM image; SU8-5 as patterning mask. (For near-infrared Si nanomembrane patterning, Zep520-A e-beam resist was utilized as mask or pattern transferring medium, not shown here.)[4, 122]

Large-area Si MRs were fabricated based on photolithography and deep reactive-ion etching (DRIE) process on SOI substrates with different top-Si thicknesses. The patterned Si membrane structures were later released by selective buffered HF (BHF) etching of buried oxide (BOX) layer underneath, and transferred onto foreign substrates, based on wet transfer technique.

2.1.2.1 Mid-infrared Si membrane reflectors at 2.3 μm and 8 to 10 μm

We designed Si MR working at ~2.3 μm wavelength band as the material system has the minimized intrinsic absorption to the interested wavelength region. Here we showed a basic simulation result according to our design as Fig. 2-10, where the design parameters were given.

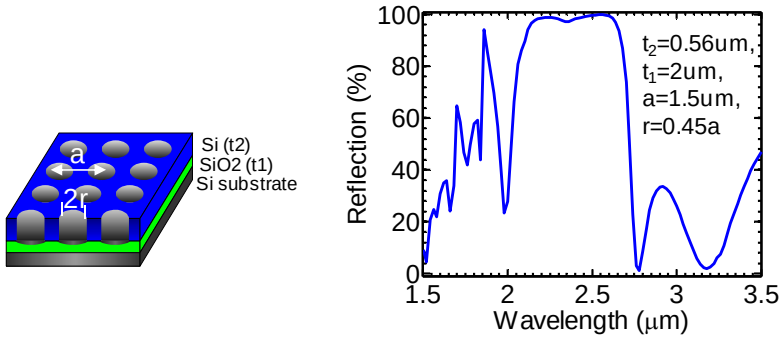

Figure 2-10 (a) design device 3-D sketch for the design parameters for SiMR working at 2.3 μm spectral band; (b) simulated reflection spectra for 2.3 μm band Si-MR.(un-published)

We also made one trying as the first time for fabrication of this device by e-beam lithography. Though lower reflectivity around 70~80% reflection peak was noticed, this is

due to the measurement incidence angle. Ideally, we are expecting a normal incidence with collimated incident beam for the device testing.

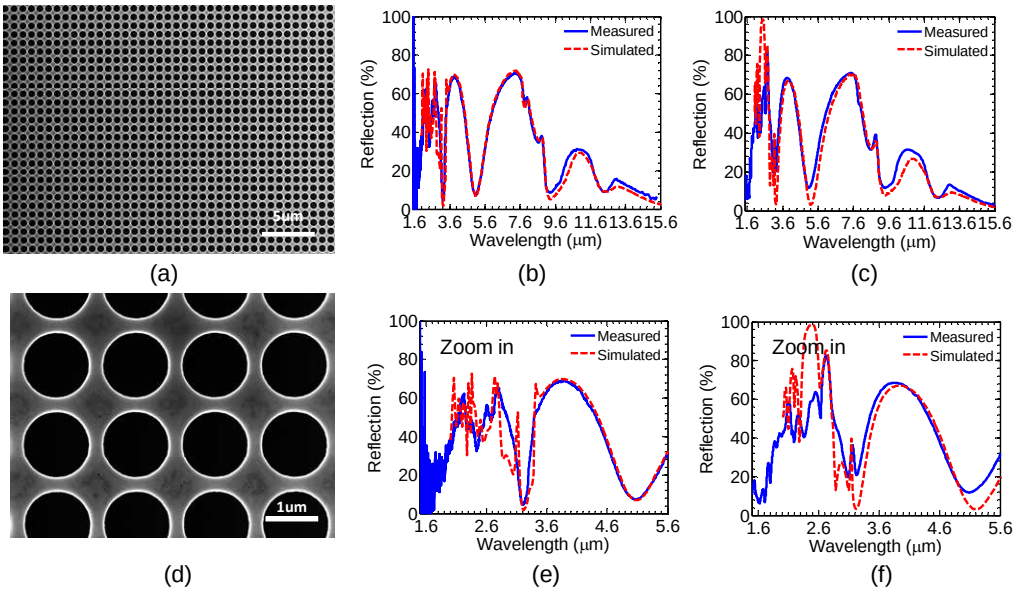

Figure 2-11 (a) and (d) are SEM topview of this fabricated sample. Notice that the Si surface was slightly attached due to RIE over etching. (b), zoomed-in (e) are measurement results using a 15X NA 0.58 objective lens with ~26 degree incidence; and (c), zoomed-in (f) are measurements using a 36X objective lens with 20 to 57 degree incidence. We tried to match all with simulations. (un-published)

The measurements were tried both on UTA Zhou's lab FTIR system with 26 degree incidence and on ASU another FTIR system, which claimed measuring with a 20 to 57 degree light incident angle. As showed in Fig. 2-11 (a) and (d) are SEM topview of this fabricated sample. Notice that the Si surface was slightly attached due to RIE over etching. Holes size are smaller than our desired parameter of r = 0.46a, instead we got measured size from SEM r = 0.41a, where a = 1.5 μm. (b) (e) are measurement results

for 26 degree incidence; and (c) (f) are for 20 to 57 degree incidence. Both of the measurements matched very well with the simulations corresponding to each measuring strategy.

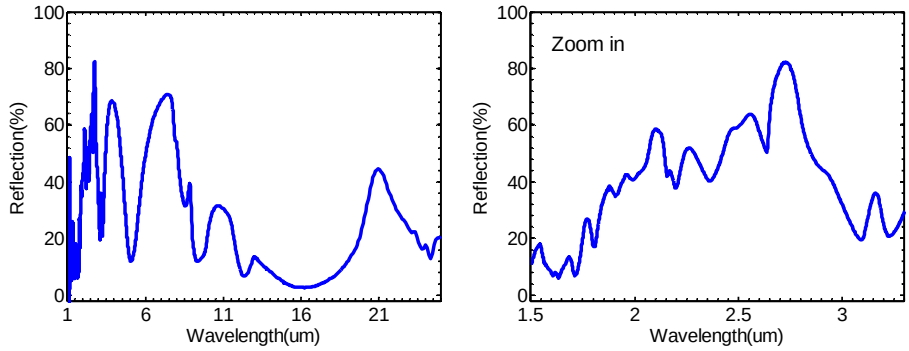

(a) (b)

Figure 2-12 2.3um reflection band Si-MR: (a) (b) are reflection measurement spectral for 5-15 degree incidence; (b) zoomed-in at 2~3 μm interested band region. (un-published)

As shown in Fig. 2-12, the later 5 to 15 degree incidence testing reviews that it has an 84 % reflection peak at the desired band. The lower reflectivity either caused by fabrication defects, smaller hole size than the designed parameter or the measurement incident angle related issue. It is still open for further investigation and potential applications at this highly interested low absorption wavelength region.

For the 8~10 μm operation wavelength Mid-infrared MR devices, AZ5214 negative resist is used for the photolithography on 2.3 μm thickness Si on the SOI (with top Si 2.3 μm), which have been identified by Ultra-SOI data sheet within our design tolerance. Two dimensional holes array are focused on in our 2D PC design. We scanned the design parameters as of holes center to center separation (period) and holes' diameter. Due to the enlargement of the patterning hole size caused by RIE lateral

etching, we considered a hole size offset during the mask design and scanned the hole sizes in a 0.4 µm range with 0.1 µm steps.

In order to have a successful hole size control and uniform resist patterning, other than other specified lithography parameters, the good surface contact was found to be the most critical part for this 2~5 µm small size patterning, especially for a small piece of sample on a much bigger photolithography machine 4-inch chuck. To solve this technical issue during resist patterning for a critical dimension that approaching to resist functional patterning limit, we applied a PDMS coated chip carrier as a substrate during the exposure contact. There are two benefits by doing so, on one hand, PDMS coated substrate offers an attachment of the small chip to the chuck when one make the alignment and also easy to lift the chip up from the PDMS coated substrate after exposure; On the other side, with the soft PDMS at chip's backside, the self-balanced contact gives perfect pressure uniformity between chip top surface to the photo-mask. This engineering method can provide a large area uniform contact during exposure for small chips resist patterning photolithography when a machine chuck mechanical auto-balanced contact cannot be able to achieve. After resist patterning, we further developed a Si etching recipe with low pressure (29 mtorr) and faster etching rate and more straight vertical etching sidewall, SF6 and O2 were used as the reacting gas, RIE power set as 28 W with a 10 inch Trion chamber chuck size. The AZ5214 resist mask was utilized for 2.3 µm Si etching. The selectivity improved from (1:1.25) to (1:2) after hard baking at 150C for 2mins. Fig. 2-13 shows SEM topview of an 8~10 µm wavelength band Si-MR device in (b) and a large piece (1cm by 1cm) of pattern 2.3 µm thick Si-NM was transferred on to the Si substrate with opening hole.

Various measurement setups have been used for Si-MR reflection measurements in different spectral regions. For near IR structures (NIR), a free-space

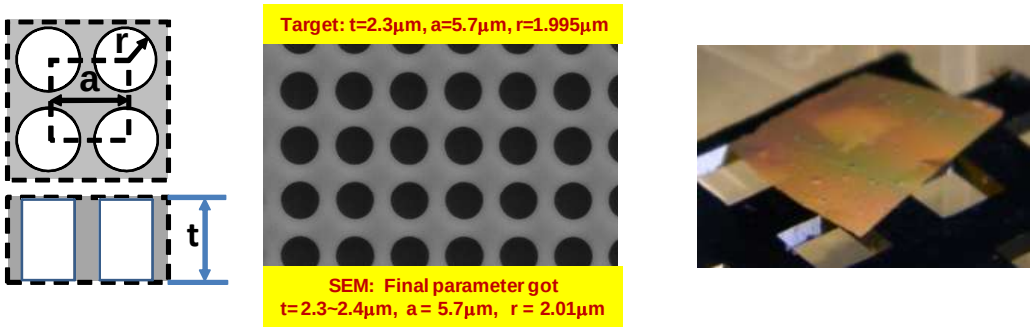

(a) (b) (c)

Figure 2-13 (a) Design parameters definition sketch. (b) SEM top view image of a patterned Mid-infrared membrane reflector device; Parameters target showed at the top and fabricated device parameters showed at bottom, which give an idea of the intrinsic off-set between design and device fabrication. Notice here we successfully patterned hole arrays with 2 μm radius and 5.7 μm spacing, SEM shows the perfect circular edge we achieved using AZ5214. (c) A large piece (1cm by 1cm) patterned Si membrane device was released and transferred on to the Si substrate as supporting with opening square holes. [4, 122]

beam-splitter was used for surface normal reflection measurement, with a gold reflector used as reference. [124] For Mid-infrared wavelengths (MWIR) MR devices measurements, a Nicolet micro-Fourier Transform Infrared (FTIR) system was used, where the reflection measurement was carried out with a 23.6° off-surface-normal beam, though a 15X, 0.4 NA reflecting objective lens. Measured reflection spectrum is shown in Fig. 2-14(b), where the measured was carried out with a 23.6° off-surface-normal beam. Close to 90% peak reflection was achieved. It is worth notice that these MRs are very sensitive to incident angles. It is anticipated that the surface normal reflection for this MR can be much higher.

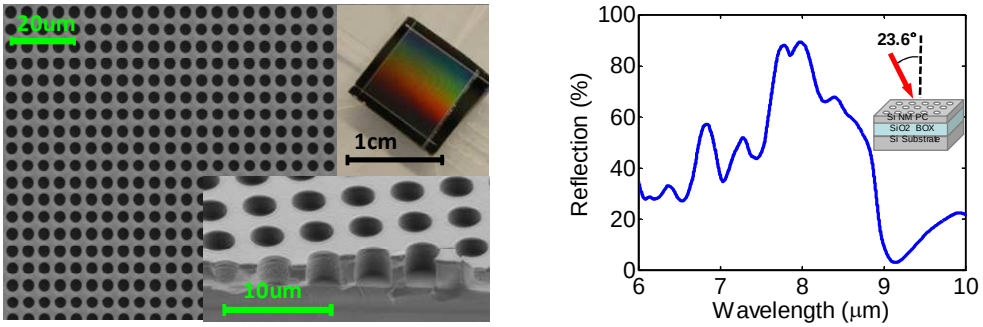

(a) (b)

Figure 2-14 (a) A SEM top view image of the fabricated Si-MR at mid-infrared, with a cross-sectional SEM image and a micrograph shown in the insets; (b) Measured reflection spectrum for a Si-MR on 4 μm SiO2 box layer measured at an incident angle of 23.60 off surface-normal measured with a micro-FTIR system. [4]

As the original optical design, we also tried to suspend the Si photonic crystal slab. The 2.3 μm thickness Si membrane reflector device layer were released by HF and transferred onto foreign Si substrate with a pre-etched 1 mm × 1 mm area of 4 μm deep trench. Both PDMS assisted and wet transferring techniques were used. We measured the reflection spectral by FTIR with a ~26 degree angled incidence. It keeps a fairly matching spectral comparing to simulation result although the membrane bending issue may cause some uncertainty. The bright side is, as we expected, the reflectivity improved from 90% to almost 96% at the peak reflection region. Sample picture Fig. 2-15 (a), SEM sample topview as Fig. 2-15 (c), SEM angled views as Fig. 2-15 (b,d,e) and measured reflection spectral Fig. 2-15 (f) were showed here.

It is also worth to mention that the 2.3 μm thickness Si membrane with 1cm × 1cm size is still quite flexible but strong for handling. It is feasible for later investigation of it potential properties as bending, multilayer transferring and stacking. One most direct

idea might be stacking double-layer 2.3 µm thick PCS to achieve high-Q resonance in Mid-infrared or even Far-infrared wavelength region. This could be the same idea as we will discuss in Chapter 3. We showed here some pictures of transferred 2.3 µm thickness PCS devices on PDMS substrate in Fig. 2-16 (a), (b) and (c), with different shapes and sizes.

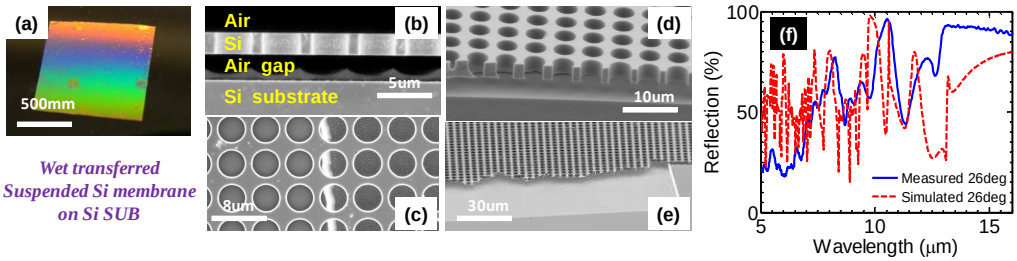

Figure 2-15 (a) A SEM top view image of the fabricated Si-MR at mid-infrared, with a cross-sectional SEM image and a micrograph shown in the insets; (b) Measured reflection spectrum for a Si-MR on 4 µm SiO2 box layer measured at an incident angle of 23.60 off surface-normal measured with a micro-FTIR system. (un-published)

(a) (b) (c)

Figure 2-16 (a) PCS device layer on PDMS, comparing with one Dime (b) PCS device layer with different shapes on PDMS, comparing with one Dime. (c) One large PCS membrane bended and broke on PMDS. (un-published)

The following pictures show in Fig. 2-17 is the FTIR testing system that used for suspending Mid-infrared MR device (8 μm ~ 10 μm) reflection spectral characterization, which can handle the device operation wavelength from 1 μm to 16 μm.

Figure 2-17 Reflection test with an incident angle of 26°off surface-normal measured with a micro-FTIR system. (Zhou' NPLab facility, NanoFAB, UTArlington)

The scope reflection and transmission special design enables the on stage sample testing with a well defined focusing square spot size from 5 μm × 5 μm to 150 μm × 150 μm. The scope testing modes showed below as the sketch in Fig. 2-18 left and right. (Copied from FTIR software, "help" document.)

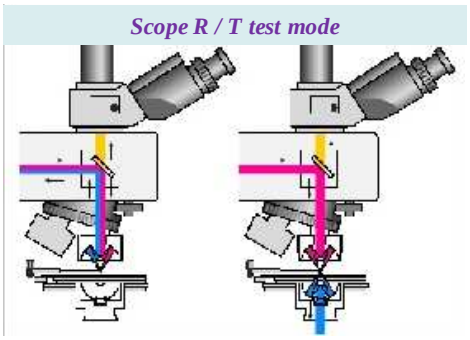

Figure 2-18 FTIR measurement: test system. R/T mode. (Zhou' NPLab facility, NanoFAB, UTArlington)

2.1.2.2 Far-infrared Si membrane reflectors at 76 μm

The fabrication on the 18 μm thickness Si membrane is quite different to 2.3 μm thickness Si membrane. The SU-8-5, which has typical 5 μm spin thickness, was used for patterning and etching mask. The hole size is well controlled after 18 μm deep Si etching in around 40 mins. (Using the same Si etching recipe) After that, the resist remaining as a membrane on Si top surface is hard to remove possibly because of the long time etching temperature rising and several times pre- and reverse bake during SU-8 patterning, but a HF dip can help to remove the SU-8 resist mask after Si etching.

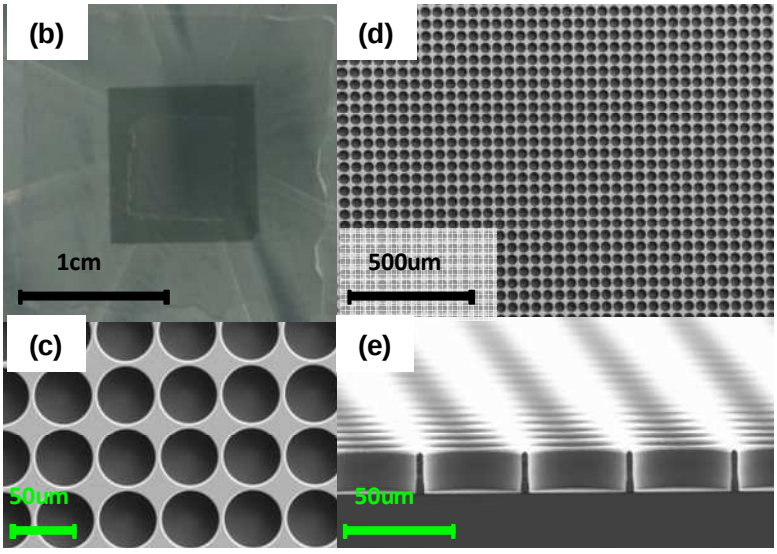

Figure 2-19 (a) A suspended 1cm by 1cm Si-MR at far-infrared sitting on glass substrate where have an opening hole in the center. (b) SEM large scale top-view of the Si-MR at far-infrared device. (c) A SEM zoomed-in top-view image of the fabricated Si-MR at Far-infrared, with a cross-sectional SEM image in (e).[4]

The pattern 18 μm thick PCS then was transferred onto a glass substrate with an opening hole in the center by wet transferring techniques. The attachment between the Si membrane and the glass substrate can be enhanced by annealing the sample at 200 C to 300 C for 10 mins.

To estimate the reflectivity of the Fano reflector at far-infrared (FIR), a Fabry-Perot interferometer was formed from two identical reflectors and its finesse characterized. The finesse F may be determined from the free spectral range (FSR, Δλ) and the resonance full width at half maximum (FWHM, δλ) according to F = Δλ / δλ. The reflectivity R is then found from the measured finesse according to F = $(\pi\sqrt{R})/(1-R)$.[125]

The measurement setup is shown in Fig. 2-20 (a). One of the Fano reflectors was mounted on a fixed mirror mount. The second was mounted on a motorized precision translational stage controlled by a Labview program. Radiation from a quantum cascade laser (QCL) at 70 micron wavelength was collimated by a 90° off axis parabolic mirror and passed through the Fabry Perot, where it was focused onto a slow but sensitive Golay cell detector by a second off-axis paraboloid. The QCL (Trion) was held at 77 K inside a liquid nitrogen cryostat with polyethylene output window. The collimating optic was inside the cryostat. The laser was excited with a burst of fifty 10-μs-long pulses. The repetition rate of the burst was ~10 Hz and the burst duty cycle was 50%. The bursts were integrated by the Golay cell, lock-in amplified at the slow burst repetition rate, and recorded with the Labview program.

Shown in Fig. 2-21 (b) are measured and simulated surface-normal reflection spectra outputs derived from transmission measurements. Assuming no absorption in

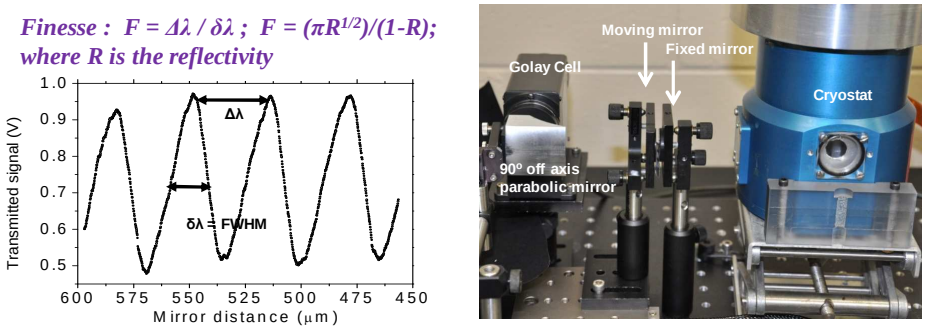

(a) (b)

Figure 2-20 (a) Measured Transmission spectra for two suspended Si-MRs. [4, 122] (Professor Robert Peale Lab facility, UCF) (b) A micrograph of the experimental setup for the measurement of Si-MR reflection at 76 μm spectral band.

the spectral band, we can obtain close to 100% reflection at roughly 76 μm wavelength. The experimental results agree reasonably well with the simulation results.

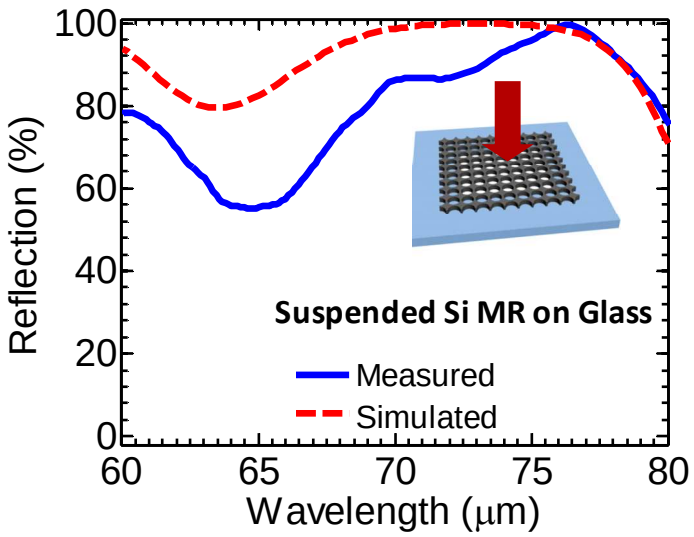

Figure 2-21 Measured and simulated reflection spectra for a suspended Si-MR on glass.[4]

Chapter 3

Photonic Crystal Nanomembrane Optical High-Q Filters

Traditional thin-film based filters, operating in the infrared regime for dense wavelength division multiplexing (DWDM) applications, usually require hundreds of or more individual layers, with stringent thickness tolerances for each layer and are thus very difficult to satisfy missions of nanophotonics. As one solution, Wang and Magnusson showed that a slab can function as a notch filter with a Lorentzian reflection line shape, when the slab thickness is appropriately chosen and a single resonance is placed within the vicinity of the signal frequency.[126] However, Fano resonances in photonic crystal slabs [60, 127-133] can provide a very compact way to generate useful spectral functions for externally incident light.

Recently, Fano resonances, known from atomic physics, have been employed for a wide variety of nanophotonic structures, such as quantum dots, photonic crystals (PhCs), plasmonics, and metamaterials [1, 134-136]. With modal dispersion engineering, Fano filters and reflectors can all be realized in single-layer dielectric PhC structures. [7, 135, 137] With in-plane periodic modulation of dielectric constant in PhC slabs (PCS), the out-of-the-plane optical mode coupling is feasible with the Fano resonance effect, where the in-plane guided resonances above the lightline are strongly coupled to the out-of-the-plane radiation modes due to the phase matching provided by the periodic lattice structure. Therefore, these guided resonances can provide an efficient way to channel light from within the slab to the external environment, and vice versa. Such phenomenon was also investigated in one-dimensional grating structures, known as guided mode resonances (GMRs) [36, 138], or high index contrast gratings (HCGs) [38, 95]. The investigation of guided resonance has resulted in using various one dimensional (1D) and

two dimensional (2D) dielectric structures in applications, such as filters [41-43, 137, 139], modulators [45, 140], sensors [141, 142], as well as broadband reflectors, lasers, and beam shaping structures, etc. [8, 139, 143-150]

Surface-normal ultra-compact optical filters are of great importance in optical fiber communications, optical sensors, and millimeter-wave communication systems. Photonic crystal slabs (PCS) as one of the most promising artificial platforms with in-plane periodic modulation of dielectric constant on a wavelength scale, can function either as an all-pass transmission filter or as a flattop reflection filter, thus providing an extremely compact way of generating useful filter functions, and further demonstrating the versatility of photonic crystal structures. [87] Note that it was shown that by coupling two photonic slabs together, all-pass transmission or flattop reflection could be synthesized. [151] Recently, we also experimentally demonstrated the double layer ultra-high Q filters based on coupled two PCSs, which will be discussed in the later sections in this chapter. As a general conclusion we can reached to is, based upon guided resonance effects, we strongly expect the potential integrate these compact novel spectral filter devices [152-160] into ultra-compact optical communication system, as well as using them as sensors and optomechanical integration platforms.

3.1 Different approaches for optical high-Q filters

The most common type of optical filter is the thin-film filter. [161] It was used widely as narrowband filters in laser cavities, light modulators, and optical telecommunication components. Some advantages of thin-film optics are high efficiency and versatility. However, narrowband filters with subnanometer passbands are difficult to fabricate. One needs to make more than handred individual layers with stringent tolerance on each layer. [162] to achieve narrow band high-Q filters. [85]

Mirco-ring resonator showed much more potential as one high resonance platform, a demonstration of Polymer Micro-Ring Filters and light modulation was made in 2002 by Rabiei et al. The Micro-ring give rising to the resonance thus can provide a high Q factor. [163] In the next year, a tunable Polymer Double Micro-Ring Filters was also achieved, which provide tuning rate for thermo optic device is 120GHz/mW and for electro optic device is 120GHz/12V with a wide thermal tuning over 35nm and a tunable laser with side-mode suppression ratio greater than 30dB. [164] Later on, Si_3N_4 was considered as a low loss waveguides material for the micro-scale high-Q ring resonator. Q factors upto 3,000,000, operating in the telecommunication C-band, was achieved in single mode ring resonators. [165] Due to the high stiffness of SiC, it was also utilized as the high resonance ring resonator mode supporting material, a 20 μm radius suspended microring resonator with Q factor of 18,000 was fabricated on commercially available SiC-on-silicon substrates. [166] A fast all-optical switching on silicon using highly light-confining silicon ring structures was present to enhance the sensitivity of light to small changes in refractive index [167] Extremely high Q factor of 100million, that previously attainable only by droplets or microspheres, was also achieved in a toroid microcavity on a chip by using combination of lithography, dry etching and selective reflow process. [168]

Other than the micro rings, another similar idea for high resonance structure, microdisk resonator filters and switches played an important part in the high-resonance optical design. [169] In a silicon nitride microdisk resonator with a 40-nm-thin horizontal air slot was demonstrated, an intrinsic Q factor of ~34,000 at the resonance wavelength 1523.7nm was observed. [170] Ultra-high Q silicon microdisk resonator on silicon-on-insulator (SOI) platform was reported with Q factor of 3 million, corresponding to a propagation loss around 0.16dB/cm. [171]

High-Q measurement also was realized in micro structure as microspheres. [172] However, base on these mode highly confined microdisk or ring resonators strategies, high-Q cavity of optical wavelength size is still difficult to achieve, as radiation loss increases in inverse proportion to cavity size. [173] Therefore, photonic crystal nanocavity attracted much more attention, a high-Q photonic nanocavity in a two–dimensional photonic crystal was realized with 545,000 Q factor, and it shows that light should be confined gently in order to be confined strongly. [173, 174] It is quite straightforward that this photonic crystal nanocavity high-Q design will lead into high-Q cavity integration with other photonic elements.

Fano resonance or guided-mode resonance filters are a new class of narrowband filters that could be important in a number of applications, including laser cavity reflectors, [57, 95] polarizers,[175] light modulators,[176-179] biosensors,[89, 180-182] and WDM filters.[43, 45, 85] One advantage of Fano resonance filters is that they operate on a resonance effect, which can be exhibited by relatively simple structures. Thus, it would be able to replace hundreds of layers thin-films filter with a single or double-layer membrane. The resonance effect is associated with leaky modes that are supported by index modulated patterned membrane structure. At resonance, energy from an incident plane wave is coupled into a leaky mode and then back into one or more radiation modes. The coupling is highly sensitive to the wavelength of light and angle of incidence, and a sharp resonant peak might be observed in the reflected light when either of these parameters is varied.

More attractions have been focused on these Fano resonance based high-Q photonics strategy due to the fact that, the theoretical prediction of these coupled double-layer PCSs structure is possible to offer an extremely high-Q factor that without a theoretical limitation. The dark modes that can be excited in both of these coupled

double-layer PCSs with or without lattice offsets. In the lattice aligned double-layer stacked PCSs structure, proper choices for set of parameters as PCSs thicknesses, lattices can leads to infinite Q. On the other hand, with the PCSs lattice misaligned double-layer stacking structure, infinite Q is also possible from theory. Moreover, one can have even better chances to expecting a practical extremely high-Q.

We have successfully demonstrated these ideas by experimental ways. It has been confirmed that these expectation of extremely high-Q filters are highly desirable and achievable. We will discuss these experimental results in details in the later sections. Nevertheless, these crystalline semiconductor nanomembranes (NMs), which are transferable, stackable, bondable and manufacturable, offer unprecedented opportunities for unique electronic and photonic devices for vertically stacked high density photonic/electronic integration, high performance flexible electronics and flexible photonics. [118]

3.2 Fano resonance high-Q filter design, simulation techniques.

The design was based on 3D finite difference time-domain (FDTD) and rigorous coupled-wave analysis (RCWA) techniques. The transmission or reflection spectrum and field plots were computed based on the Fourier Modal Method using a freely available Stanford Stratified Structure Solver (S4) software package [183]. Comparing the commercial RCWA package GD-Calc we used before [184], S4 software package offers much higher resolution due to the consideration of higher diffraction orders and also takes much less computation time.

Photonic-crystal slabs (PCSs) are one of the most promising artificial platforms with in-plane periodic modulation of dielectric constant on a wavelength scale. Shown in Fig. 3-1 (a) is the schematic of a square lattice PCS, where key lattice parameters are

denoted as r, a and t, for air hole radius, lattice constant and slab thickness, respectively. The outof- the-plane optical mode coupling is feasible with the Fano or guided resonance effect, [135, 185-187] where these in-plane guided resonances above the lightline are also strongly coupled to out-of-the-plane radiation modes due to phase matching provided by the periodic lattice structure. Therefore, the guided resonances can provide an efficient way to channel light from within the slab to the external environment, and vice versa [48]. In recent years, devices based on Fano resonance such as narrowband filters [49, 67, 135] or broadband reflectors [87, 188] have been reported. Shown in Fig. 3-1 (b) is the simulated dispersion plot for the square lattice PCS structure shown in Fig. 3-1 (a), based on a three-dimensional (3D) plane wave expansion (PWE) technique. The Fano resonance modes operating above the lightline region, denoted as the shaded area, are shown in Fig. 3-1 (b). The properties of a few Fano resonance modes (ω1, ω2, ω3) will be discussed later in this paper.

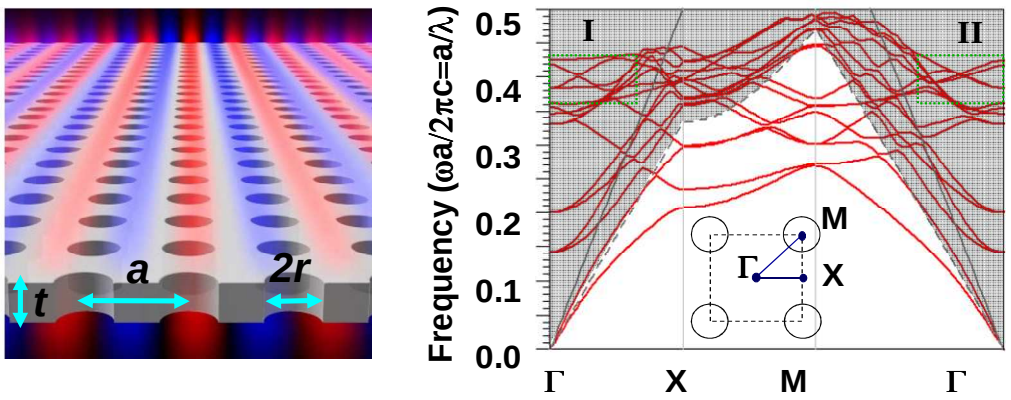

Figure 3-1 (a) Schematic of PCS with square lattice air hole patterns for surface-normal Fano filters and (b) Simulated dispersion characteristics for the square lattice Si PCS structure transferred onto glass/PET substrates with substrate index of 1.5. [118, 189]

Photonic-crystal (PC) structures were first designed with a three-dimensional finite-difference time domain (3D FDTD) technique by using a periodic boundary condition (PBC) and a perfectly matched layer (PML) in the four lateral and two vertical directions, respectively [3], as shown in Fig. 3-2 (a). A Gaussian source is launched from the top of the PCS structure, with two power monitors monitoring the power both reflected and transmitted. Depending on the PCS lattice parameters, either Fano resonance filters or broadband reflectors can be realized with different Q values. A set of simulated spectra for transmission and for reflection spectra is shown in Fig. 3-3 (a). High Q filters with Q greater than 1000 can be easily obtained when a smaller r/a value is used (r/a = 0.08 for high Q case here). On the other hand, a larger r/a value can lead to lower Q filters for broadband reflector design (r/a = 0.28 for low Q case here).

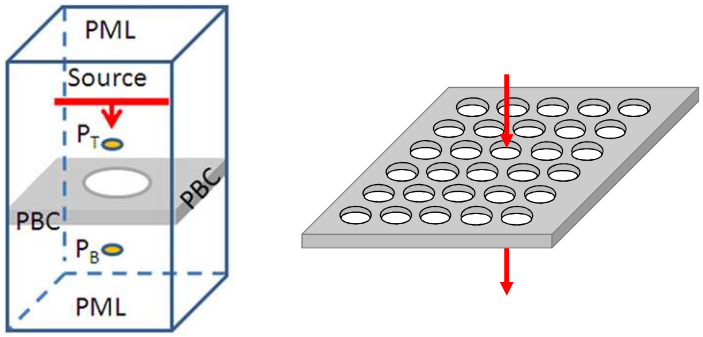

Figure 3-2 (a) Schematic of a unit cell used in the simulation based on the 3D FDTD technique; Simulated (b) Transmission on PCS 3D-sketch [118]

The resonance modes were further verified with the field propagation plots based on 3D FDTD simulations. Snapshots of field propagation for the on- and the off-resonance modes are shown in Fig. 3-3 (b) and (c), respectively. Note that, for the on-

resonance mode (λ1), the surface-normal incident light is bounced back from the patterned Si-NM structure due to the coherence (in-phase) reflection, which leads to the dip in the transmission spectra. On the other hand, light at other spectra locations (off-resonance) can pass through the patterned Si-NM Fano filter with its maximum transmission efficiency.

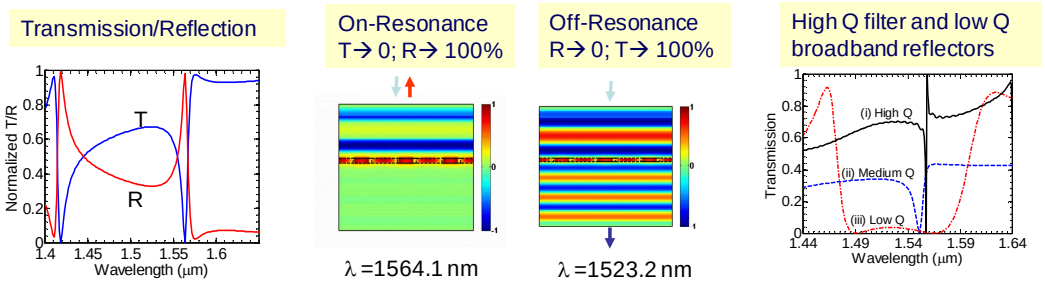

Figure 3-3 (a) Simulated transmission and reflection spectra for surface-normal Fano filters with different quality factors (Qs) (d) for either highly spectrally selective filters or broadband reflectors. Snapshots of electric field distribution of Fano filters under (b) on-resonance and (c) off-resonance conditions. [118]

It is shown that both narrow band filters and broadband reflectors can all be realized based on the design and the control of lattice parameters of PCs. Our results show that Fano resonance based silicon NM devices can be ultra compact and flexible (note that typically a lateral lattice period of 15a is sufficient to achieve compact, yet high performance photonic devices [95]). With further process optimizations, transferred NMs can find wider and practical applications in various electronic and photonic device and integration system applications [190-192]

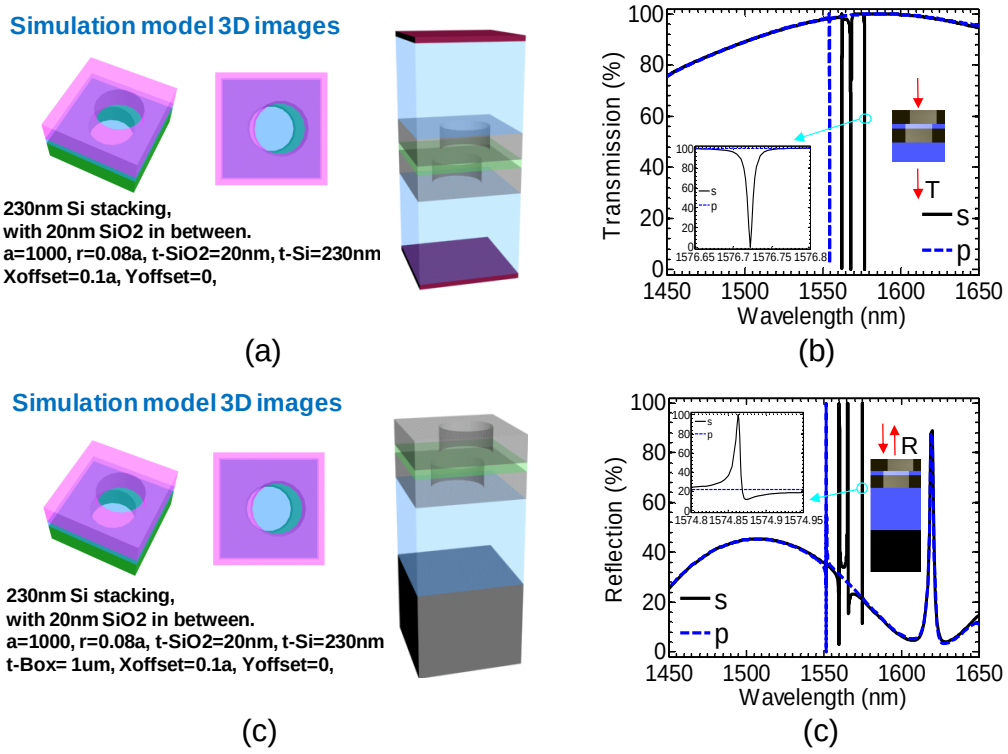

Figure 3-4 two example for simulation 3-D structures (a),(b) for surface normal transmission spectra and (c), (d) for surface normal reflection spectral. Refer to [10, 11, 193]

3.2.1 Single layer photonic crystal nanomembrane high-Q filters

Single-layer Fano resonance PhC filters were first patterned on silicon-on-insulator (SOI) substrates based on electron-beam lithography (EBL) and reactive-ion etching (RIE) processes. It was then transferred onto glass substrates using transfer printing process. [124] Shown in Fig. 3-5 (a) and (b) are scanning electron microscope (SEM) images of the fabricated single layer Fano filters on glass substrate. The single layer Fano filters were characterized with a tunable laser (1 pm tuning step) based setup for transmission measurement over wavelengths of 1490 nm to 1650 nm. The measured

(blue solid line) and simulated (red dash line) transmission spectra are shown in Fig. 3-5 (c), with zoom-in shown in Fig. 3-5 (d). Two transmission dips were found, at 1529.88 nm and 1564.62 nm. For the 1564.62 nm dip, the Q value of 1,737 was obtained, with 26 dB extinction ratio.

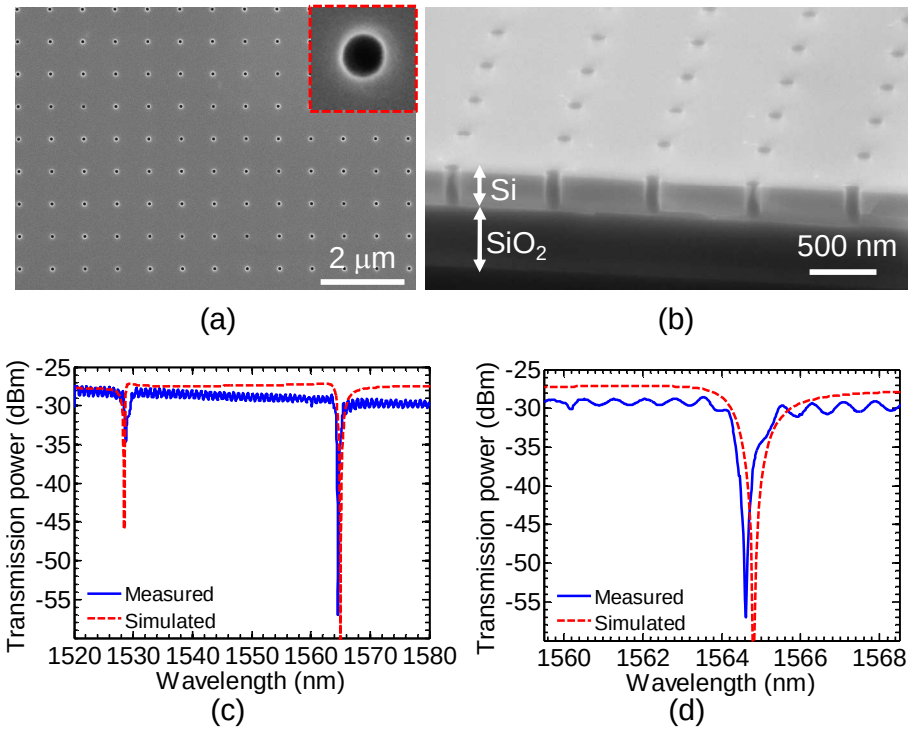

Figure 3-5 Experimental results for Design S1: (a) Top and (b) Cross-section views of fabricated single-layer PhC Fano resonance filters on oxide buffer; (c) Measured (blue solid line) and simulated (red dash line) transmission spectra for the fabricated single-layer PhC Fano resonance filter transferred on glass substrates; and (d) Zoom-in of (c) over the second dip (λ=1564.62 nm) region. [10]

In an optimized single layer Fano filter design, Quality factor Q of 4,500 can be achieved with r/a ratio of 0.08, as shown in Table 3-1, S3. For the lattice constant a of

780 nm (Case S3), the corresponding air hole radius r is 62.4 nm. Though even higher Q is expected with further reduction in r/a ratio, achieving air holes with radius much smaller than 60 nm is challenging in fabrication. And potential degradation of air hole quality with radius smaller than 60 nm will lead to significant reduction in filter Q. Experimentally, we have demonstrated single layer filters based on PDMS transfer printing of single crystalline Si PhC nanomembranes on transparent low index glass substrate. A Q factor of 1,727 was obtained with 26 dB extinction ratio, for Design S1 with r/a = 0.08 and a = 765 nm.

3.2.2.1 Coupled double-layer PC NM high-Q filters with aligned lattices.

In previous works, we reported Fano resonance filters on both glass and plastic substrate, employing polydimethylsiloxane (PDMS) transfer printing technique [7, 194-196]. However, single layer PhC Fano filters offer limited quality factor Q and limited dispersion engineering capabilities for fine-tuning the output spectrum. It was reported that much higher Q Fano filters can be realized by multi-layer PhC coupling and lattice offset control [136, 137]. Employing PDMS transfer printing technique [124, 197] and poly-crystalline-Si deposition processes [198, 199], we report here single and double-layer Fano filters on silicon and on quartz substrates, with symmetric spectral lineshapes and much higher Q factors of 98,000-10,000,000 by design. We experimentally demonstrated double-layer filters with Q factors of 22,000 by design and ~10,000 by measurement. These high Q filters, can have extraordinary potentials in integrated photonics, optical communications, and sensing applications.

Practically, we firstly proposed a double-layer PCSs stacking structures with a buffer low index oxide layer sandwiched between the two patterned Si nanomembranes. The incident light would be a surface normal collimated beam at near-infrared wave-

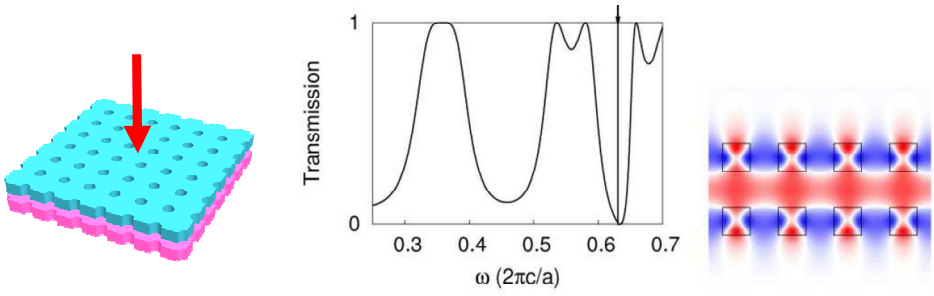

(a) (b)

Figure 3-6 Dark state arising from coupled bright resonances in coupled symmetric PCSs. [9]

length region, covering S, C and L band. By proper design and parameters optimizing, we can obtain high-Q filters operating at all bands. As has been discussed in the beginning, in this case, dark state can arise from coupled bright resonances in coupled symmetric PCSs and give extremely high-Q factor when applying a set of optimized simulation parameters. This proposed structure is highly desirable for high-Q factor and, at the same time, it is relatively simple for processing.

Shown in Fig. 3-7 are the schematics of double-layer Fano resonance PhC optical filters on low index glass substrates, where key lattice parameters are defined as air hole radius (r), lattice period (a), thicknesses for top (t1), bottom (t2) Si PhC layers and the oxide buffer layer (tb) in between. Both single- and double-layer Fano resonance Si PhC filters were designed and optimized for high Q around 1550 nm spectral band. The transmission spectrum and field plots were computed based on the Fourier Modal Method using a freely available Stanford Stratified Structure Solver (S4) software package [183]. Comparing the commercial RCWA package GD-Calc we used before [184], S4 software package offers much higher resolution due to the consideration of higher diffraction orders and also takes much less computation time.

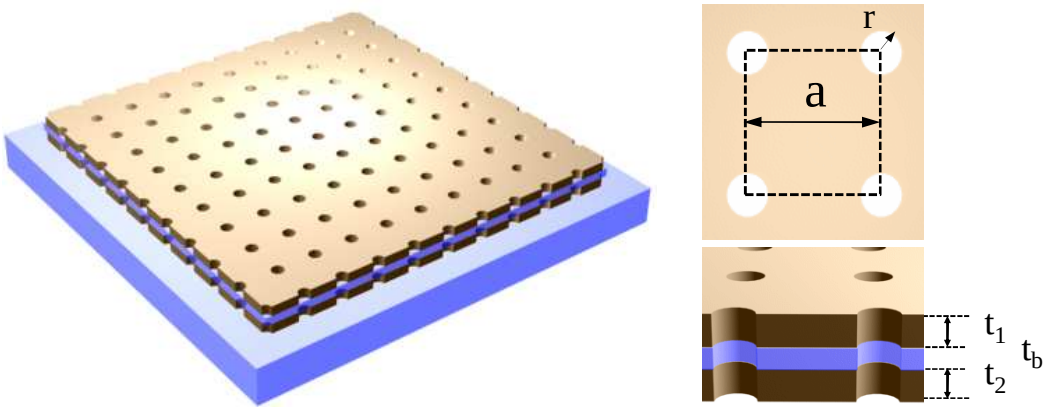

(a) (b)

Figure 3-7 Schematics of double-layer Fano resonance photonic crystal optical filters: (a) 3D sketch; and (b) Key parameters defined for the square lattice photonic crystal double layer.[10]

Shown in Table 3-1 are key design parameters for a few optimized design structures, where S1-S3 are for single-layer and D1-D3 are for double-layer designs.

Table 3-1 Key design parameters and Q's for selected single- (S1-S3) and double- (D1-D3) layer filters.[10]

	a	r/a	t_1	t_2	t_b	Q
Unit	nm		nm	nm	nm	
S_1	765	0.08	260	---	---	4,100
S_2	765	0.1	260	---	---	1,900
S_3	780	0.08	260	---	---	4,500
D_1	1000	0.2	230	230	160	$1.2x10^4$
D_2	1000	0.08	230	230	20	$2.2x10^4$
D_3	1000	0.05	230	230	20	$9.8x10^4$

It was clearly shown in the comparison of single and double-layer designs, much higher Q's can be achieved by coupled double-layer Fano resonance PhC structures. Liu and Fan et al [136] reported earlier that much higher Q can arise from the coupled dark states in the double-layer stacked PhC structures. We report here design and experimental demonstrations of coupled double-layer Fano resonance PhC filters. Some designs are summarized in Table 3-1, for cases D1 to D3. With the reduction in r/a value to 0.05, the filter Q increases to 98,000 which is one order of magnitude higher than the value in single-layer structure. Shown in Fig. 3-8 are the simulated transmission spectra for Designs S3 and D3, with Q of 4,500 and 98,000 respectively. Additionally, it was predicted that the double-layer PhC structure can excited extremely high Q mode (infinite in theory), by varying the coupling condition between two PhC layers. [136] Based on the Design D2 parameters, transmission spectra were simulated by varying the buffer layer oxide thickness tb.

For the double-layer structure, the simulated transmission spectra are plotted in Fig. 3-9 (a), with oxide buffer thicknesses range from 0 to 160 nm. With the increase of oxide buffer layer thicknesses, the high Q modes (shorter wavelength modes shown in Fig. 3-9 (a)) shift towards shorter wavelengths, with the filter Q value maximizes around 10,000,000 for buffer layer thickness tb = 60 nm, as shown in Fig. 3-9 (b). Shown in Fig. 3-9 (c) is the zoom-in spectral plot for the transmission dip with Q of 10,000,000. Simulated field distribution profiles for three cases close to the maximum Q are shown in Fig. 3-9 (d), where strong field confinement is evident for the high Q transmission dips at optimal buffer layer thickness.

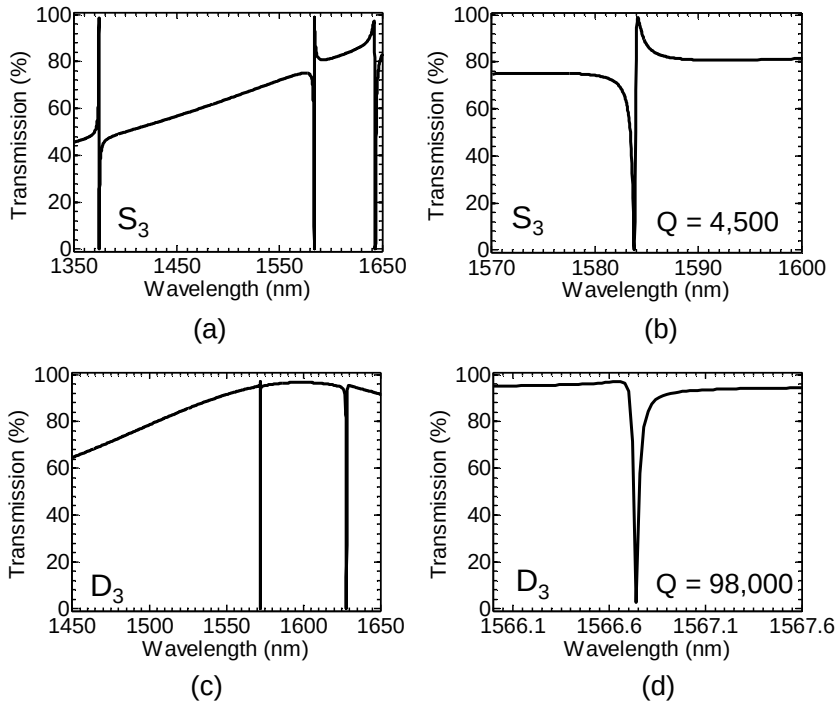

Figure 3-8 Simulated transmission spectra for (a,b) single- and (c,d) double-layer Fano resonance PhC filters, where (b) and (d) are zoom-in plots of (a) and (c), respectively. The design parameters are summarized in Table 1 for Case S3 and D3, respectively.[10]

Two types of structures were prepared for double-layer PhC Fano filters on silicon and on quartz substrates, respectively. For the double-layer PhC Fano filters on SOI, low index oxide buffer layer was first formed by thermal oxidation of single-crystalline Si layer on the SOI substrate, followed by low pressure chemical vapor deposition (LPCVD) poly-Si deposition process, to form a poly-Si/thermal SiO2/crystalline-Si double-Si-layer structure.

A single EBL pattern was used to etch through the complete poly-Si/SiO2/c-Si structure, with a combination of two RIE steps for two Si layer etching and a short buffer oxide etch (BOE) dip for SiO2 buffer layer etching. For better etching selectivity, e-beam

resist pattern was transferred onto a Cr metal layer to form a hard mask for the double-layer Si dry etching. Shown in Fig. 3-10 (a)-(c) are cross-sectional SEM images for double-layer poly-Si/SiO2/c-Si filter structure, with different thermal oxide thicknesses.

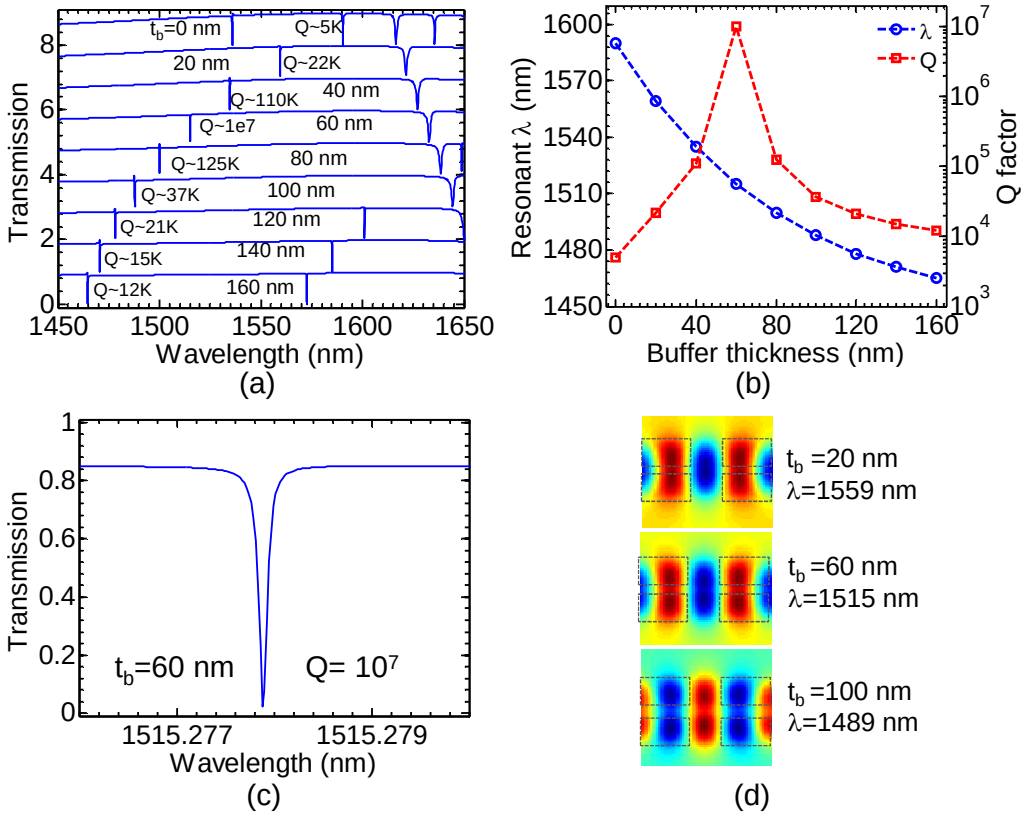

Figure 3-9 Simulation results for Design D2 with different buffer layer thicknesses tb: (a) Transmission spectra with different tb from 0 nm to 160 nm; (b) High Q resonant wavelengths and the corresponding Q values for different buffer thicknesses tb; (c) Zoom-in spectrum for the buffer thickness tb = 60 nm and filter Q of 10,000,000; and (d) Simulated E-field intensity profile at resonant wavelengths for three different tb values, where tb = 60 nm representing the highest Q condition for this design.[10]

The other double-layer PhC Fano filters on quartz substrates were formed by two steps of LPCVD poly-Si deposition process, with a plasma-enhanced chemical vapor deposited (PECVD) SiO2 layer sandwiched in between these two LPCVD poly-Si layers. The same E-beam patterning and etching processes were utilized for the 2D-PhC patterning. A SEM image is shown in Fig. 3-10 (d).

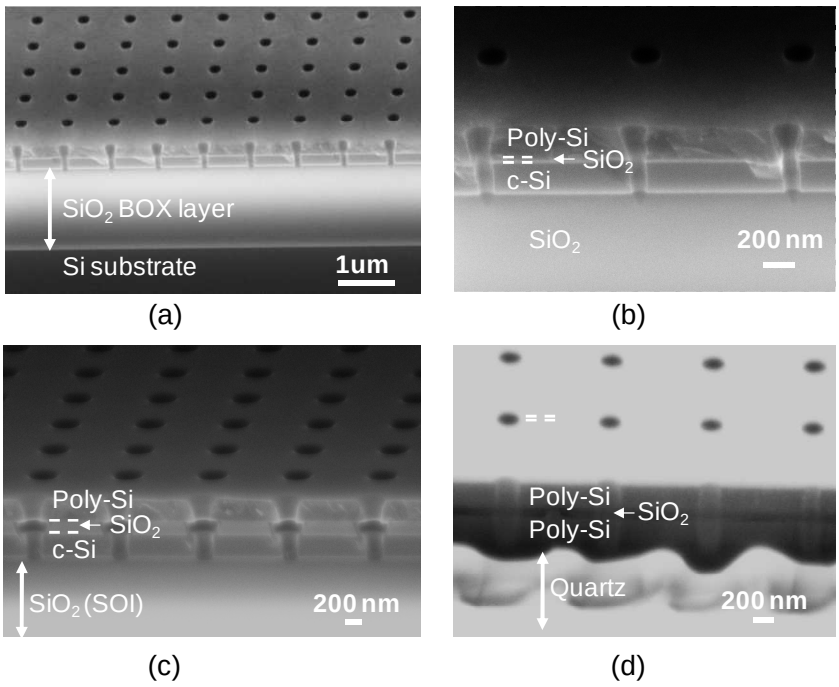

Figure 3-10 Cross-sectional SEM images for fabricated double-layer PhC Fano resonance filters based on Design D2 parameters: (a, b, c) Double-layer PhC structure was formed by poly-Si deposition on top of the SOI substrates; and (d) Double-layer PhC structure was formed by two steps of poly-Si deposition on quartz substrate. Notice the oxide buffer thicknesses are 20 nm, 160 nm, and 20 nm, for cases (b), (c), and (d), respectively. [10]

The double-layer Fano filters were characterized by measuring transmission or reflection spectra for the two different configurations respectively. For the transmission measurement on a double-layer filter quartz substrate, a transmission dip at 1545.2 nm was obtained, with an estimated Q of 5,000 and 2.7dB extinction ratio (Fig. 3-11 (a) and (b)). For the reflection measurement on a double-layer filter on SOI substrate, a reflection peak was obtained at 1567 nm with Q factor of 9,734 and an 8dB extinction ratio (Fig. 3-11 (c) and (d)).

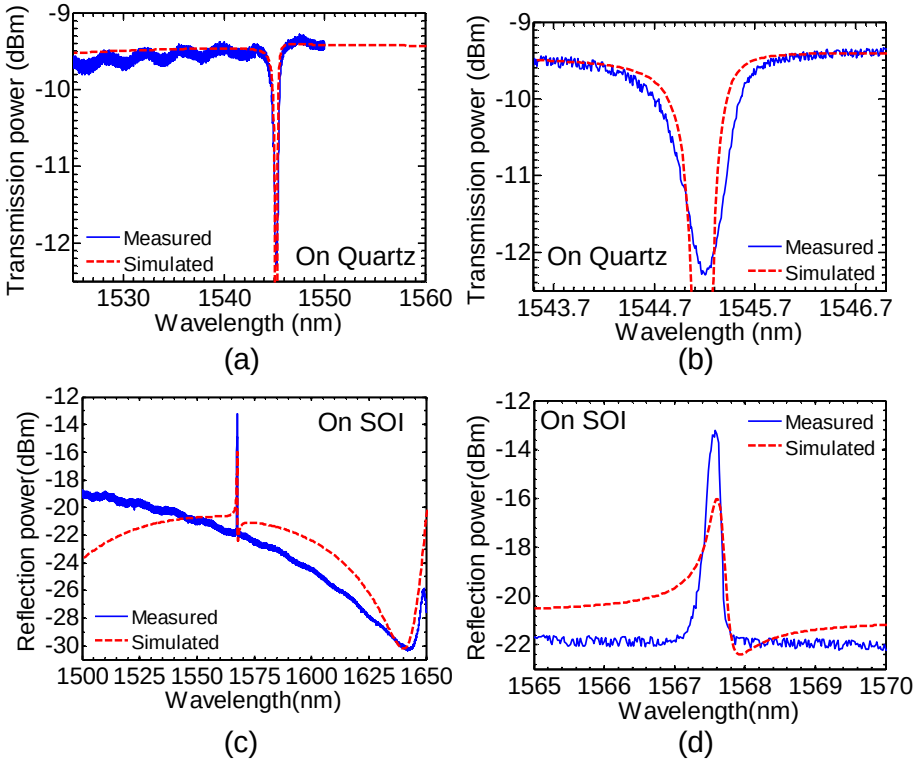

Figure 3-11 (a, b) Measured (blue solid line) and simulated (red dash line) transmission spectra for the double-layer PhC Fano resonance filters on quartz; and (c, d) Measured (blue solid line) and simulated (red dash line) reflection spectra for the

double-layer PhC Fano resonance filters on SOI. (b), (d) are zoom-in's of (a), (c), respectively. [10]

All these measured spectra match well with the simulated ones at these resonance locations (wit spectral dips or peaks). Measured Q values are less than the designed ones, which may come from the imperfect etching process of air holes, such as the conical shape and different hole sizes in this trilayer structure. We expect the filter performance can be improved with much higher Q factors by optimizing the fabrication process.

In conclusion, high Q surface-normal Fano resonance filters were designed and demonstrated experimentally based on single and double-layer PhC structures. Higher Q filters can be obtained in double-layer PhC structures, with optimized Q of 22,000 by design and experimentally demonstrated Q close to 10,000. With fining tuning of double layer buffer layer thicknesses, it is possible to obtained extremely high Q (10,000,000 or higher) from the coupled dark state resonances [136].

3.2.2.2 Coupled double-layer PC NM high-Q filters with lattice displacement

In recent years, great interests have been attracted to single layer ultra-compact surface-normal nanostructure optical filters and reflectors[6-8, 38, 138, 139, 150, 200, 201] mostly based on one-dimensional high contrast gratings (1D HCGs) [38, 95] and two-dimensional photonic crystal slabs (2D PCSs) [8, 150, 200, 202]. Owing to the phase matching provide by in-plane periodic index modulation, the out-of-the-plane optical mode coupling is feasible with the Fano or guided mode resonance (GMR) effect,[1, 6, 36, 138] where these in-plane discrete guided resonances above the lightline are also strongly coupled to the out-of-the-plane continuum radiation modes[139]. Similar to Fano resonances in other types of nanoscale structures, extremely high quality factor (Q)

optical filters can be obtained in these structures with asymmetric resonance lineshapes and extremely sharp transition between transmission peak and dip. [1] Optical filters based on single layer 2D PCSs have been investigated extensively [41-43, 137, 139].

We reported earlier single layer Fano resonance filters fabricated on SOI (silicon on insulator), as well on glass and flexible plastic substrates, employing polydimethylsiloxane (PDMS) transfer printing technique[7, 194-196]. However, single layer PCS Fano filters offer limited Q factor and limited dispersion engineering capabilities for fine-tuning the output spectrum. Coupled bi-layer PCS structures, on the other hand, were proposed and reported to have much high Q factors, and strong optomechanical forces[142, 203]. Suh et al. and Liu et al. reported earlier the optical Q-factors and the optomechanical interactions can be controlled by precisely tuning the gap and the lattice displacement between two coupled PCS[136, 137]. Under theoretical considerations, infinite Q factors can be achieved in the dark states arising from coupled bright or dark resonances in symmetric or asymmetric coupled bi-layer PCSs, respectively[136]. With single step e-beam lithography patterning process, coupled bi-layer PCS structures have been experimentally demonstrated in InP material systems, with strong optomechanical interactions and modest Q factors (~1600) [204]. We also reported coupled double-layer Fano resonance PCS filters with experimentally demonstrated Q factor of 9,734 and extinction ratio of 8 dB, for a filter design with target Q of 22,000. [205] However, experimental demonstration of coupled double-layer PCS structures with controlled lattice displacement has not been reported, due to the challenges associated with the fabrication.

Spectral high-Q factors predicted in such an asymmetric system with dark state arising from dark resonance in the coupled asymmetric PCSs [9] was illustrated in the following Fig. 3-12.

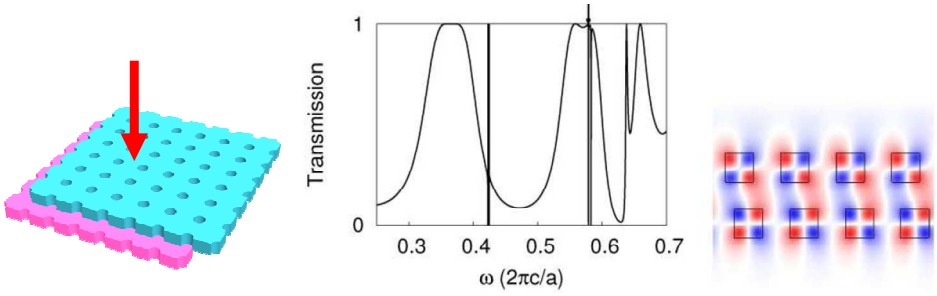

(a) (b)

Figure 3-12 Dark state arising from coupled dark resonances in coupled asymmetric PCSs.[9]

Employing PDMS nanomembrane transfer printing technique, it is possible to stack multi-layers of semiconductor and other dielectric materials. [8, 206] We report here the design and first experimental demonstration of coupled double-layer PCS with precisely controlled lattice displacement, based on transfer printing and multi-layer e-beam patterning alignment processes. [206, 207] Both simulation and measurement suggest optical filter Q-factors are very sensitive the lattice displacement. For one structure with relatively large lattice displacement, we demonstrated Q factor of 80,000 experimentally. Further design and process optimization give us an expectation of much higher Q-factors with simulation Q factor of 2.11×10^8 for coupled double-PCS structures with optimal lattice displacement.

The optical filter is shown schematically in Fig. 3-13, where two single layer PCSs (with thicknesses t1 and t2) are stacked with controlled lattice displacement (Δx, Δy). An ultra-thin low index oxide buffer layer (with thicknesses tb) is sandwiched in between, serving as the field coupling tuning layer. Square lattice PCS structure was considered here with air hole radius (r) and lattice period (a). The filter transmission and

reflection spectra were computed using the Fourier Modal Method using a freely available Stanford Stratified Structure Solver (S4) software package. [183]

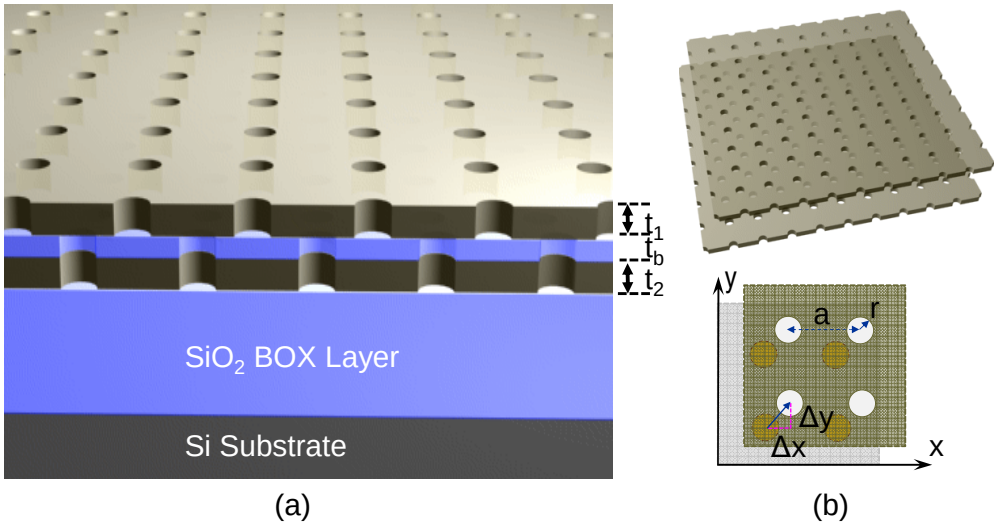

Figure 3-13 (a, b) Schematics of Fano resonance filters based on PDMS transfer printed coupled double layer photonic crystal slab (nanomembrane) on silicon substrate (a) 3D close-up view with lattice displacement and thin oxide buffer layer (tb) sandwiched in between two single layer crystalline silicon PC layers (t1 and t2); and (b) Illustration and definition of key design parameters, including lattice constant (a), air hole radius (r), and lattice displacement (Δx, Δy) between two layers. [11]

Shown in Fig. 3-14 are simulated transmission and reflection spectra for double layer stacked Fano filters without (Fig. 3-14 (a, c)) and with (Fig. 3-14 (b, d)) lattice offset (Δx = 0.2a, Δy = 0.5a), with the insets shown the zoom-in plot for the dominant (highest Q) resonance for each case. Also shown in the insets are the schematics of the structures considered in the simulation. For the transmission spectra shown in (Fig. 3-14

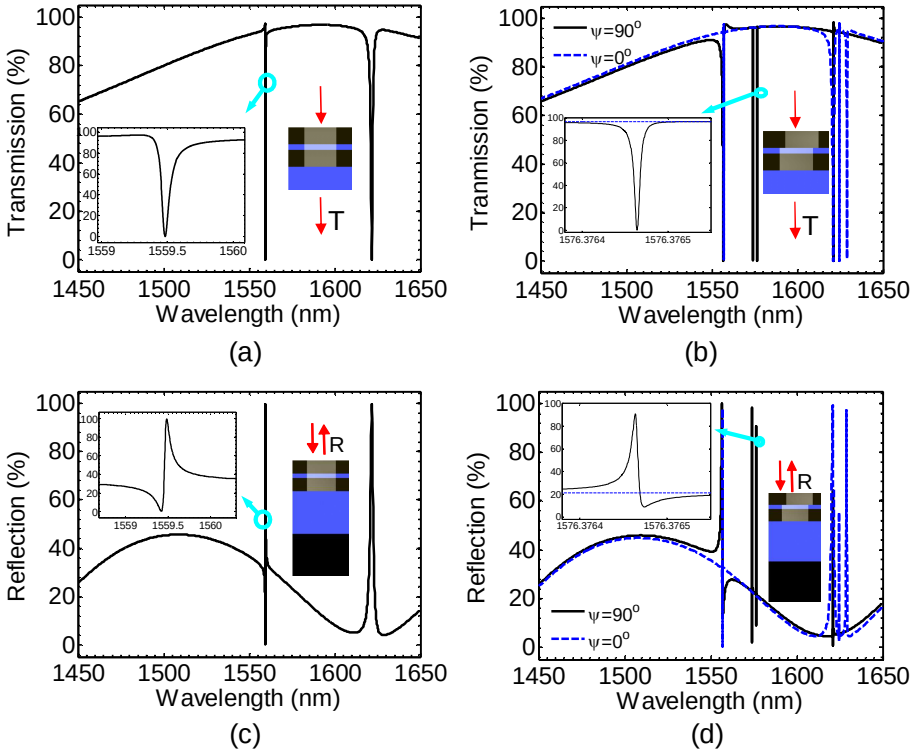

Figure 3-14 Simulated transmission and reflection spectra for double layer stacked Fano filters (a, c) without and (b, d) with lattice offset (Δx = 0.2a, Δy = 0.5a), with the insets shown the zoom-in plot for the dominant (high Qs) resonance for each cases. Also shown in the insets are the schematics of the structures considered in the simulation. For the transmission spectra shown in (a, b), glass substrate was considered. For the reflection spectra shown in (c, d), SOI substrate was considered. [11]

(a, b)), glass substrate was considered. For the reflection spectra shown in (Fig. 3-14 (c, d)), SOI substrate was considered. The design parameters are a = 1000 nm, r/a = 0.08, t1 = t2 = 230 nm, tb = 20 nm. Simulations were carried out to find the Q factors for different lattice displacements. The results shown in Fig. 3-14 (b, d) correspond to the highest Q value obtained for this set of design parameters. Notice that Fano filter Q

increases from 26,000 and 28,000 for lattice perfectly aligned structures (Fig. 3-14 (a, c)) to 2.11x108 and 1.76x108 for lattice misaligned structures (Fig. 3-14 (b, d)), respectively, with optimal lattice displacement of Δx = 0.2a and Δy = 0.5a. It is also worth mentioning that the low index buffer layer (e.g. SiO2 used here) thickness can also be varied for with Q-factors approaching infinite. [136, 205]

For the double-layer surface normal high-Q filters with lattice offsets, we started our examination from fixed lattice period and thicknesses.

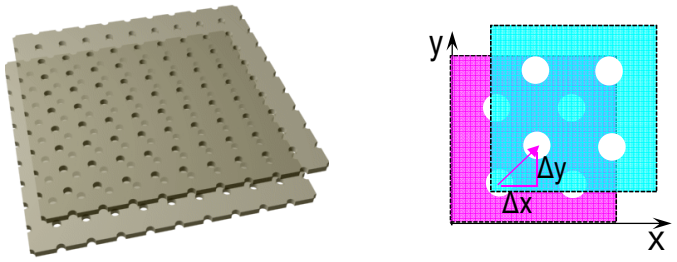

(a) (b)

Figure 3-15 (a) 3D sketch of double-layer Si-NMs with lattice offset. (b) Definition of Δx and Δy offsets along both X and Y directions.

Simulation contour mapping of the calculated Q factors were compared when applying large, medium and small hole sizes, as shown in Fig. 3-16 from r = 0.4a to r = 0.2a and r = 0.08a. Results shows that the high Q factors one can obtain from these structures are from 5,000 to 14,000 and 211,000,000 respectively.

Though the simulation frequency scanning resolution and offsets XY-mapping definition might not be able to show us the highest Q that one can expect from these structures, the direct proof has been given that --- from this comparison, a smaller hole in design is preferred for achieving relatively higher Q factors.

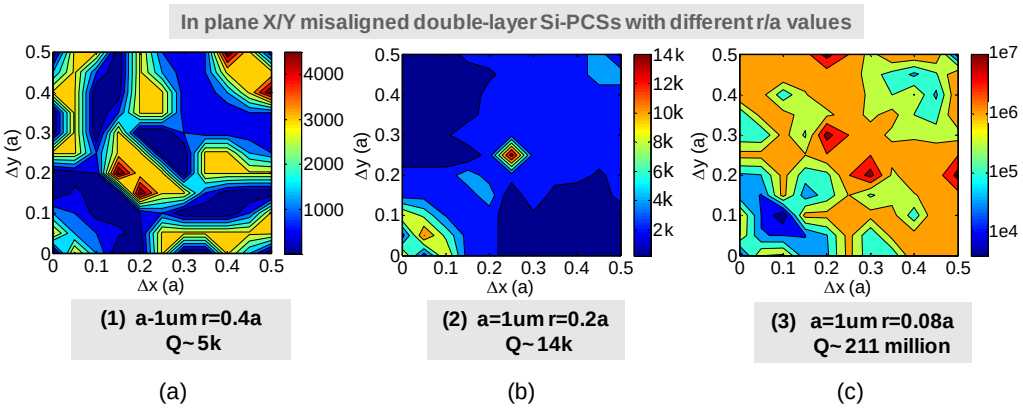

Figure 3-16 Q mapping contour for different offsets along both X and Y directions,three holes sizes examined: t1 = t2 = 230nm, tb = 20nm, a=1um. Simulation tool: V. Liu and S. Fan, "S4: A free electromagnetic solver for layered periodic structures," Computer Physics Communications 183, 2233-2244 (2012). [11]

Thin oxide buffer layer (tb = 20 nm in this case) was first formed by thermal oxidation of single crystalline Si layer on a SOI substrate, followed by definition of Cr/Au global alignment marks based on e-beam lithography (EBL) and metal lift-off processes. Bottom PCS structure was then formed by 2nd EBL patterning, aligned to the Cr/Au global marks, and reactive-ion etching (RIE) dry etching processes. A piece of single crystalline Si nanomembrane (1 mm × 2 mm size) was released from another unpatterned SOI substrate, and stacked onto the patterned bottom PCS SOI substrate with PDMS transfer printing process [57, 208]. A 3rd EBL step was used for the patterning of top PCS layer, aligned to the same global marks. With the control of the pattern location, precise control of lattice displacement can be achieved between top and bottom PCS layers.

Shown in Fig. 3-18 are scanning electron microscope (SEM) images of fabricated double layer PCS Fano filters with displaced lattices between coupled PCS layers. The

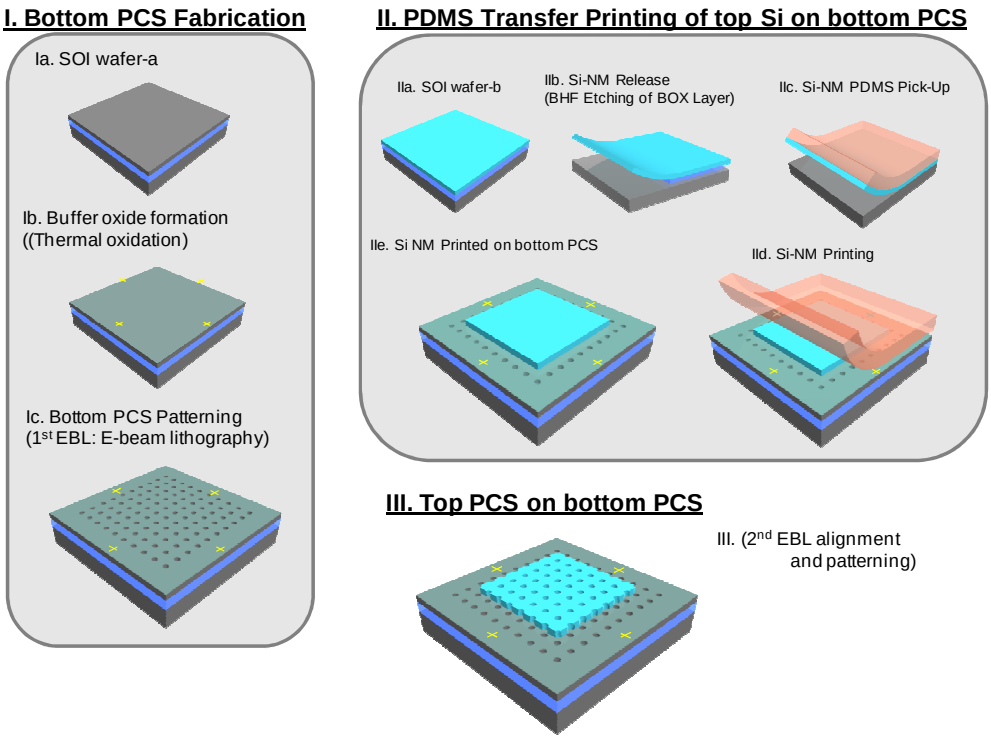

Figure 3-17 Process flow for this double-layer high-Q filters with lattice offsets: Transfer Printing and EBL Alignment. [11]

cut-out cross-sectional view SEM image shown in Fig. 3-18 (c) was prepared with focused ion beam (FIB) technique. Clearly, coupled double-layer PCS structures with oxide buffer were realized with precisely controlled lattice displacement ($\Delta x = 0.2a$, $\Delta y = 0$). Also shown in the inset of Fig. 3-18 (a) is a microscope image of coupled double layer PCS optical filters with six patterned device structures (bottom squares) and patterned top PCS structures on a piece of transferred crystalline Si nanomembrane.

Samples with different buffer oxide thickness may show different colors under microscope with same illumination intensity. Large Si-NM with 1mm to 2 mm sizes were

transferred onto the previously patterned SOI. All the different offsets can be achieved by e-beam writing at one time by program controlling the top Si-NM patterning positions, with the same patterning sizes of 400 µm x 400 µm as the previous patterns on SOI.

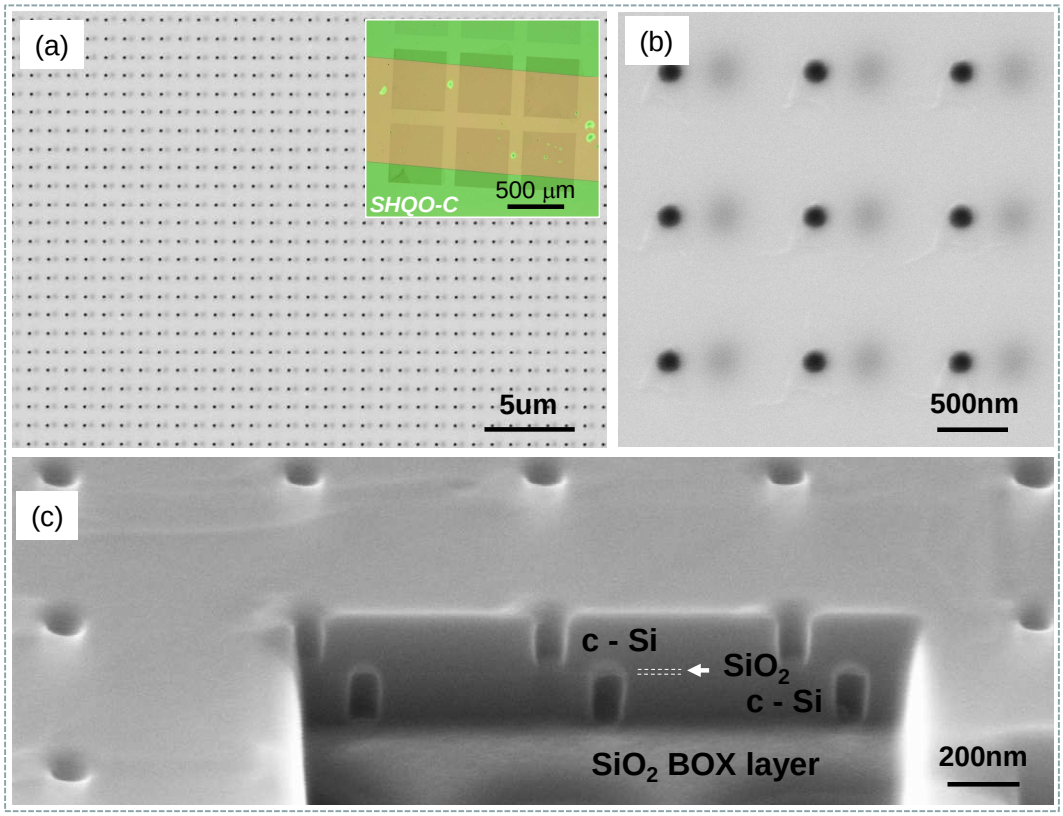

Figure 3-18 Fabricated Fano filter scanning electron micrograph (SEM) images: (a) top view; (b) zoom-in top view; and (c) cross-sectional view of double layer Fano filter on SOI, with controlled lattice misalignment offset ($\Delta x = 0.2a$, $\Delta y = 0$). Show in the inset of (a) is a micrograph showing multiple device structures with top and bottom PhC pattern areas. [11]

The Fano filters are characterized by measuring the reflection spectra with an Agilent tunable laser system with 1pm resolution and 9dBm output power. The incident

beam goes through an optical circulator, a laser beam collimator, an optical lens, a linear polarizer and a beam splitter.

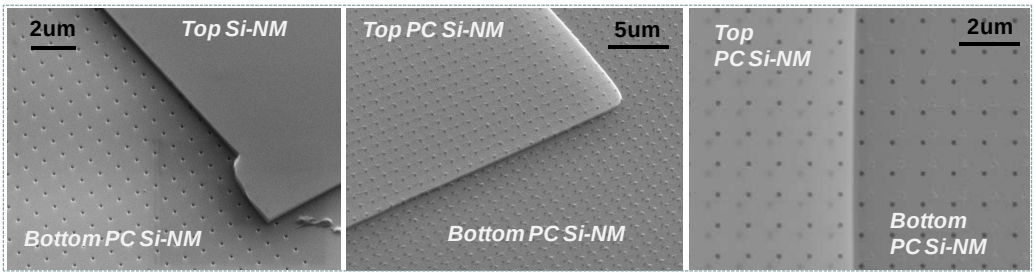

(a) (b) (c)

Figure 3-19 Top and angled views of stacked double layer PC Si-NM. [11]

Two identical results are shown in Fig. 3-23 (a, b) and Fig. 3-23 (c, d) for two cases with relatively small and large lattice displacements, respectively. For the small lattice displacement case shown in Fig. 3-23, the lattice offsets are $\Delta x = 0.045a$ and $\Delta y = 0.015a$, obtained based on the estimate from the top view SEM image shown in the inset of Fig. 3-23(a).

Measured resonance was also simulated based on S4 package and fitted with Fano resonance formula. The results are shown in Fig. 3-23(b) for the zoom-in plot of the dominant resonance at 1549 nm. The results agree very well. The fitted Q factor is 11,500 with an extinction ratio (ER) of 5.5 dB. The other peak at 1569 nm shown in Fig. 3-23(a) is less profound and we did not consider this one here. This case is very similar to the results we reported earlier, for coupled double-layer PCS filters without lattice displacement. [205]

Since the optical Q factors are very sensitive to the lattice displacement, we expect much higher Q factors can be obtained for different set of lattice displacement.

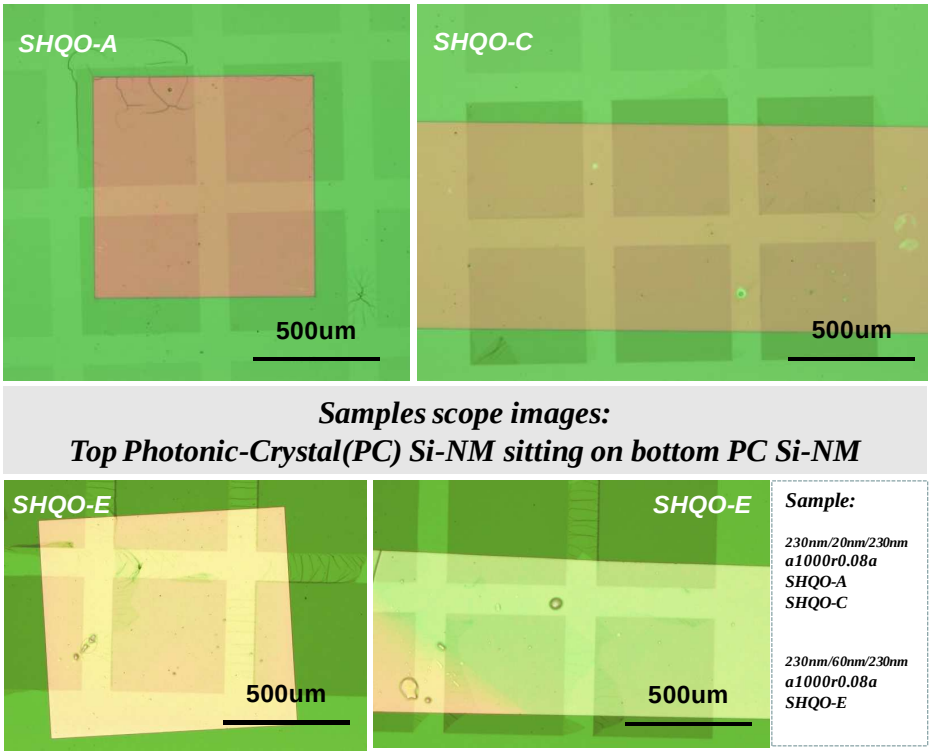

Figure 3-20 Double-layer high-Q devices with different lattice offsets and oxide buffer layer thicknesses. [11]

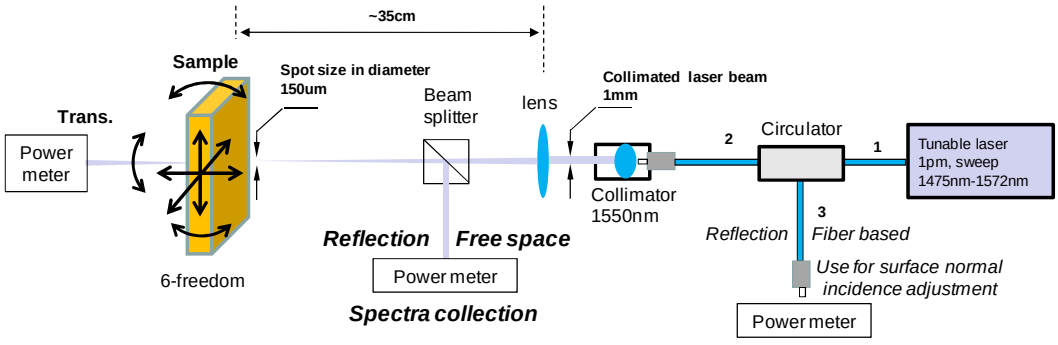

Figure 3-21 The high-Q testing setup sketch.[11]

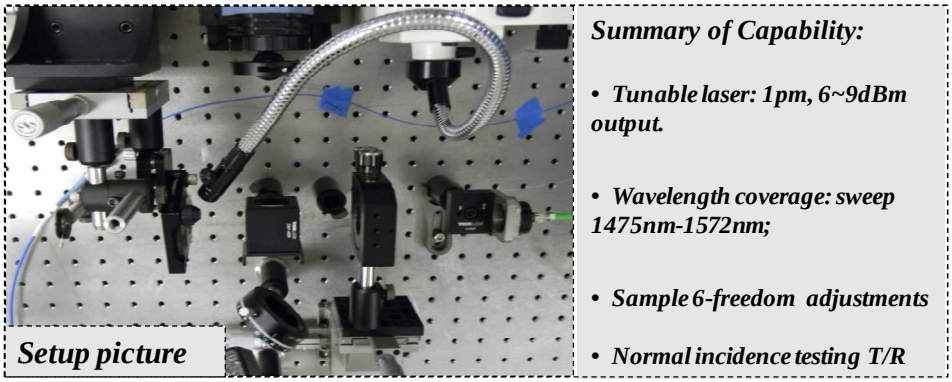

Figure 3-22 The high-Q testing setup picture. [11]

Shown in Fig. 3-23 (c) is the results obtained for the coupled double layer PCSs, with large lattice displacement (Δx = 0.495a, Δy = 0.45a). Measured reflection spectrum is shown in Fig. 3-23 (c), along with top SEM image shown in the inset. We obtained two resonant locations, around 1548.6 nm and 1567 nm, with zoom-in plot around 1548.6 nm resonant shown in Fig. 3-23 (d).

Again, simulation and Fano fit were carried out and the results match well with the measured one. In this case, we obtained Q factor of 80,000 and ER of 4.2 dB. This value is highest experimental Q factors reported so far, for all different cases we fabricated. While the value is still far from the optimal Q factor of 2.11x108, the results demonstrate great potential of coupled double-layer PCS structures with controlled lattice displacement. During testing, we also noticed that the performance of these filters is very sensitive to incident beam direction, collimation and polarization orientation. We anticipate much higher Q-factors can be obtained with precisely controlled displacement and optimized fabrication process.

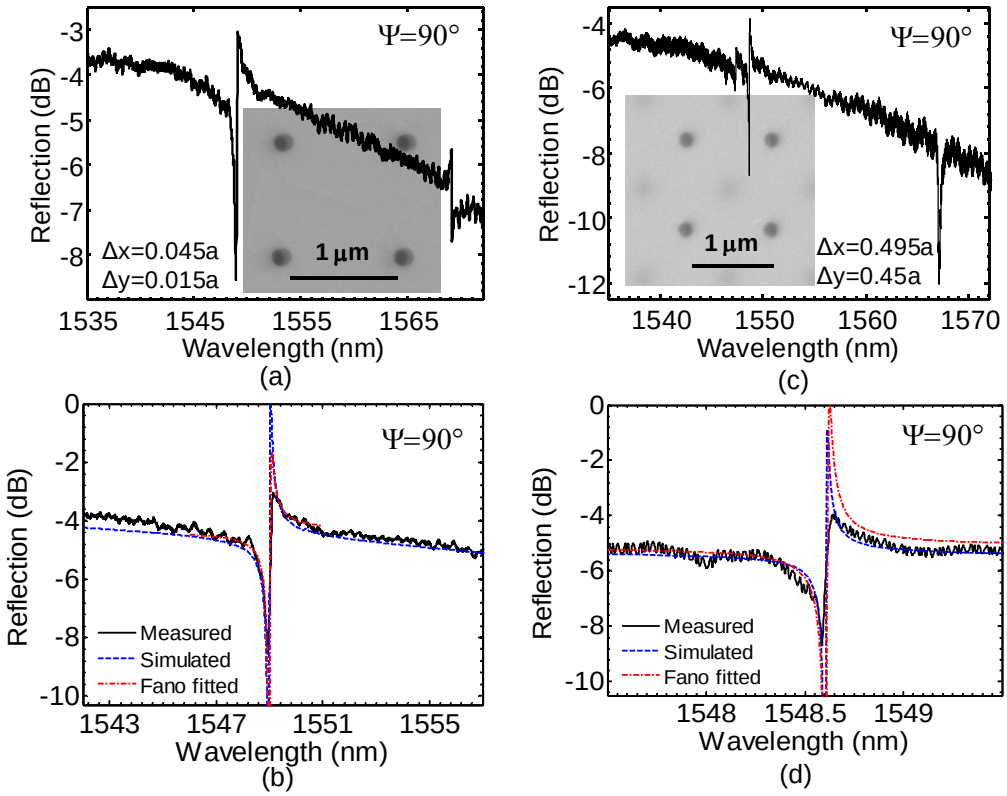

Figure 3-23 Measured reflection spectra for a displaced Fano filter with very small offset (Δx = 0.045a, Δy = 0.015a), with a top view SEM image shown in the inset; and (b) Zoom-in plots around the dominant resonance with measured, simulated, and Fano fitted reflection spectra. (c) Measured reflection spectra for a displaced Fano filter with large offset (Δx = 0.495a, Δy = 0.45a), with a top view SEM image shown in the inset; and (d) Zoom-in plots around the dominant resonance with measured, simulated, and Fano fitted reflection spectra. [11]

In conclusion, coupled double-layer PCS Fano resonance filters with controlled lattice displacement have been investigated theoretically and experimentally, based on PDMS transfer printing technique, and aligned EBL pattern processes. Theoretically, optical filter Q factors can approach 2.11×10^8 or even higher. Experimentally Q factors of

11,500 to 80,000 have been demonstrated. The results suggest this type of coupled bi-layer PCS structure can offer a platform for high Q optical filters, as well as platforms for optomechanics, reconfigurable optics, integrated photonics, and sensing systems.

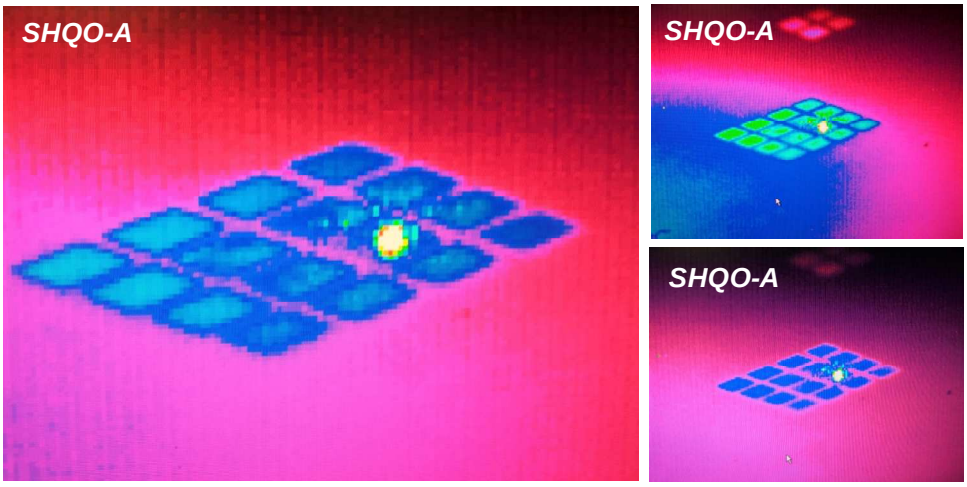

Figure 3-24 IR- camera capturing a double-layer high-Q device under test. (SHQO-A offset X=0.495a; Y=0.45a). [11]

Polarization tests were carried out use the same setup with linear polarized laser beam incidence on sample SHQO-A-P4. Due to the asymmetric of the lattice displaced double-layer structures, we may make the conclusion that they are incidence polarization sensitive devices.

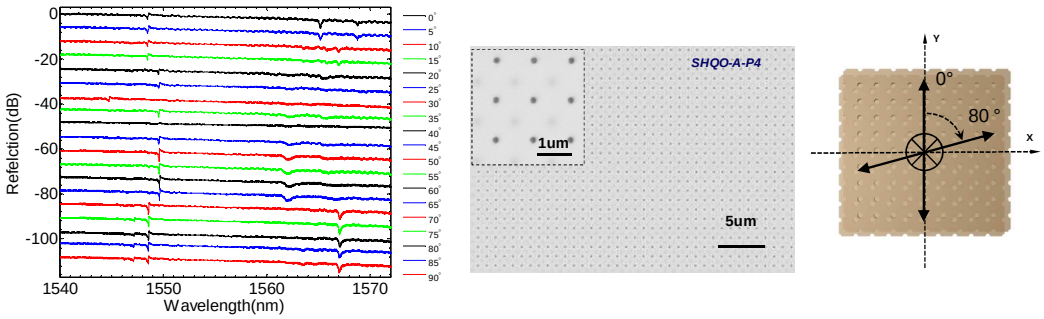

(a) (b) (c)

Figure 3-25 Polarization tests. (SHQO-A offset ΔX=0.495a; ΔY=0.45a) [11]

Chapter 4

Photonic Crystal Membrane Modulators

4.1 Photonic crystal membrane based Electro-Optical (EO) modulator design and simulations.

If agreement can be made that silicon photonics is the leading candidate technology of optical interconnect, then the workhorse of such a interconnect is the optical modulator. [209] The development of silicon optical modulators has clearly gone through a period of rapid improvement over the past 10 years. It ideally need to have high modulation speeds, large bandwidths and small footprints, as well as low loss, ultralow power consumption and compatibility with the world's most successful technology for producing electronics, CMOS. To achieve an optimal trade-off among these requirements is still significant challenging since these requirements often contradict each other when one try to obtain the performance metrics' practical limit. Significant amount of attention is currently focused on research into optical interconnect technology, simply because it is urgently required in many applications. It enables the separation of electronic devices, and thus allows optimization of the chip layout while retaining high data rates, introduces chances of reduction of electromagnetic interference, cable length and cable weight. It can also save energy, retain precise clock and signal timing, and allow interconnect densities to be reduced.

Modulators are used to modulate a light beam propagating either in free space or in an optical waveguide. It can be also classified as either electro-refractive or electro-absorptive. The primary electric field effects that are traditionally useful in semiconductor materials for causing either electro-absorption or electro-refraction are the Pockels effect, the Kerr effect and the Franz–Keldysh effect. However, it has been shown that these

effects are weak in pure silicon at the telecommunications wavelengths of 1.3 μm and 1.55 μm. [210] Thermo-optic coefficient of silicon is large, but the speed is too slow [211] Though poled polymers can have electro-optic coefficients ranging from moderate r33 = 10pm/V [212, 213] to extremely high values of r33 = 170 pm/V [213, 214], thus enabling operation with low drive voltage, the most common method of achieving modulation in silicon devices so far has been to exploit the plasma dispersion effect, in which the concentration of free charges in silicon changes the real and imaginary parts of the refractive index. The evaluation have been given [210].

Being widely used in communication systems, electro-optical (EO) modulator as an important member of the optical communication devices family has been well investigated and developed. Listed here three general structures that have been utilized, such as the classic MZI structure, high resonance rings structure [215,216], FP cavity [217,218] or the combinations of between them. Examples have been shown separately in Fig. 4-1 (a), (b) and (c).

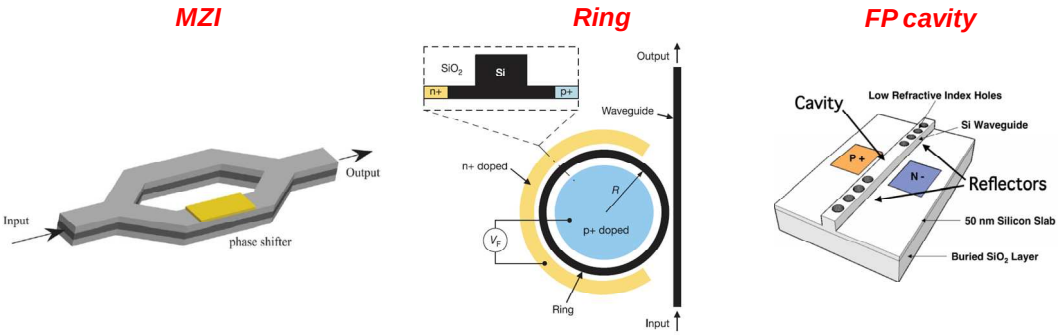

(a) (b) (c)

Figure 4-1 A general optical structures (in plane and relative larger size) (a) Classic MZI modulators (b) Micro scale ring resonator for EO modulation [215] and (c) FP cavity structure [218].

As the state-of-the-art devices, EO modulators have been exploited using different approaches. Carrier injection [219-238], accumulation [239-242] or depletion [242-249] were utilized to modulate the Si refractive index, shown in Fig. 4-1 (b), (c) and (d). Attempts have also been made to investigate other materials potentially compatible with silicon technology, such as Ge and SiGe, to achieve efficient modulation. Two related effects --- Franz-Keldysh effect [250] and the quantum-confined Stark effect(QCSE) [251] were considered to induce changes in optical absorption for optical modulation. Notice the free carrier accumulation modulation can work not only in a PN junction but also possible in a capacitor like double-layer structures with an electrical isolation layer in between. [246, 252]

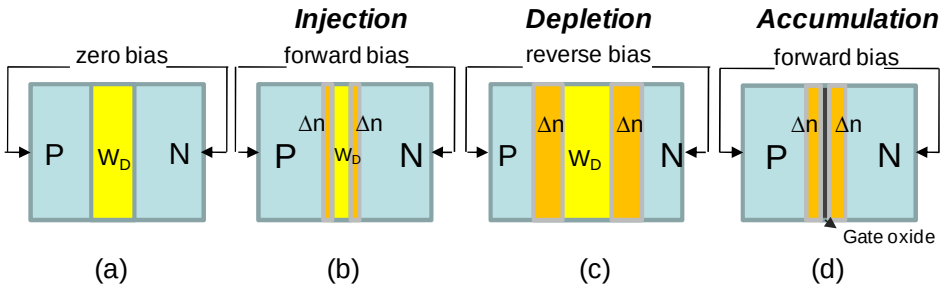

Figure 4-2 Electrical modulation mechanism in Si EO modulators: (a) Si PN junction without bias (b) carrier injection, when the PN junction have a forward bias. (c) carrier depletion, when reserse biased. (d) carrier accumulation with a forward bias in a PN junction.

We proposed here a single layer PCS Fano resonance novel modulator device, which can modulate the light with normal incidence. The desired design parameters was target at near 1.5 μm communication wavelength band. The single layer patterned Si-NM

can be transferred on to transparent foreign substrate such as glass or flexible PET substrate. A 3-D sketch was given in Fig. 4-3 below.

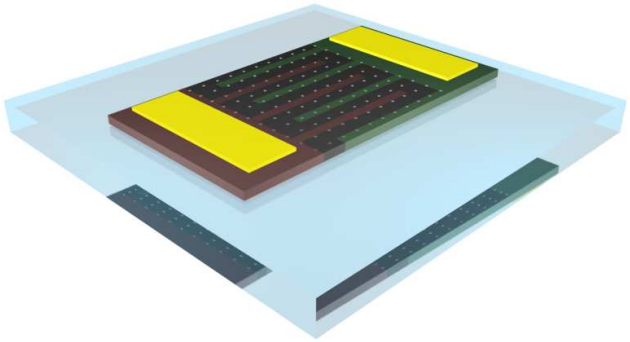

Figure 4-3 PC based surface normal Fano resonance modulator: single layer PC device sitting on glass substrate.

The basic design parameters were shown in the following Table 4-1. For the finger-print lateral junction design, we consider different PIN region width as from 2 μm to 4 μm. Total thickness of the Si-NM is desired as 260nm for one ideal optical thickness for 1550nm optical resonance application.

Photonic crystal 2D holes array was patterned with scanned periods “a” from 0.765 μm to 0.78 μm and radius of “r = 0.08a”. Si-NM on an infinite thickness glass substrate was assumed in simulation.

We simulated the device electrical and optical responses when applying 1volt forward bias. The Fig. 4-4 show the simulation results for electrical properties by Medicii [253] and correspond optical spectral of bias and no bias case in Fig. 4-5.

Table 4-1 PC based surface normal Fano resonance modulator design parameters, including lattice parameters and thickness of Si-NM. PIN region widths were given as shown in table from 2 µm to 4 µm. Different refractive index were used for doped and undoped Si.

Layer	Material	Refractive index n_{eff} / Width w(µm)						Total thickness t_{total} (nm)	PhC period a (µm)	Hole radius r(a)
		P+ region		I region		N^+ region				
2	Silicon	3.48	2~4	3.46	2~4	3.48	2~4	**260**	**0.765-0.78**	**0.08**
1	SiO_2	1.48						Infinite		

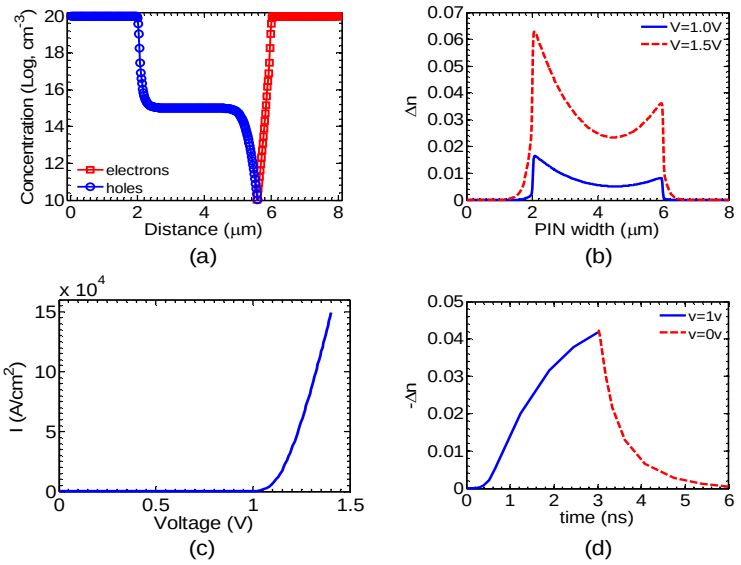

Figure 4-4 Simulation of the electrical property. (a) Free carrier concentration distribution along the direction that across the fingers. (b) Free carrier concentration change when applied an electrical injection with 1 volt and 1.5 volts. (c) I-V property simulated by Medicii. [253] (d) Free carrier concentration change inside the "undoped Si" I region in time-domain when apply 1 volt forward bias.

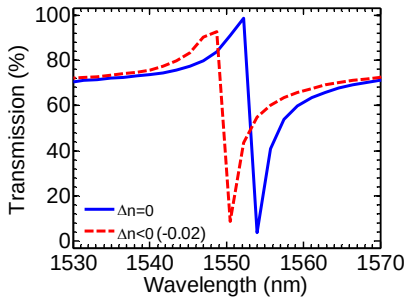

Figure 4-5 Simulation of optical surface normal transmission property when applying the 1 volt forward bias.

4.2.1 Single layer photonic crystal spatial modulators

We introduce a unique membrane modulator device which based on Photonic-crystal Fano Resonance. Transmission of certain wavelength can be modulated by membrane material effective refractive index change, which due to electrical carrier injection. A finger-print PIN lateral junction within Photonic-crystal Si nanomembrane is demonstrated, by PDMS transferring the nanomembrane device on glass, it promised a surface normal transmission light modulation. Such photonic-crystal Fano resonance based crystalline semiconductor nanomembrane spatial modulators, which are transferrable, stackable and bondable, propose divertive opportunities for silicon photonic integration and ultra-compacted high speed communication system.

Fig. 4-8 is scope view of the PIN lateral junction by two time implantations with AZ5214 photo-resist as masks. Red and green colors areas turns to be the P and N implanted surface on the Si–NM. Notice the color contract becomes much lower after dopants activation, which requires 980C for several minutes of the RTA process. PC patterns have been pre-patterned but not able to be seen because of that the hole size is as small as 100nm in diameter and the scope views are in relative low magnifications.

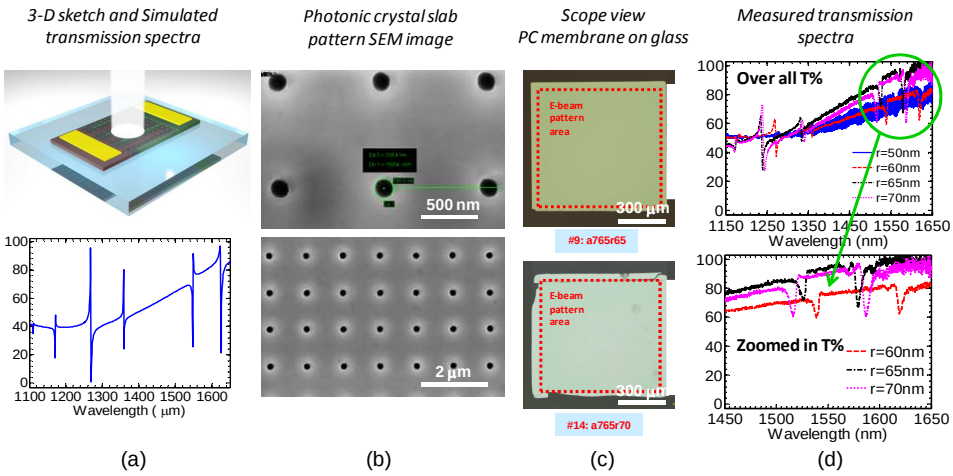

Figure 4-6 Patterned Si nanomembrane transferred on glass: (a) 3D-image for the device under transmission testing using white light source. (b) SEM top view of square lattice holes array patterning on SOI. (c) Patterned Si nanomembrane single layer PCS high-Q devices transferred on glass slides. (d) Transmission dip testing results at 1550nm region were measured by white-light source (beam focused by a 4X objective lens with NA 0.1) and the OSA testing setup.

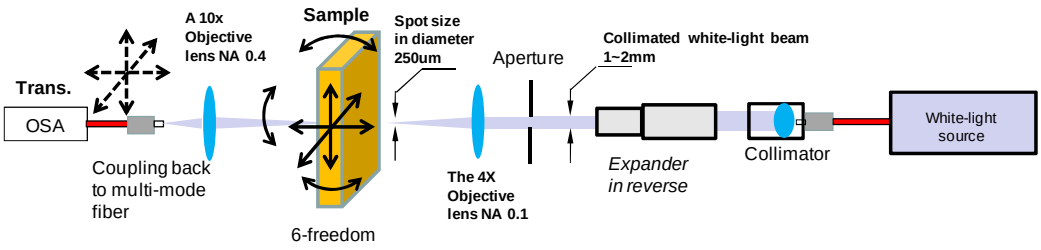

Figure 4-7 A basic optical testing setup sketch: white-light source coverage of 800nm to 1650nm. Fiber and free space coupling for the transmission tests or reflection tests (by inserting a beam splitter between aperture and the 4X objective lens and collecting light in the same way as transmission) and later light modulation test.

But we are still able to see PC pattern area in the shadow that has been high-lighted in red square regions.

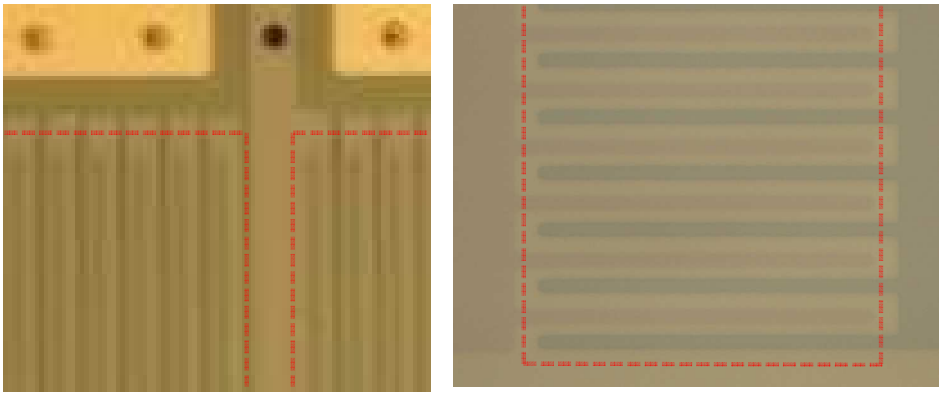

(a) (b)

Figure 4-8 (a) Scope zoomed-in view between two 300um PC area devices, which have been finished with final electrodes metallization. (b) Scope zoomed-in view of a 100um PC area device after two step implantations. PC pattern areas have been high-lighted in red square regions.

A group of single layer Fano resonance modulator devices with finger-print PIN lateral junctions was demonstrated. The Si-NM was transfer-printed onto glass substrates by PDMS mode following with the electrode metallization processes, as in Fig. 4-9 (c). I –V measurement as Fig. 4-9 (d) shows a perfect lateral Si PIN junction have been formed. The microscope topviews and zoomed-in topviews have been given in Fig. 4-9 (a), (b), (c), (d)inset. The designed N type doping concentration should be as least 1×10^{19} as well as for P type doping. The N type dopant is phosphorous and P type dopant is Boron. They were implanted at Innovion Inc. by 7-degree tilted off surface normal.

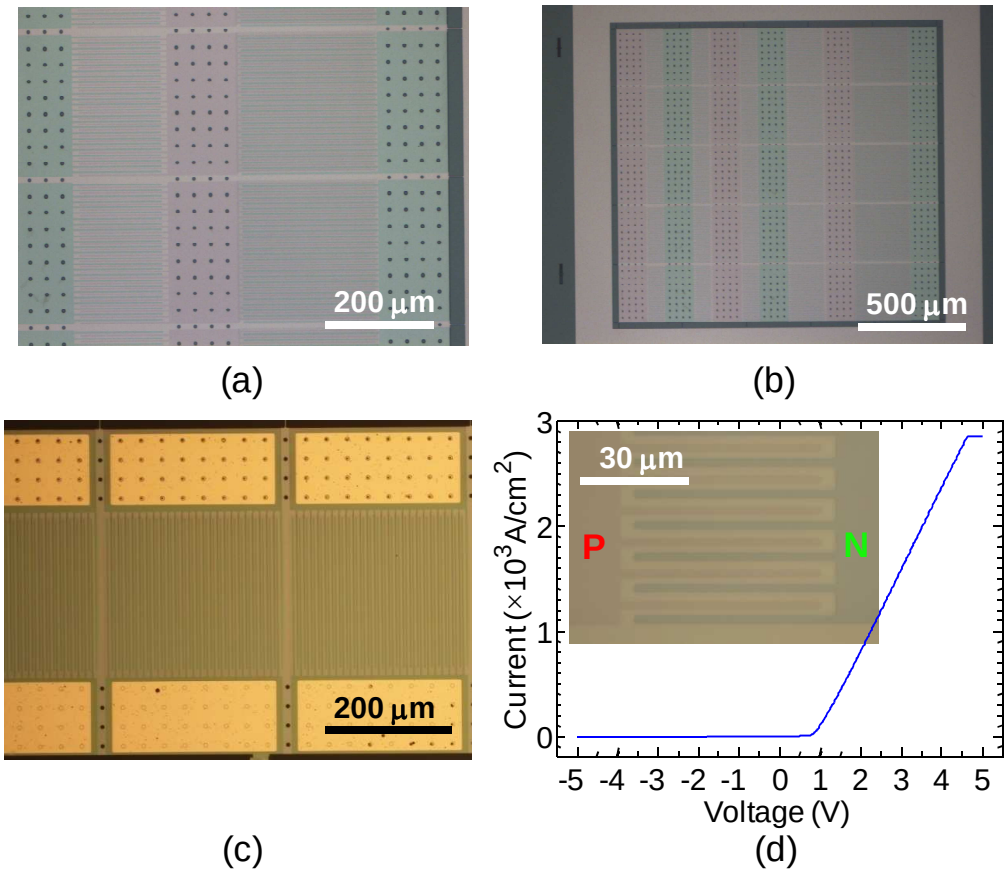

Figure 4-9 (a) 3D image of device. (b) Devices microscope top view after P/N implantation. (c) Microscope top view of PDMS transferred Si nanomembrane device on glass with electrodes. (d) I-V testing results.

In the Fig. 4-10 (a) a group of 300 µm PC area modulator devices transferred on glass substrate are under testing. The blue spot reflects the actual white-light spot position shining on the center PC region. The two electrical pins are probing on the electrode pads at two sides. By bias the PIN junction with different voltages, the transmission dip shifting was successfully demonstrated. This red shifting is dominant mainly due to the strong thermal tuning effect that have been expected, the electrical

injected free carriers concentration changes induced blue shift may not be noticeable in this case. Fig. 4-10 (b) shows transmission spectra shifting when membrane material effective refractive index changes. Around 6nm red shifting has been noticed with a 4 volts forward bias.

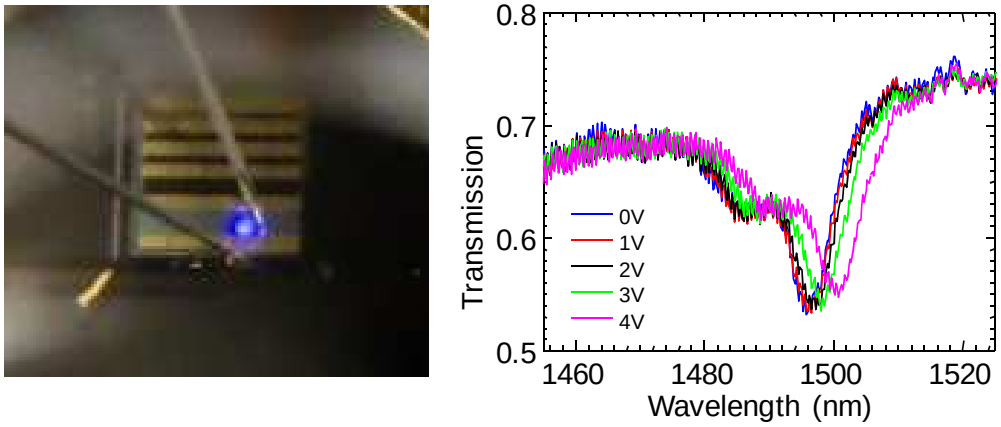

Figure 4-10 Fano Resonance modulators based on transferred Si membranes on glass with lateral PIN junction: (a) Picture of a group of devices on glass under testing. (b) One 300um PC area device under electro-optical testing and its transmission dip shifting with applied forward bias.

Low speed EO optical switching was demonstrated on those single layer PCS Fano resonance novel modulator devices. The electrical driving patterns are still in a very low speed as shown in Fig. 57 (a), (b), (c), (d). It is true that the thermal effect is dominant when the system work at a relatively lower frequency. It could be meaningful to do more study on the electrical injection induced free carrier concentration change, since one should start to see the free carrier injection induced modulation when the system work at the thermal response cut-off frequency, even the modulation depth could be very

small due to the small EO coefficient in Si material. And further investigation is needed to identify the maximum modulation speed of these devices.

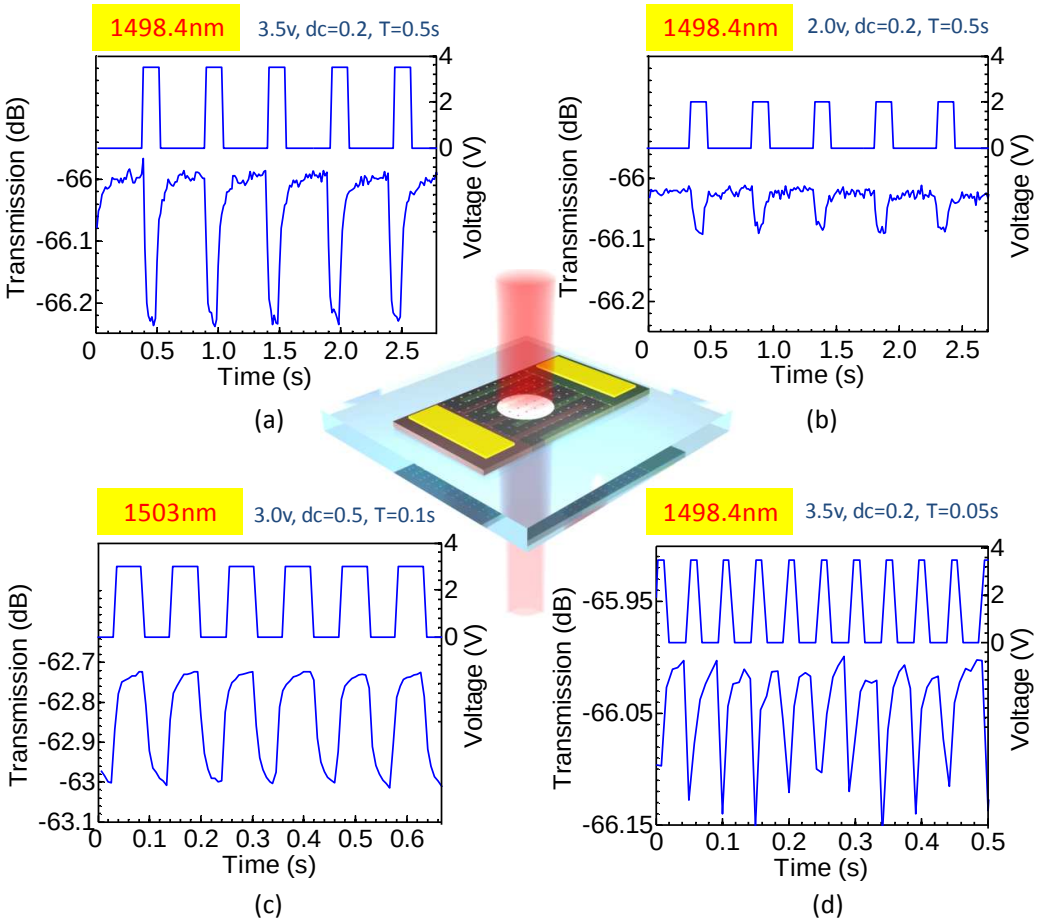

Figure 4-11 Single layer lateral junction modulators: Device under modulation testing: (a,b,c,d) Modulation to wavelengths with different duty cycle and bias, in time domain, each operation probe wavelength and electrical pulse pattern have been illustrated on top of each figure. Insert here in the center with a 3-D sketch of this single layer Si nanomembrane based PCS Fano resonance modulator device.

Such photonic-crystal Fano resonance based crystalline semiconductor nanomembrane modulators are transferrable, stackable, bondable, and thus could be compatible with vertical emitting light sources. Its vertical incidence and PCS membrane based Fano resonance property may provide a unique way for further shrinking the optical interconnect footprint and increasing on-chip integration density.

4.2.2 Double- layer photonic crystal slabs modulators

We proposed here double–layer photonic crystal slabs Fano resonance modulator novel devices, which are transferable, stackable, bondable and manufacturable, offering unprecedented opportunities for unique and novel electronic and photonic devices for vertically stacked high density photonic/electronic integration.

With the membranes bases Fano resonance physics, it can provide great opportunities for ultra-high Q resonance, ultra-compact on-chip integration and smaller device footprint. Double layer design is based on e-beam patterned stacking Si-NM bi-layer structure, which has much higher Q-factor comparing to a single layer Si-NM device due to its strong coupling effect by inserting a lower refractive index layer between the two patterned Si-NMs. A Q factor of 10K with 8dB extinction ratio has been achieved experimentally with lattice aligned double layer structure near 1.5um wavelength region. Experimentally, 80K high-Q factor also has been achieved most recently by this double-layer PCS stacking configuration with lattice displacement at 1550nm. Based on these achievements, we start to pursue further applications on these extremely high-Q resonance structures.

Two configurations have been considered in the double-layer Fano resonance PCSs novel modulator design: one is the stacking on SOI for a refletion mode strategy; the other is stacking double-layer PCSs on transparent substrate such as glass for a

transmission mode strategy. The basic idea of these device structures have been illustrated as following Fig. 4-12. (a),(b) by 3D sketches.

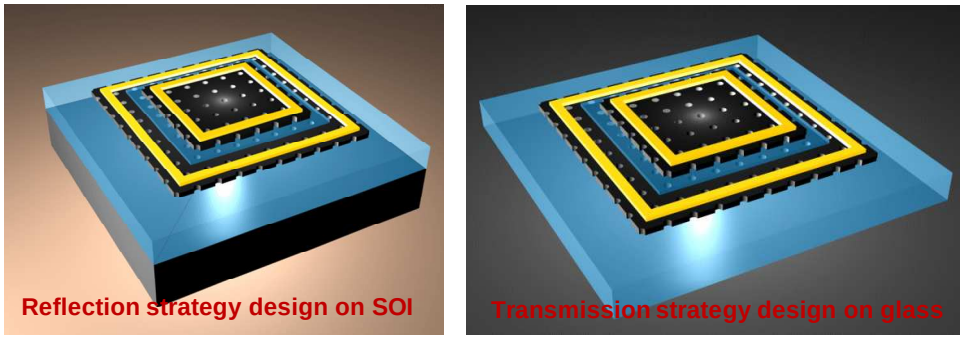

(a) (b)

Figure 4-12 (a) 3-D sketch for reflection strategy staked double-layer PC Si-NM Modulator on SOI substrate. (b) 3-D sketch for transmission strategy staked double layer PC Si-NM Modulator on transparent substrates, such as glass.

In the vertical dimension, we proposed a PIN bi-layer Si-NMs stacked structure. 230 nm poly-Si layers were grown on quartz substrates or SOI wafer by LPCVD. Utilizing Cr metal thin layer as hard mask, 2-D circles array patterning was firstly written by E-beam writer, then was transferred onto Cr mask. Stacked layers were etched through to the bottom box layer by Si/SiO2 RIE with high aspect ratio. Both thermal Si dioxide and PECVD oxide were considered as the low index separation layer. High-Qs can be found with oxide thicknesses range from tens to hundreds of nm. By an examination into the electro-optical modulation configurations, we applied here a vertical PIN structure of the electrical carriers accumulation mechanism for EO modulation. As shown in Fig. 59, the optimized overall doping profile has been investigated to achieve the largest index change and a high intrinsic modulation speed of ~20GHz. Device size and GSG pad

size were also taken into consider based on electrical and optical testing setups capabilities. A modulation speed of 11GHz was expected according to a simulation of a 20 μm size modulator device. (Real device size from ~30 μm to ~300 μm)

Based on a 20 μm by 20 μm device in its lateral dimensions, we pursued an examination into this basic semiconductor material physics. Simulation tool Medici was utilized for electrical properties study. In this simulation model (Fig. 4-13), one lateral dimension, which is normal to the paper, was set to be infinite. In the Fig. 4-13, a cross-sectional view of this 2D model we are looking at in this simulation was shown. The desired multi-layers doping profile was determined and then a calculation towards the modulation effect was proceeded.

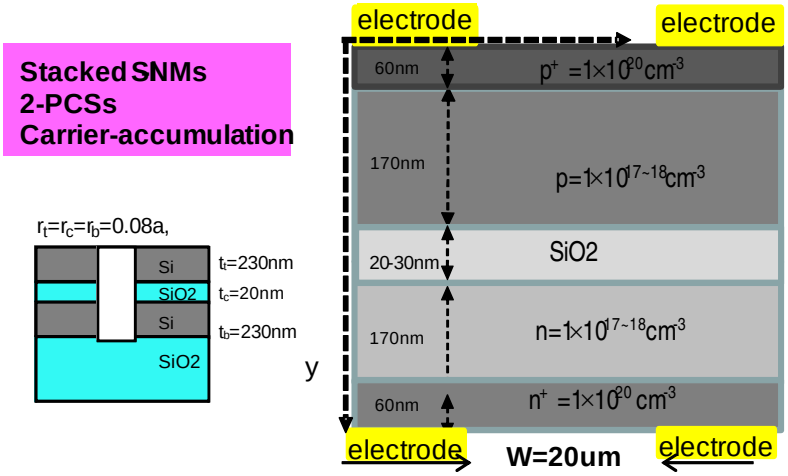

Figure 4-13 Electrical design key parameters for the carrier-accumulation double-layer PCSs surface normal modulator.

The double layer vertical stacked Si-NMs PIN structure was doped by Boron/Phosphorous ion implantation according to optimized doping profile for refractive index modulation. The doping levels are designed $1\times10^{19}/cm^3$ ~ $1\times10^{20}/cm^3$ in the top

region of the up Si-NM layer and at bottom region of the second Si-NM layer that at beneath. A lower doping level of 1×10^{17}~1×10^{18} in the middle of the overall vertical PIN region were utilized in order to achieve the highest modulation of the averaged effective refractive index per volume.

In this structure, the carrier accumulation is the fundamental that was considered in the simulation. Carrier concentration changes along vertical direction was estimated when applying reverse bias of 5 volts and 10 volts (Fig. 4-14 (a));

The profile shows that most accumulation happens near to the two interfaces between Si layer and the electrical isolation layer, which is identical. The magnitude of the concentration changes in the double layer middle region are profound, however, it is not uniform along vertical direction in this Si double layers stacking structure.

Based on the index change profile caused by the carrier concentration changes along vertical direction, we then gave a calculated resonance mode shifting spectra in Fig. 4-14 (c). 0.3 nm and 0.65 nm blue shifting (Fig. 4-14. (c)) were noticed when applying 5 volts and 10 volts reverse bias respectively.

The intrinsic electrical response study was carried out by Medici in time domain. The carrier concentration change rise and fall-time are 0.04ns and 0.01ns respectively which will promise a 20GHz intrinsic modulation speed or even higher if one consider the 3D real device electrical contact. Device capacitance and other electrical parameters are also estimated.

Assuming a 20 μm by 20 μm device in lateral dimension with 50Ω resistance of the device, the intrinsic capacitance can be estimated as around 2.7×10^{-4} nF, its Maximum cut-off frequency will be 11GHz.

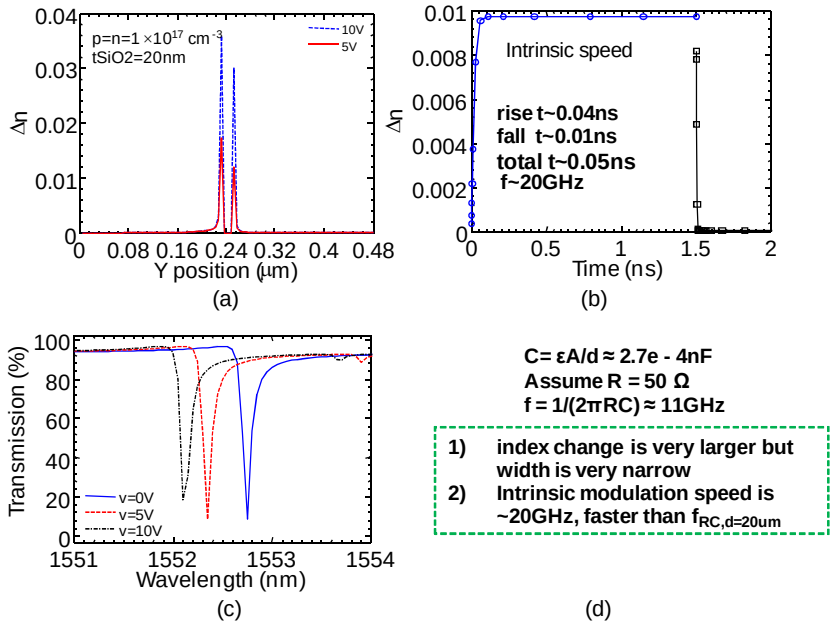

Figure 4-14 Simulation for modulation speed: By an examination into the electro-optical modulation configurations, we applied here a vertical PIN structure of the electrical carriers accumulation mechanism for EO modulation.

The conclusion can be arrived at that the Maximum working frequency of this double-layer PCSs modulator design can reach to 11GHz and it may increase by square of the device size decrease, till it reach to its intrinsic frequency 20GHz as calculated here. We might also want to know that when we consider the 60nm oxide buffer layer in this double-layer modulator structure, the intrinsic frequency will increase to around three times of 20GHz and the cut-off frequency will be 33GHz in this case. Additionally, from achieving even higher Q factor point of view, the 60nm buffer oxide also give a plus to the high-speed modulation with low power consumption. Please refer to the double-layer high-Q we have demonstrated in chapter 3 for supporting this conclusion.

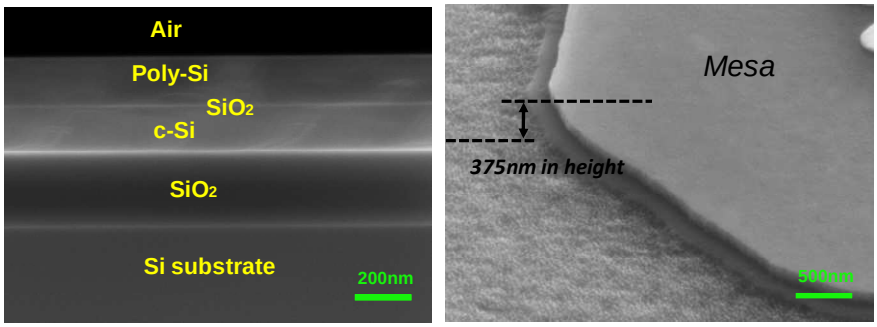

(a) (b)

Figure 4-15 Fabrication: Implanted PIN bi-layer Si-NMs; Thermal growth and wet etching; Poly-Si LPCVD; Ion-implantation and E-beam lithography and RIE processes.

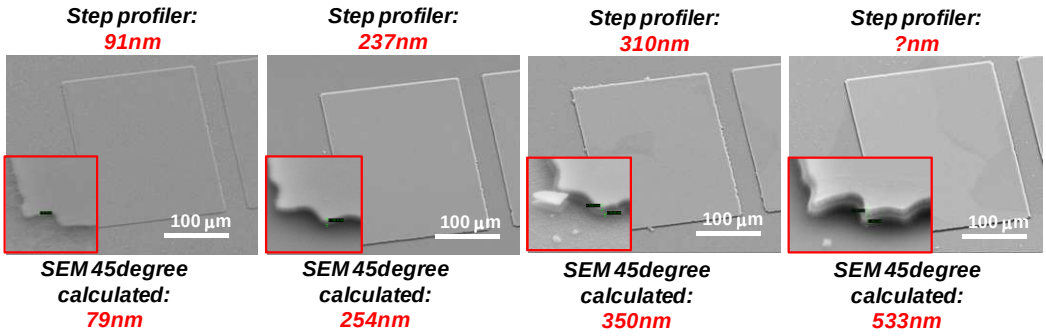

(a) (b) (c) (d)

Figure 4-16 Vertical I-V electrical properties study: RIE depths.

With 20nm PECVD SiO2 working as an isolation layer and a mesa etching depth of 375nm, IV tests results show high conductivity of the top/bottom surfaces. When probe on the Top-bottom, IV rectifying can be observed, but very low forward bias current --- only ~1/1000 of a junction forward bias current level that it should be.

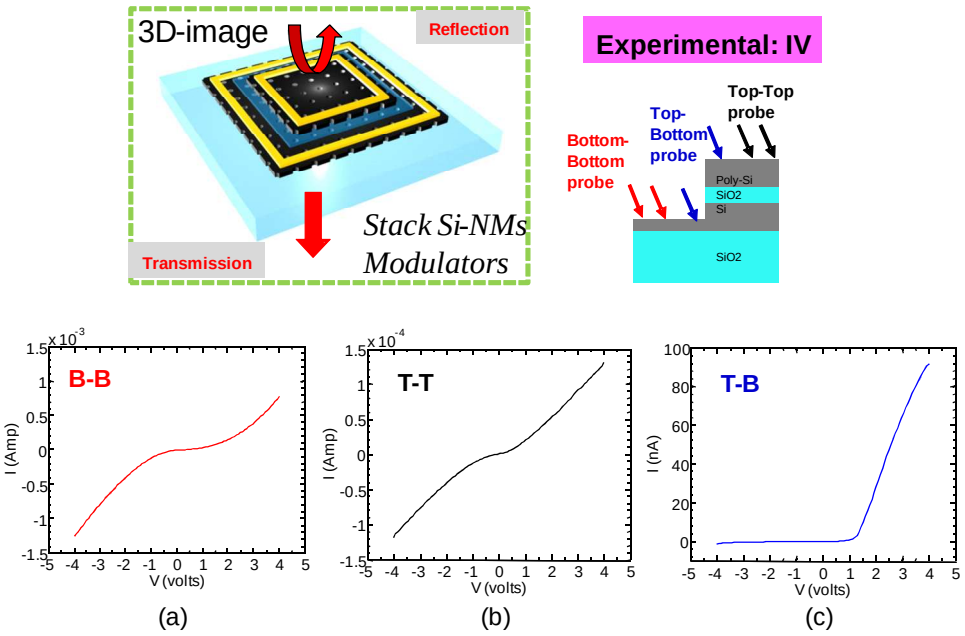

Figure 4-17 Stacked PC Si-NMs modulators: Implanted stacked vertical PIN junction IV tests: With 20nm PECVD SiO2 working as an isolation layer and a mesa etching. IV tests results show high conductivity of the top/bottom surfaces in (a) and (b); I-V rectifying was noticed in (c) with much lower current in tens of nA at forward bias.

In a sum, as a Fano-resonance based Si-NM modulator design, we applied here a stacked Si-NMs PIN structure with optical low index separation layer which also work as an electrical isolation layer. Thin oxide thicknesses show junction IV rectifying, though thicker then 20nm oxide may isolate the up N-type poly-Si layer and the P-type Si layer beneath.

Fabricated sample images and microscope images of devices group and individual device were shown in following Fig. 4-18 and Fig. 4-19, along with the SEM angled views of these double-layer PCSs stacked novel modulator devices in different sizes in Fig. 4-20

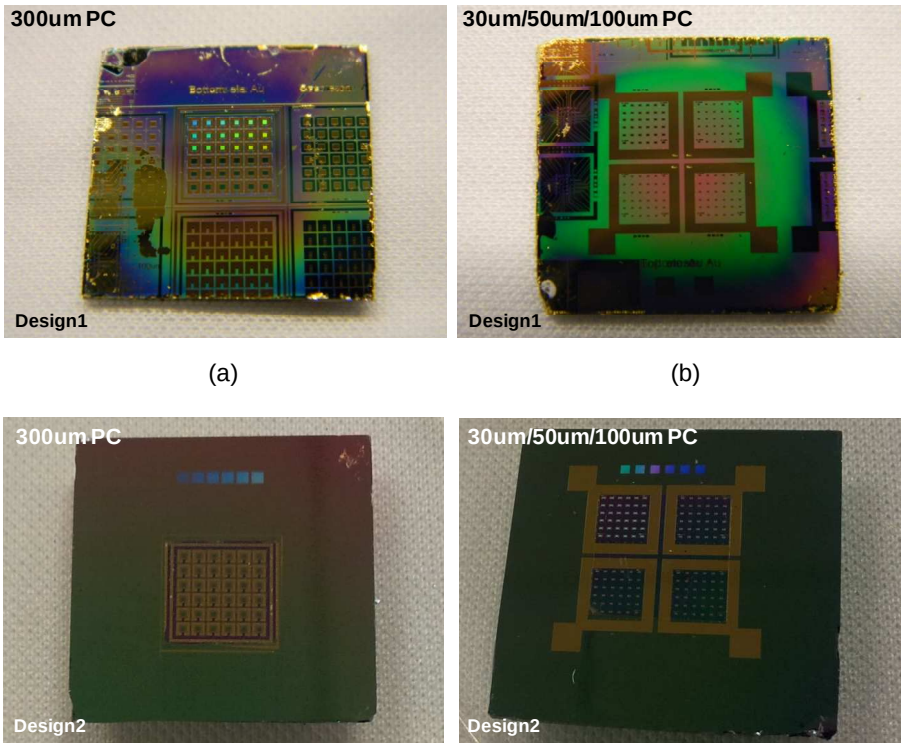

Figure 4-18 Stacked PCSs Si-NMs based modulators device groups pictures (a) 300 µm PC area, device group with design1 (b) 30 µm / 50 µm / 100 µm PC area devices groups with design1 (c) 300 µm devices group with design2 (d) 30 µm / 50µm / 100 µm PC area devices groups with design2.

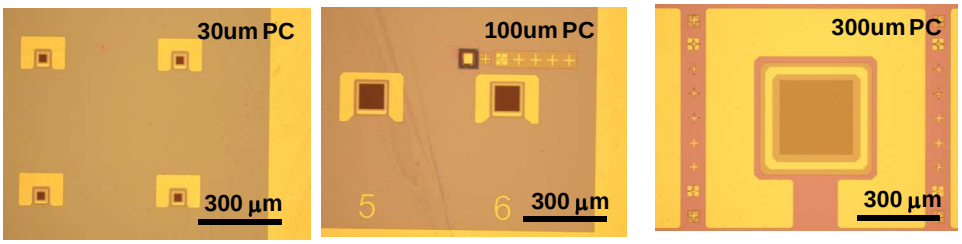

Figure 4-19 Device scope view after electrodes metallization.

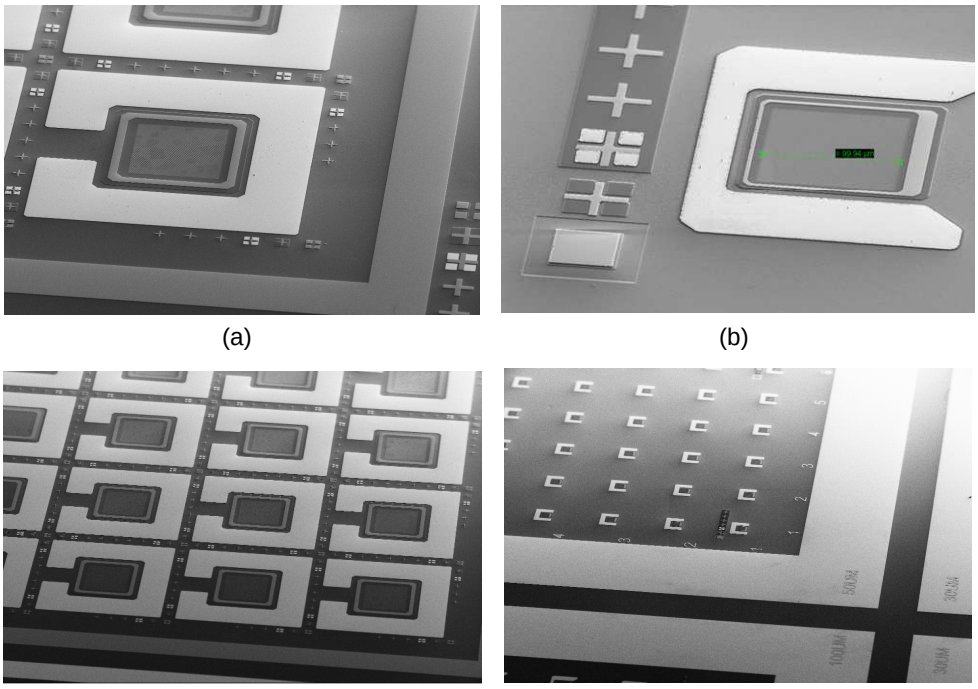

(a) (b)

(c) (d)

Figure 4-20 Stacked PC Si-NMs modulators: SEM angled-view images (a) 300 µm PC area device at the group corner. (b) 100 µm PC area device along with alignment marks (c) 300 µm PC area modulator devices group (d) 30 µm PC area devices group.

Chapter 5

Conclusion And Future Work

5.1 Photonic crystal membrane based Fano resonance reflectors

We demonstrated single layer ultra-compact Si-MRs with their operation wavelength bands covering through Near-infrared, mid-infrared to far-infrared. In this study, Si based material system was carefully investigated, the simulation shows that broadband reflection with close to 100% peak reflection can be achieved for designed wavelength bands, with the optimal selection of lattice parameters and Si thicknesses. Based on scaling principles, it was found that the optimal Si-MR thickness (t) is ~0.75-0.85 (λ/n), and the optimal lattice constant (a) is ~1.9-2.1 (λ/n), where λ is the wavelength and n is the refractive index of Si.

High performance reflectors were experimentally demonstrated for surface-normal incidence with center operation wavelengths of 1.5 μm, 2.3μm, 8~10 μm, 76 μm, respectively. Large area patterned membrane reflectors were fabricated and transferred onto foreign substrates using wet or PDMS stamp assisted membrane transfer printing processes.

5.2 Photonic crystal membrane based Fano resonance filters

Fano resonance or guided-mode resonance filters are a new class of narrowband filters that could be important in a number of applications, including laser cavity reflectors, [57, 95] polarizers,[175] light modulators,[176-179] biosensors,[89, 180-182] and WDM filters.[43, 45, 85] One advantage of Fano resonance filters is that they operate on a resonance effect, which can be exhibited by relatively simple structures. Thus, it would be able to replace hundreds of layers thin-films filter with a single or

double-layer membrane. The resonance effect is associated with leaky modes that are supported by index modulated patterned membrane structure. At resonance, energy from an incident plane wave is coupled into a leaky mode and then back into one or more radiation modes. The coupling is highly sensitive to the wavelength of light and angle of incidence, and a sharp resonant peak might be observed in the reflected light when either of these parameters is varied.

In an optimized single layer Fano filter design, Quality factor Q of 4,500 can be achieved with “r/a” ratio of 0.08, as shown in Table 3-1, S3. For the lattice constant “a” of 780 nm (Case S3), the corresponding air hole radius “r” is 62.4 nm. Though even higher Q is expected with further reduction in “r/a” ratio, achieving air holes with radius much smaller than 60 nm is challenging in fabrication. And potential degradation of air hole quality with radius smaller than 60 nm will lead to significant reduction in filter Q. Experimentally, we have demonstrated single layer filters based on PDMS transfer printing of single crystalline Si PhC nanomembranes on transparent low index glass substrate. A Q factor of 1,727 was obtained with 26 dB extinction ratio, for Design S1 with r/a = 0.08 and a = 765 nm.

Fano resonance filters on both glass and plastic substrate have been reported, employing polydimethylsiloxane (PDMS) transfer printing technique [2, 92, 93, 189]. However, single layer PhC Fano filters offer limited quality factor Q and limited dispersion engineering capabilities for fine-tuning the output spectrum. The resonance-enhancement between coupled photonic crystal slabs was theoretically investigated by Liu. et al. The results show that much higher Q Fano filters can be realized by multi-layer PhC coupling and lattice offset control [9, 39]. In such double-layer PCSs systems, the presence of in-plane periodic index contrast enables phase-matched coupling between externally

incident plane waves and guided modes that are supported by the slab, leading to strong resonant behaviors of individual slabs [6, 254].

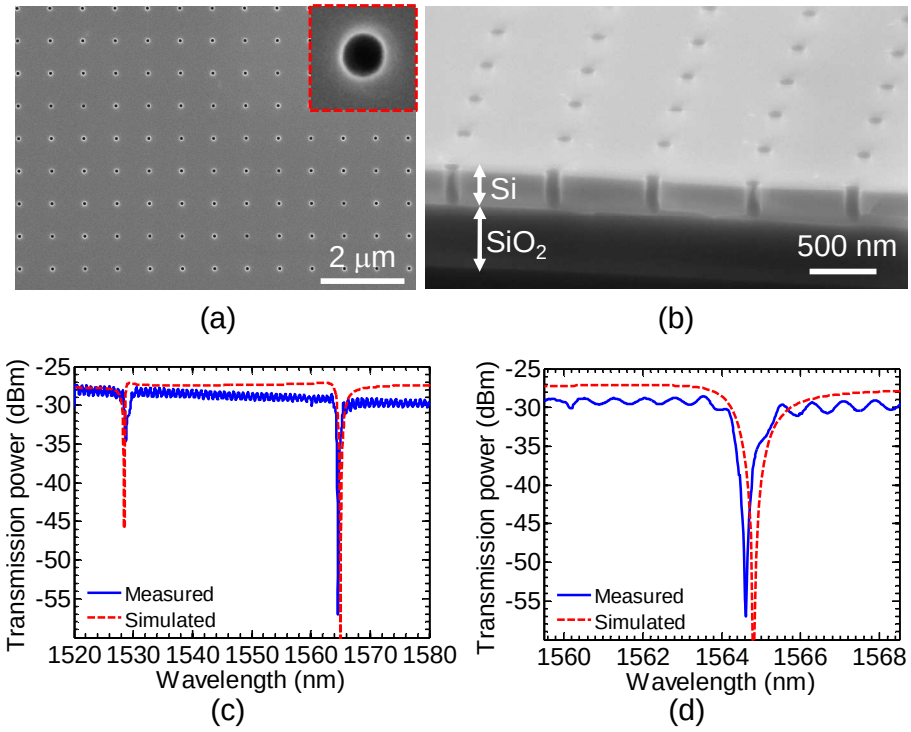

Figure 5-1 Experimental results for Design S1: (a) Top and (b) Cross-section views of fabricated single-layer PhC Fano resonance filters on oxide buffer; (c) Measured (blue solid line) and simulated (red dash line) transmission spectra for the fabricated single-layer PhC Fano resonance filter transferred on glass substrates; and (d) Zoom-in of (c) over the second dip (λ=1564.62 nm) region.

The dark states that exist in Photonic Crystal Slab (PCS), can be excited in a two adjacent PCSs system, either arising from coupled bright guided resonances or coupled dark resonances of single labs, when the mode frequency and in-plane wave vectors satisfying the phase-matching conditions for coupling and de-coupling between in-plane

modes and external plane waves due to either symmetric or dynamic reasons. [9, 39, 255]

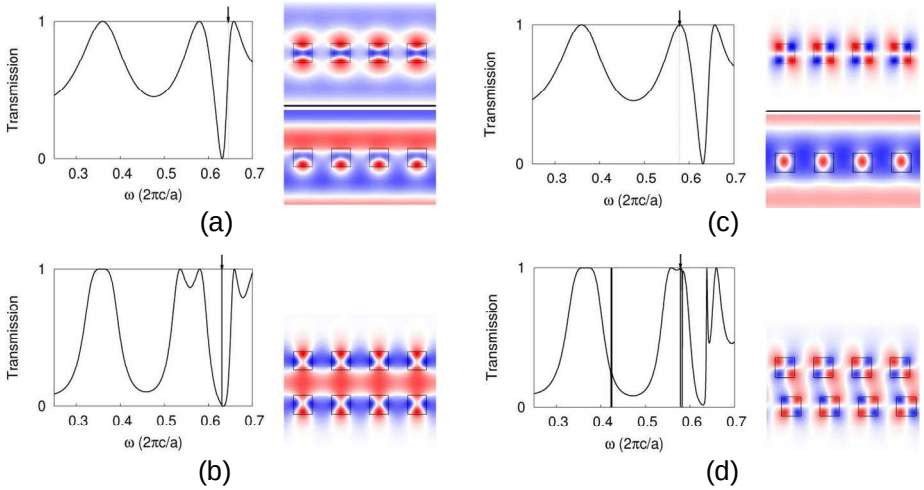

Figure 5-2 Dark state arising from coupled bright guided resonances: (a) Left: Single slab transmission spectrum; the arrow indicates the frequency of a Fano resonance mode. Right: Mode profile calculated by MPB (top) and field profile computed with SMM at the frequency indicated by the arrow in left. (b) Left: Double slab transmission spectrum for d = 0.65a; note the extremely sharp resonance peak. Right: Field profile at peak of resonance in left; Dark states in the two-slab system that arise from coupled dark resonances from single slabs: (c) Left: Single slab transmission spectrum; the arrow indicates the frequency of a dark state. Right: Mode profile calculated from MPB at the dark state frequency (top) and field profile computed with SMM at the frequency indicated by the arrow in left. (d) Left: Double slab transmission spectrum for d = 0.5a, lateral offset x = 0.15a; note the appearance of pairs of sharp resonances. Right: Field profile at lowest frequency resonance from left.[9]

More attractions have been focused on these Fano resonance based high-Q photonics strategy due to the fact that, the theoretical prediction of these coupled double-layer PCSs structure is possible to offer an extremely high-Q factor that without a theoretical limitation. The dark modes that can be excited in both of these coupled double-layer PCSs with or without lattice offsets. In the lattice aligned double-layer stacked PCSs structure, proper choices for set of parameters as PCSs thicknesses, lattices can leads to infinite Q. On the other hand, with the PCSs lattice misaligned double-layer stacking structure, infinite Q is also possible from theory. Moreover, one can have even better chances to expecting a practical extremely high-Q.

We have successfully demonstrated these ideas by experimental ways. It has been confirmed that these expectation of extremely high-Q filters are highly desirable and achievable. These crystalline semiconductor nanomembranes (NMs), which are transferable, stackable, bondable and manufacturable, offer unprecedented opportunities for unique electronic and photonic devices for vertically stacked high density photonic/electronic integration, high performance flexible electronics and flexible photonics. [118]

Employing poly-crystalline-Si deposition processes [198, 199], double-layer nanomenbranes Fano filters on silicon and on quartz substrates were reported with symmetric spectral lineshapes and much higher Q factors of 98,000-10,000,000 by design; A double-layer filter device with Q factors of 22,000 by design and ~10,000 by measurement was also successfully demonstrated [10]. The etching profile and side-wall control turn to be the most critical part of the desirable quality factors.

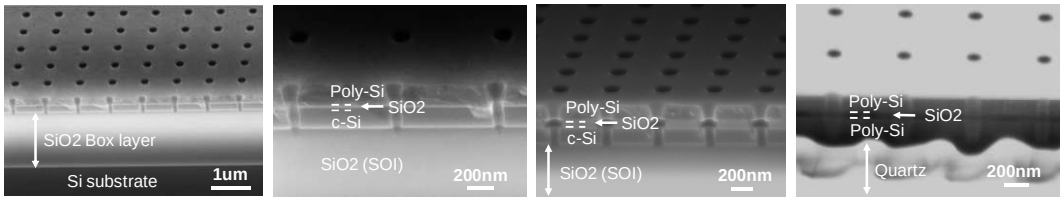

(a) (b) (c) (d)

Figure 5-3 Cross-sectional SEM images for fabricated double-layer PhC Fano resonance filters based on Design D2 parameters: (a, b, c) Double-layer PhC structure was formed by poly-Si deposition on top of the SOI substrates; and (d) Double-layer PhC structure was formed by two steps of poly-Si deposition on quartz substrates. Notice the oxide buffer thicknesses are 20 nm, 160 nm, and 20 nm, for cases (b), (c), and (d), respectively. [10]

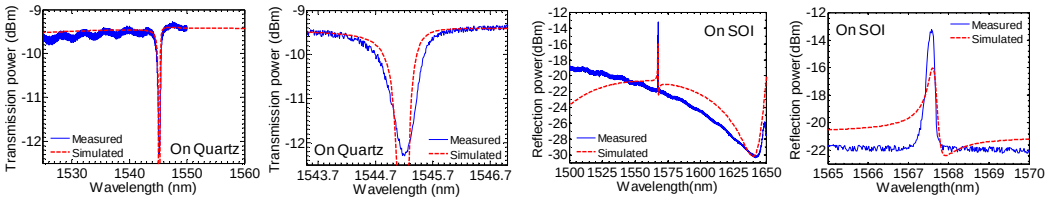

(a) (b) (c) (d)

Figure 5-4 (a, b) Measured (blue solid line) and simulated (red dash line) transmission spectra for the double-layer PhC Fano resonance filters on quartz; and (c, d) Measured (blue solid line) and simulated (red dash line) reflection spectra for the double-layer PhC Fano resonance filters on SOI. (b), (d) are zoom-in's of (a), (c), respectively.

In the same year of 2013, we reported ultra-compact high-Q Fano resonance filters with displaced lattices between two coupled photonic crystal slabs, fabricated with crystalline silicon nanomembrane transfer printing and aligned e-beam lithography techniques. Experimentally Q factors up to 80,000 have been demonstrated [256] (and APL submitted). Similar to Fano resonances in other types of nanoscale structures,

extremely high quality factor (Q) optical filters was obtained in these structures with asymmetric resonance lineshapes and extremely sharp transition between transmission peak and dip. [1, 35] Polarization tests were also carried out use the same setup with linear polarized laser beam incidence on sample SHQO-A-P4. Due to the asymmetric of the lattice displaced double-layer structures, these lattice displaced double-layer PCSs high-Q devices are incidence polarization sensitive.

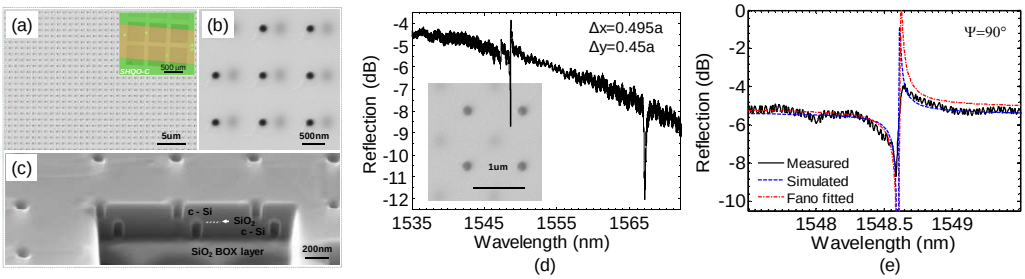

Figure 5-5 Fabricated Fano filter scanning electron micrograph (SEM) images: (a) top view; (b) zoom-in top view; and (c) cross-sectional view of double layer Fano filter on SOI, with controlled lattice misalignment offset (Δx =0.2a, Δy = 0). Show in the inset of (a) is a micrograph showing multiple device structures with top and bottom PhC pattern areas. (d) Measured reflection spectra for a displaced Fano filter with large offset (Δx = 0.495a, Δy = 0.45a), with a top view SEM image shown in the inset; and (e) Zoom-in plots around the dominant resonance with measured, simulated, and Fano fitted reflection spectra.

The conclusion terms to be that, ideally, assuming zero material intrinsic absorption and no fabrication defects, with a proper separation between two PCSs and the optimized set of PCS thicknesses and lattice parameters design, the optical Q factor of this lattice aligned double-layer PCSs system can go extremely high without a

theoretical limitation. However, instead of extremely accurate controlling of those fabrication parameters in such a lattice aligned double-layer PCSs system, less engineering challenge for achieving the practical high-Q factors was addressed to controlling the lattice displacements between two coupled PCS layers. This mostly due to the processes alternativities were utilizing in the two kinds of fabrication approaches: either one-time masking for dry etching through the double-layer Si-NMs or applying PDMS transfer printing to separate the one-time masking into twice for the two Si-NMs. Note that it can be also achievable to make a lattices aligned double-layer PCSs structure when apply PDMS transfer printing for top-layer Si-NM and pattern for the two Si-NMs separately, thus, can lead to a much higher-Q factor with a better dry-etching overall profile comparing to the double-layer one-time masking and etching result. These high Q filters, will have extraordinary potentials in integrated photonics, optical communications, and sensing applications.

In sum, 1) Employing poly-crystalline-Si deposition processes, double-layer nanomenbranes Fano filters on silicon and on quartz substrates were reported with symmetric spectral lineshapes and much higher Q factors of 98,000-10,000,000 by design; A double-layer filter device with Q factors of 22,000 by design and ~10,000 by measurement was demonstrated. 2) Coupled double-layer PCS Fano resonance filters with controlled lattice displacement have been investigated theoretically and experimentally, based on PDMS transfer printing technique, and aligned EBL pattern processes. Theoretically, optical filter Q factors can approach 2.11x108 or even higher. Experimentally Q factors of 11,500 to 80,000 have been demonstrated. These results suggest this type of coupled bi-layer PCS structures can offer a platform for high Q optical filters, as well as platforms for optomechanics, reconfigurable optics, integrated photonics, and sensing systems.

5.3 Photonic crystal membrane based Electro-Optical (EO) modulator

Photonic-crystal-based slow-light MZI modulators [257-261] have given main advantages of the ability to engineer the group velocity to allow device lengths of the order of 100um, but this is often at the cost of optical bandwidth.[261] Here we proposed two kinds of novel Si membrane EO modulator devices base on single layer PCS or double-layer PCSs. Notice that the double-layer modulator design offers additional freedom for ultra-high-Q resonance and engineering. Benefiting from the ultra-compact photonic crystal slabs device small size and ultra-high Q it promises, we are expecting a Si nanomembrane based surface normal incidence optical modulator novel device by going through the foreseen engineering challenges, such as devices size minimization and thermal related consideration.

The thermal effect, on one hand, could be the domain effect that has been noticed in our previously demonstrated single layer PCS surface normal optical switching devices. But it can be significantly minimized in the double-layer stacked new design when we consider the carrier accumulation physics by introduce an electrical isolation oxide layer between two Si PCS layers. Nevertheless, from optical point of view, ultra-high Q can be expected from this double-layer PCSs structure design, which may offer chances for higher modulation speed and lower modulation power consumption. Moreover, the thermal effect, on the other hand, could also provide chances for bandwidth engineering by controlling the device operation temperature when an electrical injection frequency is much higher than the thermal response intrinsic frequency, even though it may require additional power consumption.

From the simple RC circuit intrinsic physics bandwidth point of view, we should also note that the device physical dimensions will also make a big difference in modulation speed and bandwidth. This can be solved by the available engineering

approach; however, for example, in the vertical junction single layer membrane modulators design or the double-layer stacked membranes modulator design, devices' lateral dimensions mostly determine the device capacitance, which will be a first barrier of approaching high speed. We need to continue working on to find the optimized PCS device lateral dimensions by balancing between the desirable high-Q factor that the Fano resonance membranes can provide with certain lateral dimensions and its corresponded RC magnitude.

In the end, as an overall view, we should mention that the arguments for a hybrid modulator are perhaps reinforced if one accept that other devices such as an optical sources or detectors can be usefully integrated through a hybrid approach, which have been focused on in past several years. Nevertheless, silicon photonics still offers one of the most promising approaches to achieving the high-density electronics/photonic integration necessary for developing a range of prospective applications --- most notably for the optical interconnects required in high-performance computing. And as for the modulator, monolithic variants continue to improve but it is entirely possible, given the wealth of expertise currently devoted to this subject, that a new device design could change the landscape overnight. Although debate still rages as to whether on-chip integration of hybrid component is required, what we do know is that silicon photonics will make the difference.

5.4 Photonic crystal membrane based optomechanics applications: investigation and attemption.

Optomechanics related optical force was investigated theoretically in two-dimensional photonic crystal slab where the radiation force can be further enhanced due to the stored and strongly localized electromagnetic field inside the PCSs. Other than the systems have been well studied, including coupled waveguides, waveguides coupled to substrates, as well as a variety of resonator structures such as micro-rings, disks or toroids that support whispering gallery modes, and point defects in photonic crystal slab structures that support standing-wave optical modes, the behaviors of lateral and normal optical forces between coupled photonic crystal slabs attract a lot of interests, where near the frequencies of guided resonances, we see significant enhancement of the optical forces [9]. The theoretical analysis showed that the optical force is periodic with displacement, resulting in stable and unstable equilibrium positions. Moreover, the forces are strongly enhanced by guided resonances of the coupled slabs. Such enhancement is particularly prominent near dark states of the system, and the enhancement effect is strongly dependent on the types of guided resonances involved. Worth to notice that these structures were proposed can lead to enhancement of light-induced pressure over larger areas, in a configuration that is directly accessible to externally incident, free-space optical beams. It was also being highly expected that the force enhancement scales with the Q of the resonances in the structure even for moderate values of Q. By placing the system configuration in the vicinity of a dark state, a dramatic enhancement of the optical forces may be obtained due to the large resonant enhancement of the fields. Moreover, the enhancement behavior is closely related to some of the symmetry properties of the system. Both attractive or repulsive force were induced depending on the spatial symmetry of the stored electromagnetic field profile in double-layer PC slab cavity

structures and air-slot cavity structures [262]. As one experimental demonstration in 2010 from NTT group, strong optomechanical interaction was detected with estimation of optomechanically generated force per unit stored energy as 0.4 uN / pJ [204]. High Q factor was indicated as preference for practical experiments that the induced force on a photonic crystal slab was so strong that it can be detected experimentally with the microelectromechanical systems technique. Similar to symmetric-membrane systems, tunable attractive and repulsive forces can also arise in highly asymmetric structures coupled to external radiation. One recent theoretical work in 2011 shows the generality by demonstrating that tunable attractive and repulsive forces can also arise in highly asymmetric structures coupled to external radiation [263].

Membrane based single layer and double-layer PCS high-Q filters have been highly motivated for possible optomechanics application, especially for the ultra-high Q Fano resonance that we have recently demonstrated. It would be more interesting to make further exploring for the optical forces related physics in those coupled double-layer high-Q resonator structures that have been obtained for the Fano filters. This is another direction for proposed future work. Worth to mention that we also have demonstrated one suspending double-layer PCSs resonator structures which show here in the Fig. 72 as following. It is approved that such kind of MEMS double-layer PCSs structure could be achievable and have extraordinary potentials for proposed optomechanical applications.

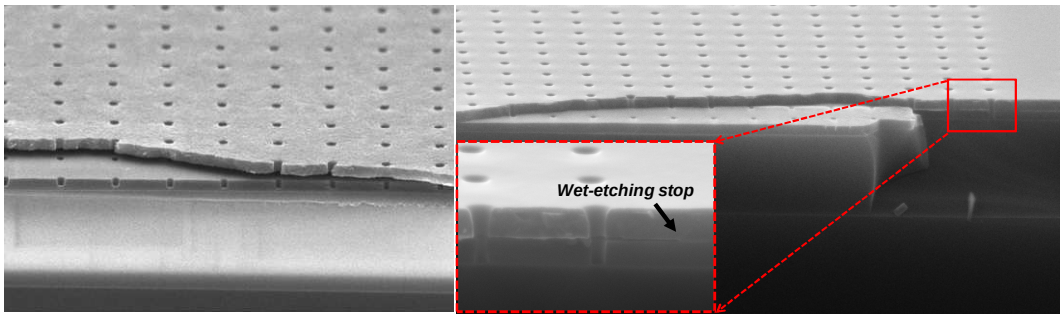

(a) (b)

Figure 5-6 A demonstration of double-layer PCSs stacking on SOI substrate, with removed thin oxide buffer layer of 20nm. Large area of the top Si-NM PCS layer was suspended on top of bottom PCS layer. This can be seen from the SEM image (a) top poly Si layer broke through a curved line shape but not aligned with the bottom PCS's straight breaking line. Shown in (b) is a larger scale view of the free-standing PCS sitting on the bottom PCS, with a inset of zoomed-in SEM image where one can notice the separation between the two layers and the oxide buffer wet-etching stop position.

References

[1] A.E. Miroshnichenko, S. Flach, Y.S. Kivshar, Fano resonances in nanoscale structures, Reviews of Modern Physics 82 (2010) 2257.

[2] W. Zhou, Z. Ma, H. Yang, Z. Qiang, G. Qin, H. Pang, L. Chen, W. Yang, S. Chuwongin, D. Zhao, Flexible photonic-crystal Fano filters based on transferred semiconductor nanomembranes, Journal of Physics D: Applied Physics 42 (2009) 234007-234017.

[3] Z. Qiang, H. Yang, L. Chen, H. Pang, Z. Ma, W. Zhou, Fano filters based on transferred silicon nanomembranes on plastic substrates, Applied Physics Letters 93 (2008) -.

[4] Y. Shuai, D. Zhao, G. Medhi, R. Peale, Z. Ma, W. Buchwald, R. Soref, W. Zhou, Fano Resonance Photonic Crystal Membrane Reflectors at Mid-and Far-Infrared, (2013).

[5] K. Balasundaram, P.K. Mohseni, Y. Shuai, D. Zhao, W. Zhou, X. Li, Photonic crystal membrane reflectors by magnetic field-guided metal-assisted chemical etching, Applied Physics Letters (in press) (2013).

[6] S. Fan, J.D. Joannopoulos, Analysis of guided resonances in photonic crystal slabs, Phys. Rev. B 65 (2002) 235112.

[7] W. Zhou, Z. Ma, H. Yang, Z. Qiang, G. Qin, H. Pang, L. Chen, W. Yang, S. Chuwongin, D. Zhao, Flexible photonic-crystal Fano filters based on transferred semiconductor nanomembranes, Journal of Physics D: Applied Physics 42 (2009) 234007.

[8] H. Yang, D. Zhao, S. Chuwongin, J.H. Seo, W. Yang, Y. Shuai, J. Berggren, M. Hammar, Z. Ma, W. Zhou, Transfer-printed stacked nanomembrane lasers on silicon, Nature Photonics 6 (2012) 617-622.

[9] V. Liu, M. Povinelli, S. Fan, Resonance-enhanced optical forces between coupled photonic crystal slabs, Opt. Express 17 (2009) 21897-21909.

[10] Y. Shuai, D. Zhao, Z. Tian, J.-H. Seo, D.V. Plant, Z. Ma, S. Fan, W. Zhou, Double-layer Fano resonance photonic crystal filters, Optics Express 21 (2013) 24582-24589.

[11] Y. Shuai, D. Zhao, J.-H. Seo, H. Yang, S. Fan, Z. Ma, W. Zhou, in: Photonics Conference (IPC), 2013 IEEE, (2013).

[12] B. Jalali, S. Fathpour, Silicon photonics, Lightwave Technology, Journal of 24 (2006) 4600-4615.

[13] R. Soref, Silicon photonics: a review of recent literature, Silicon 2 (2010) 1-6.

[14] IBM, (Webpage, http://www.slashgear.com/ibm-silicon-nanophotonics-speeds-servers-with-25gbps-light-10260108/, 2013).

[15] Intel, (Webpage, http://discover.osa.org/optical-society-blog/bid/276528/Photonics-Integration-and-its-future-at-Advanced-Photonics-2013, 2013).

[16] Intel, (Webpage, http://www.intel.com/content/www/us/en/research/intel-labs-silicon-photonics-research.html, 2013).

[17] Intel, (Webpage, http://www.intel.com/pressroom/archive/releases/2010/20100727comp_sm.htm?iid=pr1_marqmain_si-photonics#highlights, 2013).

[18] Optics, (Webpage, http://optics.org/indepth/3/2/4, 2013).

[19] G.T. Reed, W.R. Headley, C.J. Png, in: Integrated Optoelectronic Devices 2005, (International Society for Optics and Photonics, 2005).

[20] R. Soref, The past, present, and future of silicon photonics, Selected Topics in Quantum Electronics, IEEE Journal of 12 (2006) 1678-1687.

[21] www.slate.com, (Webpage, http://www.slate.com/blogs/future_tense/2012/07/13/global_internet_map_geotel_fortune_maps_show_how_cable_infrastructure_connects_the_world.html, 2013).

[22] www.opral.com, (Webpage, http://www.optral.com/blog/, 2013).

[23] D.A. Miller, Optical interconnects to silicon, Selected Topics in Quantum Electronics, IEEE Journal of 6 (2000) 1312-1317.

[24] N. Sherwood-Droz, M. Lipson, Scalable 3D dense integration of photonics on bulk silicon, Opt. Express 19 (2011) 17758-17765.

[25] P. Koka, M.O. McCracken, H. Schwetman, X. Zheng, R. Ho, A.V. Krishnamoorthy, in: ACM SIGARCH Computer Architecture News, (ACM, 2010).

[26] A. Joshi, C. Batten, Y.-J. Kwon, S. Beamer, I. Shamim, K. Asanovic, V. Stojanovic, in: Proceedings of the 2009 3rd ACM/IEEE International Symposium on Networks-on-Chip, (IEEE Computer Society, 2009).

[27] A. Shacham, K. Bergman, L.P. Carloni, Photonic networks-on-chip for future generations of chip multiprocessors, Computers, IEEE Transactions on 57 (2008) 1246-1260.

[28] L. Chen, K. Preston, S. Manipatruni, M. Lipson, Integrated GHz silicon photonic interconnect with micrometer-scale modulators and detectors, arXiv preprint arXiv:0907.0022 (2009).

[29] D. Wentzlaff, P. Griffin, H. Hoffmann, L. Bao, B. Edwards, C. Ramey, M. Mattina, C.-C. Miao, J.F. Brown, A. Agarwal, On-chip interconnection architecture of the tile processor, Micro, IEEE 27 (2007) 15-31.

[30] D. Vantrease, R. Schreiber, M. Monchiero, M. McLaren, N.P. Jouppi, M. Fiorentino, A. Davis, N. Binkert, R.G. Beausoleil, J.H. Ahn, Corona: System implications of

emerging nanophotonic technology, ACM SIGARCH Computer Architecture News 36 (2008) 153-164.

[31] Y. Pan, J. Kim, G. Memik, in: High Performance Computer Architecture (HPCA), 2010 IEEE 16th International Symposium on, (IEEE, 2010).

[32] C. Batten, A. Joshi, J. Orcutt, A. Khilo, B. Moss, C.W. Holzwarth, M.A. Popovic, H. Li, H.I. Smith, J.L. Hoyt, Building many-core processor-to-DRAM networks with monolithic CMOS silicon photonics, Micro, IEEE 29 (2009) 8-21.

[33] J. Chan, G. Hendry, A. Biberman, K. Bergman, Architectural exploration of chip-scale photonic interconnection network designs using physical-layer analysis, Journal of Lightwave Technology 28 (2010) 1305-1315.

[34] N. Sherwood-Droz, A. Gondarenko, M. Lipson, in: Conference on Lasers and Electro-Optics, (Optical Society of America, 2010).

[35] R. Magnusson, S. S.Wang, New principle for optical filters, Appl. Phys. Lett. 61 (1992) 1022-1024.

[36] R. Magnusson, M. Shokooh-Saremi, Physical basis for wideband resonant reflectors, Optics Express 16 (2008) 3456-3462.

[37] M.C.Y. Huang, Y. Zhou, C.J. Chang-Hasnain, A surface-emitting laser incorporating a high-index-contrast subwavelength grating, Nat Photon 1 (2007) 119-122.

[38] C.J. Chang-Hasnain, High-contrast gratings as a new platform for integrated optoelectronics, Semiconductor Science and Technology 26 (2011) 014043.

[39] W. Suh, M.F. Yanik, O. Solgaard, F. Shanhui, Displacement-sensitive photonic crystal structures based on guided resonance in photonic crystal slabs, Applied Physics Letters 82 (2003) 1999-2001.

[40] Y. Kanamori, T. Kitani, K. Hane, Control of guided resonance in a photonic crystal slab using microelectromechanical actuators, Applied Physics Letters 90 (2007) 031911-031911-031913.

[41] K.B. Crozier, V. Lousse, O. Kilic, S. Kim, S. Fan, O. Solgaard, Air-bridged photonic crystal slabs at visible and near-infrared wavelengths, Physical Review B 73 (2006) 115126.

[42] C. Grillet, D. Freeman, B. Luther-Davies, S. Madden, R. McPhedran, D.J. Moss, M.J. Steel, B.J. Eggleton, Characterization and modeling of Fano resonances in chalcogenide photonic crystal membranes, Optics Express 14 (2006) 369-376.

[43] L. Zhou, A.W. Poon, Fano resonance-based electrically reconfigurable add-drop filters in silicon microring resonator-coupled Mach-Zehnder interferometers, Optics Letters 32 (2007) 781-783.

[44] F. Shanhui, Sharp asymmetric line shapes in side-coupled waveguide-cavity systems, Applied Physics Letters 80 (2002) 908-910.

[45] L.Y. Mario, S. Darmawan, M.K. Chin, Asymmetric Fano resonance and bistability for high extinction ratio, large modulation depth, and low power switching, Optics Express 14 (2006) 12770-12781.

[46] C.-Y. Chao, L.J. Guo, Biochemical sensors based on polymer microrings with sharp asymmetrical resonance, Applied Physics Letters 83 (2003) 1527-1529.

[47] W. Suh, O. Solgaard, S. Fan, Displacement sensing using evanescent tunneling between guided resonances in photonic crystal slabs, Journal of applied physics 98 (2005) -.

[48] Y. Kanamori, T. Kitani, K. Hane, Control of guided resonance in a photonic crystal slab using microelectromechanical actuators, Applied Physics Letters 90 (2007) -.

[49] A. Rosenberg, M. Carter, J. Casey, M. Kim, R. Holm, R. Henry, C. Eddy, V. Shamamian, K. Bussmann, S. Shi, D. Prather, Guided resonances in asymmetrical GaN photonic crystal slabs observed in the visible spectrum, Optics Express 13 (2005) 6564-6571.

[50] N. Inoue, T. Baba, in: Asia Pacific Optical Communications, (International Society for Optics and Photonics, 2006).

[51] O. Levi, M.M. Lee, J. Zhang, V. Lousse, S.R. Brueck, S. Fan, J.S. Harris, in: Proc. SPIE, (2007).

[52] R. Harbers, S. Jochim, N. Moll, R.F. Mahrt, D. Erni, J.A. Hoffnagle, W.D. Hinsberg, Control of Fano line shapes by means of photonic crystal structures in a dye-doped polymer, Applied Physics Letters 90 (2007) 201105-201105-201103.

[53] E. Bisaillon, D. Tan, B. Faraji, A. Kirk, L. Chrowstowski, D.V. Plant, High reflectivity air-bridge subwavelength grating reflector and Fabry-Perot cavity in AlGaAs/GaAs, Optics Express 14 (2006) 2573-2582.

[54] J. Kim, L. Chrostowski, E. Bisaillon, D.V. Plant, DBR, Sub-wavelength grating, and Photonic crystal slab Fabry-Perot cavity design using phase analysis by FDTD, Opt. Express 15 (2007) 10330-10339.

[55] S. Boutami, B. Benbakir, X. Letartre, J. Leclercq, P. Regreny, P. Viktorovitch, Ultimate vertical Fabry-Perot cavity based on single-layer photonic crystal mirrors, Optics Express 15 (2007) 12443-12449.

[56] C. Sciancalepore, B.B. Bakir, X. Letartre, J. Harduin, N. Olivier, C. Seassal, J.-M. Fedeli, P. Viktorovitch, CMOS-compatible ultra-compact 1.55-μ m emitting VCSELs using double photonic crystal mirrors, Photonics Technology Letters, IEEE 24 (2012) 455-457.

[57] H. Yang, D. Zhao, S. Chuwongin, J.-H. Seo, W. Yang, Y. Shuai, J. Berggren, M. Hammar, Z. Ma, W. Zhou, Transfer-printed stacked nanomembrane lasers on silicon, Nature Photonics 6 (2012) 617-622.

[58] U. Fano, Effects of configuration interaction on intensities and phase shifts, Physical Review 124 (1961) 1866.

[59] R. Magnusson, S. Wang, New principle for optical filters, Applied Physics Letters 61 (1992) 1022-1024.

[60] S. Fan, J. Joannopoulos, Analysis of guided resonances in photonic crystal slabs, Physical Review B 65 (2002) 235112.

[61] V. Lousse, W. Suh, O. Kilic, S. Kim, O. Solgaard, S. Fan, Angular and polarization properties of a photonic crystal slab mirror, Opt. Express 12 (2004) 1575-1582.

[62] S. Fan, W. Suh, J. Joannopoulos, Temporal coupled-mode theory for the Fano resonance in optical resonators, JOSA A 20 (2003) 569-572.

[63] W. Suh, M. Yanik, O. Solgaard, S. Fan, Displacement-sensitive photonic crystal structures based on guided resonance in photonic crystal slabs, Applied Physics Letters 82 (2003) 1999-2001.

[64] K.B. Crozier, S. Kim, O. Kilic, W. Suh, S. Fan, O. Solgaard, in: Lasers and Electro-Optics, 2004.(CLEO). Conference on, (IEEE, 2004).

[65] O. Kilic, S. Kim, W. Suh, Y.-A. Peter, A.S. Sudbø, M.F. Yanik, S. Fan, O. Solgaard, Photonic crystal slabs demonstrating strong broadband suppression of transmission in the presence of disorders, Optics Letters 29 (2004) 2782-2784.

[66] F. Raineri, C. Cojocaru, R. Raj, P. Monnier, C. Seassal, X. Letartre, P. Viktorovitch, A. Levenson, in: Quantum Electronics and Laser Science, 2003. QELS. Postconference Digest, (IEEE, 2003).

[67] C. Lin, Z. Lu, S. Shi, G. Jin, D.W. Prather, Experimentally demonstrated filters based on guided resonance of photonic-crystal films, Applied Physics Letters 87 (2005) -.

[68] O.G. Schmidt, K. Eberl, Nanotechnology: Thin solid films roll up into nanotubes, Nature 410 (2001) 168-168.

[69] H.-C. Yuan, Z. Ma, Microwave thin-film transistors using Si nanomembranes on flexible polymer substrate, Applied Physics Letters 89 (2006) -.

[70] H.-C. Yuan, Z. Ma, M.M. Roberts, D.E. Savage, M.G. Lagally, High-speed strained-single-crystal-silicon thin-film transistors on flexible polymers, Journal of applied physics 100 (2006) -.

[71] H.-C. Yuan, G.K. Celler, Z. Ma, 7.8-GHz flexible thin-film transistors on a low-temperature plastic substrate, Journal of applied physics 102 (2007) -.

[72] S.A. Scott, M.G. Lagally, Elastically strain-sharing nanomembranes: flexible and transferable strained silicon and silicon–germanium alloys, Journal of Physics D: Applied Physics 40 (2007) R75.

[73] J.A. Rogers, Z. Bao, K. Baldwin, A. Dodabalapur, B. Crone, V.R. Raju, V. Kuck, H. Katz, K. Amundson, J. Ewing, P. Drzaic, Paper-like electronic displays: Large-area rubber-stamped plastic sheets of electronics and microencapsulated electrophoretic inks, Proceedings of the National Academy of Sciences 98 (2001) 4835-4840.

[74] H.C. Yuan, Z. Ma, Microwave thin-film transistors using Si nanomembranes on flexible polymer substrate, Applied Physics Letters 89 (2006) 212105.

[75] H.-C. Yuan, J. Shin, G. Qin, L. Sun, P. Bhattacharya, M.G. Lagally, G.K. Celler, Z. Ma, Flexible photodetectors on plastic substrates by use of printing transferred single-crystal germanium membranes, Applied Physics Letters 94 (2009) -.

[76] P. Zhang, E. Tevaarwerk, B.-N. Park, D.E. Savage, G.K. Celler, I. Knezevic, P.G. Evans, M.A. Eriksson, M.G. Lagally, Electronic transport in nanometre-scale silicon-on-insulator membranes, Nature 439 (2006) 703-706.

[77] M.M. Roberts, L.J. Klein, D.E. Savage, K.A. Slinker, M. Friesen, G. Celler, M.A. Eriksson, M.G. Lagally, Elastically relaxed free-standing strained-silicon nanomembranes, Nat Mater 5 (2006) 388-393.

[78] Y. Sun, J.A. Rogers, Inorganic Semiconductors for Flexible Electronics, Advanced Materials 19 (2007) 1897-1916.

[79] D.-H. Kim, J.-H. Ahn, W.M. Choi, H.-S. Kim, T.-H. Kim, J. Song, Y.Y. Huang, Z. Liu, C. Lu, J.A. Rogers, Stretchable and Foldable Silicon Integrated Circuits, science 320 (2008) 507-511.

[80] D.-H. Kim, J. Song, W.M. Choi, H.-S. Kim, R.-H. Kim, Z. Liu, Y.Y. Huang, K.-C. Hwang, Y.-w. Zhang, J.A. Rogers, Materials and noncoplanar mesh designs for integrated circuits with linear elastic responses to extreme mechanical deformations, Proceedings of the National Academy of Sciences 105 (2008) 18675-18680.

[81] J.A. Rogers, Y. Huang, A curvy, stretchy future for electronics, Proceedings of the National Academy of Sciences 106 (2009) 10875-10876.

[82] J. Lee, B. Zhen, S.-L. Chua, W. Qiu, J.D. Joannopoulos, M. Soljačić, O. Shapira, Observation and differentiation of unique high-Q optical resonances near zero wave Vector in macroscopic photonic crystal slabs, Physical Review Letters 109 (2012) 067401.

[83] C.W. Hsu, B. Zhen, J. Lee, S.-L. Chua, S.G. Johnson, J.D. Joannopoulos, M. Soljačić, Observation of trapped light within the radiation continuum, Nature 499 (2013) 188-191.

[84] D.K. Jacob, S.C. Dunn, M. Moharam, Flat-top narrow-band spectral response obtained from cascaded resonant grating reflection filters, Applied optics 41 (2002) 1241-1245.

[85] S.T. Thurman, G.M. Morris, Controlling the spectral response in guided-mode resonance filter design, Applied optics 42 (2003) 3225-3233.

[86] C.F. Mateus, M.C. Huang, L. Chen, C.J. Chang-Hasnain, Y. Suzuki, Broad-band mirror (1.12-1.62 μm) using a subwavelength grating, Photonics Technology Letters, IEEE 16 (2004) 1676-1678.

[87] W. Suh, S. Fan, All-pass transmission or flattop reflection filters using a single photonic crystal slab, Applied Physics Letters 84 (2004) 4905-4907.

[88] S. Boutami, B.B. Bakir, H. Hattori, X. Letartre, J.-L. Leclercq, P. Rojo-Romeo, M. Garrigues, C. Seassal, P. Viktorovitch, Broadband and compact 2-D photonic crystal reflectors with controllable polarization dependence, Photonics Technology Letters, IEEE 18 (2006) 835-837.

[89] Y. Ding, R. Magnusson, Resonant leaky-mode spectral-band engineering and device applications, Optics Express 12 (2004) 5661-5674.

[90] M.-L. Wu, Y.-C. Lee, C.-L. Hsu, Y.-C. Liu, J.-Y. Chang, Experimental and theoretical demonstration of resonant leaky-mode in grating waveguide structure with a flattened passband, Japanese Journal of Applied Physics 46 (2007) 5431.

[91] H. Yang, S. Chuwongin, Z. Qiang, L. Chen, H. Pang, Z. Ma, W. Zhou, Resonance control of membrane reflectors with effective index engineering, Applied Physics Letters 95 (2009) 023110-023110-023113.

[92] H. Yang, H. Pang, Z. Qiang, Z. Ma, W. Zhou, Surface-normal Fano filters based on transferred silicon nanomembranes on glass substrates, Electronics letters 44 (2008) 858-859.

[93] L. Chen, Z. Qiang, H. Yang, H. Pang, Z. Ma, W. Zhou, Polarization and angular dependent transmissions on transferred nanomembrane Fano filters, Opt. Express 17 (2009) 8396-8406.

[94] A.E. Willner, Lasers: All mirrors are not created equal, Nature Photonics 1 (2007) 87-88.

[95] M.C. Huang, Y. Zhou, C.J. Chang-Hasnain, A surface-emitting laser incorporating a high-index-contrast subwavelength grating, Nature Photonics 1 (2007) 119-122.

[96] H. Wu, W. Mo, J. Hou, D. Gao, R. Hao, H. Jiang, R. Guo, W. Wu, Z. Zhou, A high performance polarization independent reflector based on a multilayered configuration grating structure, Journal of Optics 12 (2010) 045703.

[97] Z. Huang, N. Geyer, P. Werner, J. de Boor, U. Gösele, Metal-Assisted Chemical Etching of Silicon: A Review, Advanced Materials 23 (2011) 285-308.

[98] W. Chern, K. Hsu, I.S. Chun, B.P.d. Azeredo, N. Ahmed, K.-H. Kim, J.-m. Zuo, N. Fang, P. Ferreira, X. Li, Nonlithographic Patterning and Metal-Assisted Chemical Etching for Manufacturing of Tunable Light-Emitting Silicon Nanowire Arrays, Nano Letters 10 (2010) 1582-1588.

[99] X. Li, Metal assisted chemical etching for high aspect ratio nanostructures: A review of characteristics and applications in photovoltaics, Current Opinion in Solid State and Materials Science 16 (2012) 71-81.

[100] X. Geng, B.K. Duan, D.A. Grismer, L. Zhao, P.W. Bohn, Monodisperse GaN nanowires prepared by metal-assisted chemical etching with< i> in situ</i> catalyst deposition, Electrochemistry Communications 19 (2012) 39-42.

[101] X. Li, P. Bohn, Metal-assisted chemical etching in< equation>< font face='verdana'> HF/H< sub> 2</sub>< font face='verdana'> O< sub>

2</sub></equation> produces porous silicon, Applied Physics Letters 77 (2000) 2572-2574.

[102] K. Balasundaram, J.S. Sadhu, J.C. Shin, B. Azeredo, D. Chanda, M. Malik, K. Hsu, J.A. Rogers, P. Ferreira, S. Sinha, Porosity control in metal-assisted chemical etching of degenerately doped silicon nanowires, Nanotechnology 23 (2012) 305304.

[103] P.K. Mohseni, S. Hyun Kim, X. Zhao, K. Balasundaram, J. Dong Kim, L. Pan, J.A. Rogers, J.J. Coleman, X. Li, GaAs pillar array-based light emitting diodes fabricated by metal-assisted chemical etching, Journal of applied physics 114 (2013) 064909-064909-064906.

[104] J.C. Shin, C. Zhang, X. Li, Sub-100 nm Si nanowire and nano-sheet array formation by MacEtch using a non-lithographic InAs nanowire mask, Nanotechnology 23 (2012) 305305.

[105] K. Tsujino, M. Matsumura, Boring deep cylindrical nanoholes in silicon using silver nanoparticles as a catalyst, Advanced Materials 17 (2005) 1045-1047.

[106] A.I. Hochbaum, R. Chen, R.D. Delgado, W. Liang, E.C. Garnett, M. Najarian, A. Majumdar, P. Yang, Enhanced thermoelectric performance of rough silicon nanowires, Nature 451 (2008) 163-167.

[107] Q.Q. Sun, H.L. Lu, S.J. Ding, B. Zhu, L.J. Li, W. Zhang, Formation of Cylindrical Nanoholes in Heavily Doped P-Type Si (100) Substrate via Pt Nanoparticles-Assisted Chemical Etching, Advanced Materials Research 535 (2012) 362-367.

[108] K. Tsujino, M. Matsumura, Helical nanoholes bored in silicon by wet chemical etching using platinum nanoparticles as catalyst, Electrochemical and Solid-State Letters 8 (2005) C193-C195.

[109] X.-M. Zhang, N. Fukata, Fabrication of holey silicon structures with inner radial p–n junction for solar cells, Solid State Communications 156 (2013) 76-79.

[110] Y. Oh, C. Choi, D. Hong, S.D. Kong, S. Jin, Magnetically Guided Nano–Micro Shaping and Slicing of Silicon, Nano Letters 12 (2012) 2045-2050.

[111] Y. Shuai, D. Zhao, G. Medhi, R. Peale, Z. Ma, W. Buchwald, R. Soref, W. Zhou, Fano Resonance Photonic Crystal Membrane Reflectors at Mid-and Far-Infrared.

[112] C.M. Soukoulis, M. Wegener, Optical metamaterials—more bulky and less lossy, science 330 (2010) 1633-1634.

[113] M.A. Meitl, Z.-T. Zhu, V. Kumar, K.J. Lee, X. Feng, Y.Y. Huang, I. Adesida, R.G. Nuzzo, J.A. Rogers, Transfer printing by kinetic control of adhesion to an elastomeric stamp, Nature Materials 5 (2005) 33-38.

[114] R. Soref, Mid-infrared photonics in silicon and germanium, Nat Photon 4 (2010) 495-497.

[115] G.Z. Mashanovich, M.M. Milo?evi, M. Nedeljkovic, N. Owens, B. Xiong, E.J. Teo, Y. Hu, Low loss silicon waveguides for the mid-infrared, Optics Express 19 (2011) 7112-7119.

[116] G.Z. Mashanovich, W.R. Headley, M.M. Milosevic, N. Owens, E.J. Teo, B.Q. Xiong, P.Y. Yang, M. Nedeljkovic, J. Anguita, I. Marko, Y. Hu, in: Group IV Photonics (GFP), 2010 7th IEEE International Conference on, (2010).

[117] S. Boutami, B.B. Bakir, P. Regreny, J. Leclercq, P. Viktorovitch, Compact 1.55 µm room-temperature optically pumped VCSEL using photonic crystal mirror, Electronics letters 43 (2007) 282-283.

[118] W. Zhou, Z. Ma, H. Yang, Z. Qiang, G. Qin, H. Pang, L. Chen, W. Yang, S. Chuwongin, D. Zhao, Flexible photonic-crystal Fano filters based on transferred

semiconductor nanomembranes, Journal of Physics D: Applied Physics 42 (2009) 234007.

[119] Z. Qiang, H. Yang, S. Chuwongin, D. Zhao, Z. Ma, W. Zhou, Design of Fano Broadband Reflectors on SOI, Photonics Technology Letters, IEEE 22 (2010) 1108-1110.

[120] E.D. Palik, Handbook of Optical Constants of Solids: Index (Access Online via Elsevier, 1998).

[121] D. Zhao, H. Yang, S. Chuwongin, J. Seo, Z. Ma, W. Zhou, Design of photonic crystal membrane-reflector-based VCSELs, Photonics Journal, IEEE 4 (2012) 2169-2175.

[122] Y. Shuai, D. Zhao, W. Yang, W. Zhou, J.-H. Seo, Z. Ma, G. Medhi, R. Peale, W. Buchwald, R. Soref, in: Photonics Conference (PHO), 2011 IEEE, (IEEE, 2011).

[123] H.-C. Yuan, Z. Ma, Microwave thin-film transistors using Si nanomembranes on flexible polymer substrate, Applied Physics Letters 89 (2006) 212105-212105-212103.

[124] H. Yang, D. Zhao, J. Seo, S. Kim, J. Rogers, Z. Ma, W. Zhou, Broadband Membrane Reflectors on Glass, IEEE Photonics Technology Letters 24 (2012) 476-478.

[125] B.E.A. Saleh, M.C. Teich, B.E. Saleh, Fundamentals of photonics (Wiley New York, 1991).

[126] S. Wang, R. Magnusson, Design of waveguide-grating filters with symmetrical line shapes and low sidebands, Optics Letters 19 (1994) 919-921.

[127] M. Kanskar, P. Paddon, V. Pacradouni, R. Morin, A. Busch, J.F. Young, S. Johnson, J. MacKenzie, T. Tiedje, Observation of leaky slab modes in an air-

bridged semiconductor waveguide with a two-dimensional photonic lattice, Applied Physics Letters 70 (1997) 1438-1440.

[128] V. Astratov, D. Whittaker, I. Culshaw, R. Stevenson, M. Skolnick, T. Krauss, R. De La Rue, Photonic band-structure effects in the reflectivity of periodically patterned waveguides, Physical Review B 60 (1999) R16255.

[129] M. Boroditsky, T.F. Krauss, R. Coccioli, R. Vrijen, R. Bhat, E. Yablonovitch, Light extraction from optically pumped light-emitting diode by thin-slab photonic crystals, Applied Physics Letters 75 (1999) 1036-1038.

[130] A.A. Erchak, D.J. Ripin, S. Fan, P. Rakich, J.D. Joannopoulos, E.P. Ippen, G.S. Petrich, L.A. Kolodziejski, Enhanced coupling to vertical radiation using a two-dimensional photonic crystal in a semiconductor light-emitting diode, Applied Physics Letters 78 (2001) 563-565.

[131] H. Ryu, Y. Lee, R. Sellin, D. Bimberg, Over 30-fold enhancement of light extraction from free-standing photonic crystal slabs with InGaAs quantum dots at low temperature, Applied Physics Letters 79 (2001) 3573-3575.

[132] M. Meier, A. Mekis, A. Dodabalapur, A. Timko, R.E. Slusher, J.D. Joannopoulos, O. Nalamasu, Laser action from two-dimensional distributed feedback in photonic crystals, Applied Physics Letters 74 (1999) 7-9.

[133] S. Noda, M. Yokoyama, M. Imada, A. Chutinan, M. Mochizuki, Polarization mode control of two-dimensional photonic crystal laser by unit cell structure design, science 293 (2001) 1123-1125.

[134] B. Luk'yanchuk, N.I. Zheludev, S.A. Maier, N.J. Halas, P. Nordlander, H. Giessen, C.T. Chong, The Fano resonance in plasmonic nanostructures and metamaterials, Nature Materials 9 (2010) 707-715.

[135] S. Fan, J.D. Joannopoulos, Analysis of guided resonances in photonic crystal slabs, Physical Review B 65 (2002) 235112.

[136] V. Liu, M. Povinelli, S. Fan, Resonance-enhanced optical forces between coupled photonic crystal slabs, Optics Express 17 (2009) 21897-21909.

[137] W. Suh, M.F. Yanik, O. Solgaard, S. Fan, Displacement-sensitive photonic crystal structures based on guided resonance in photonic crystal slabs, Applied Physics Letters 82 (2003) 1999.

[138] R. Magnusson, S.S. Wang, New principle for optical filters, Applied Physics Letters 61 (1992) 1022.

[139] Y. Kanamori, T. Kitani, K. Hane, Control of guided resonance in a photonic crystal slab using microelectromechanical actuators, Applied Physics Letters 90 (2007) 031911.

[140] S. Fan, Sharp asymmetric line shapes in side-coupled waveguide-cavity systems, Applied Physics Letters 80 (2002) 908.

[141] C.Y. Chao, Biochemical sensors based on polymer microrings with sharp asymmetrical resonance, Applied Physics Letters 83 (2003) 1527.

[142] W. Suh, O. Solgaard, S. Fan, Displacement sensing using evanescent tunneling between guided resonances in photonic crystal slabs, Journal of Applied Physics 98 (2005) 033102.

[143] A. Rosenberg, M. Carter, J. Casey, M. Kim, R. Holm, R. Henry, C. Eddy, V. Shamamian, K. Bussmann, S. Shi, D.W. Prather, Guided resonances in asymmetrical GaN photonic crystal slabs observed in the visible spectrum, Optics Express 13 (2005) 6564-6571.

[144] N. Inoue, T. Baba, External control of guided resonance in photonic crystal slab by changing the index anisotropy of liquid crystal, Proc. SPIE 6352 (2006) 63520R.

[145] O. Levi, M.M. Lee, J. Zhang, V. Lousse, S.R.J. Brueck, S. Fan, J.S. Harris, Sensitivity analysis of a photonic crystal structure for index-of-refraction sensing, Proc. SPIE 6447 (2007) 64470P.

[146] R. Harbers, S. Jochim, N. Moll, R.F. Mahrt, D. Erni, J.A. Hoffnagle, W.D. Hinsberg, Control of Fano line shapes by means of photonic crystal structures in a dye-doped polymer, Applied Physics Letters 90 (2007) 201105.

[147] E. Bisaillon, D. Tan, B. Faraji, A. Kirk, L. Chrowstowski, D. Plant, High reflectivity air-bridge subwavelength grating reflector and Fabry-Perot cavity in AlGaAs/GaAs, Optics Express 14 (2006) 2573-2582.

[148] J. Kim, L. Chrostowski, E. Bisaillon, D. Plant, DBR, Sub-wavelength grating, and Photonic crystal slab Fabry-Perot cavity design using phase analysis by FDTD, Optics Express 15 (2007) 10330-10339.

[149] S. Boutami, B. Benbakir, X. Letartre, J.L. Leclercq, P. Regreny, P. Viktorovitch, Ultimate vertical Fabry-Perot cavity based on single-layer photonic crystal mirrors, Optics Express 15 (2007) 12443-12449.

[150] C. Sciancalepore, B.B. Bakir, X. Letartre, J. Harduin, N. Olivier, C. Seassal, J. Fedeli, P. Viktorovitch, CMOS-compatible ultra-compact 1.55- um emitting VCSELs using double photonic crystal mirrors, IEEE PHOTONICS TECHNOLOGY LETTERS 24 (2012) 455-457.

[151] W. Suh, S. Fan, Mechanically switchable photonic crystal filter with either all-pass transmission or flat-top reflection characteristics, Optics Letters 28 (2003) 1763-1765.

[152] H.L. Bertoni, L.-H. Cheo, T. Tamir, Frequency-selective reflection and transmission by a periodic dielectric layer, Antennas and Propagation, IEEE Transactions on 37 (1989) 78-83.

[153] M. Nevière, E. Popov, R. Reinisch, Electromagnetic resonances in linear and nonlinear optics: phenomenological study of grating behavior through the poles and zeros of the scattering operator, JOSA A 12 (1995) 513-523.

[154] A. Sharon, D. Rosenblatt, A. Friesem, H. Weber, H. Engel, R. Steingrueber, Light modulation with resonant grating-waveguide structures, Optics Letters 21 (1996) 1564-1566.

[155] G. Levy-Yurista, A.A. Friesem, Very narrow spectral filters with multilayered grating-waveguide structures, Applied Physics Letters 77 (2000) 1596-1598.

[156] Z. Liu, R. Magnusson, Concept of multiorder multimode resonant optical filters, Photonics Technology Letters, IEEE 14 (2002) 1091-1093.

[157] Y. Ding, R. Magnusson, Use of nondegenerate resonant leaky modes to fashion diverse optical spectra, Optics Express 12 (2004) 1885-1891.

[158] R. Magnusson, Y. Ding, K. Lee, P. Priambodo, D. Wawro, Characteristics of resonant leaky-mode biosensors, Nanosensing: Material and Devices II, ed. MS Islam and AK Dutta, Proc. SPIE 6008 (2005) 60080U-60081.

[159] R. Magnusson, Y. Ding, K. Lee, D. Shin, P.S. Priambodo, P.P. Young, T.A. Maldonado, in: Optical Science and Technology, SPIE's 48th Annual Meeting, (International Society for Optics and Photonics, 2003).

[160] T. Sang, L. Wang, S. Ji, Y. Ji, H. Chen, Z. Wang, Systematic study of the mirror effect in a poly-Si subwavelength periodic membrane, JOSA A 26 (2009) 559-565.

[161] H. Macleod, T.-F.O. Filters, American Elsevier, New York (1969).

[162] H.A. Macleod, in: International Symposium on Optical Science and Technology, (International Society for Optics and Photonics, 2000).

[163] P. Rabiei, W.H. Steier, C. Zhang, L.R. Dalton, Polymer micro-ring filters and modulators, Journal of Lightwave Technology 20 (2002) 1968.

[164] P. Rabiei, W.H. Steier, Tunable polymer double micro-ring filters, Photonics Technology Letters, IEEE 15 (2003) 1255-1257.

[165] A. Gondarenko, J.S. Levy, M. Lipson, High confinement micron-scale silicon nitride high Q ring resonator, Opt. Express 17 (2009) 11366-11370.

[166] J. Cardenas, M. Zhang, C.T. Phare, S.Y. Shah, C.B. Poitras, M. Lipson, High Q SiC microresonators, arXiv preprint arXiv:1306.2937 (2013).

[167] V.R. Almeida, C.A. Barrios, R.R. Panepucci, M. Lipson, All-optical control of light on a silicon chip, Nature 431 (2004) 1081-1084.

[168] D. Armani, T. Kippenberg, S. Spillane, K. Vahala, Ultra-high-Q toroid microcavity on a chip, Nature 421 (2003) 925-928.

[169] K. Djordjev, S.-J. Choi, S.-J. Choi, R. Dapkus, Microdisk tunable resonant filters and switches, Photonics Technology Letters, IEEE 14 (2002) 828-830.

[170] S. Lee, S.C. Eom, J.S. Chang, C. Huh, G.Y. Sung, J.H. Shin, A silicon nitride microdisk resonator with a 40-nm-thin horizontal air slot, Optics Express 18 (2010) 11209-11215.

[171] M. Soltani, S. Yegnanarayanan, A. Adibi, Ultra-high Q planar silicon microdisk resonators for chip-scale silicon photonics, Optics Express 15 (2007) 4694-4704.

[172] D. Vernooy, V.S. Ilchenko, H. Mabuchi, E. Streed, H. Kimble, High-< i> Q</i> measurements of fused-silica microspheres in the near infrared, Optics Letters 23 (1998) 247-249.

[173] Y. Akahane, T. Asano, B.-S. Song, S. Noda, High-Q photonic nanocavity in a two-dimensional photonic crystal, Nature 425 (2003) 944-947.

[174] K. Srinivasan, P.E. Barclay, O. Painter, J. Chen, A.Y. Cho, C. Gmachl, Experimental demonstration of a high quality factor photonic crystal microcavity, Applied Physics Letters 83 (2003) 1915-1917.

[175] K. Lee, R. LaComb, B. Britton, M. Shokooh-Saremi, H. Silva, E. Donkor, Y. Ding, R. Magnusson, Silicon-layer guided-mode resonance polarizer with 40-nm bandwidth, Photonics Technology Letters, IEEE 20 (2008) 1857-1859.

[176] D.L. Brundrett, E.N. Glytsis, T.K. Gaylord, J.M. Bendickson, Effects of modulation strength in guided-mode resonant subwavelength gratings at normal incidence, Journal of the Optical Society of America A 17 (2000) 1221-1230.

[177] D. Rosenblatt, (Google Patents, 1994).

[178] R. Reinisch, P. Vincent, M. Neviere, E. Pic, Fast Pockels light modulator using guided wave resonance, Applied optics 24 (1985) 2001-2004.

[179] T. Nagamura, T. Hamada, Novel all optical light modulation based on complex refractive index changes of organic dye-doped polymer film upon photoexcitation, Applied Physics Letters 69 (1996) 1191-1193.

[180] K.-L. Lee, S.-H. Wu, C.-W. Lee, P.-K. Wei, Sensitive biosensors using Fano resonance in single gold nanoslit with periodic grooves, Optics Express 19 (2011) 24530-24539.

[181] F. Hao, Y. Sonnefraud, P.V. Dorpe, S.A. Maier, N.J. Halas, P. Nordlander, Symmetry breaking in plasmonic nanocavities: subradiant LSPR sensing and a tunable Fano resonance, Nano Letters 8 (2008) 3983-3988.

[182] B.T. Cunningham, J. Pepper, B. Lin, P. Li, J. Qiu, H. Pien, (Google Patents, 2006).

[183] V. Liu, S. Fan, S4: A free electromagnetic solver for layered periodic structures, Computer Physics Communications 183 (2012) 2233-2244.

[184] Y. Shuai, D. Zhao, Z. Tian, J.H. Seo, R. Jacobson, D.V. Plant, M.G. Lagally, S. Fan, Z. Ma, W. Zhou, in: IEEE Photonics Conference, (San Francisco, CA, 2012).

[185] U. Fano, The Theory of Anomalous Diffraction Gratings and of Quasi-Stationary Waves on Metallic Surfaces (Sommerfeld’s Waves), Journal of the Optical Society of America 31 (1941) 213-222.

[186] U. Fano, Effects of Configuration Interaction on Intensities and Phase Shifts, Physical Review 124 (1961) 1866-1878.

[187] R. Magnusson, S.S. Wang, New principle for optical filters, Applied Physics Letters 61 (1992) 1022-1024.

[188] S. Boutami, B.B. Bakir, H. Hattori, X. Letartre, J.L. Leclercq, P. Rojo-Romeo, M. Garrigues, C. Seassal, P. Viktorovitch, Broadband and compact 2-D photonic crystal reflectors with controllable polarization dependence, Photonics Technology Letters, IEEE 18 (2006) 835-837.

[189] Z. Qiang, H. Yang, L. Chen, H. Pang, Z. Ma, W. Zhou, Fano filters based on transferred silicon nanomembranes on plastic substrates, Applied Physics Letters 93 (2008) 061106-061106-061103.

[190] T.K. Saha, W. Zhou, High efficiency diffractive grating coupler based on transferred silicon nanomembrane overlay on photonic waveguide, Journal of Physics D: Applied Physics 42 (2009) 085115.

[191] Z. Qiang, W. Zhou, M. Lu, G.J. Brown, in: Proc. SPIE, (2008).

[192] W. Zhou, Z. Ma, H. Yang, L. Chen, W. Yang, Z. Qiang, G. Qin, H. Pang, S. Chuwongin, D. Zhao, in: OPTO, (International Society for Optics and Photonics, 2010).

[193] S. Yichen, Z. Deyin, T. Zhaobing, S. Jung-Hun, R.B. Jacobson, D.V. Plant, M.G. Lagally, F. Shanhui, M. Zhenqiang, Z. Weidong, in: Photonics Conference (IPC), 2012 IEEE, (2012).

[194] H. Yang, Z. Qiang, H. Pang, Z. Ma, W.D. Zhou, Surface-Normal Fano Filters Based on Transferred Silicon Nanomembranes on Glass Substrates, Electronics Letters 44 (2008) 858-859.

[195] Z. Qiang, H. Yang, L. Chen, H. Pang, Z. Ma, W. Zhou, Fano filters based on transferred silicon nanomembranes on plastic substrates, Applied Physics Letters 93 (2008) 061106.

[196] L. Chen, Z. Qiang, H. Yang, H. Pang, Z. Ma, W.D. Zhou, Polarization and angular dependent transmissions on transferred nanomembrane Fano filters, Optics Express 17 (2009) 8396-8406.

[197] M. Meitl, Z. Zhu, V. Kumar, K. Lee, X. Feng, Y. Huang, I. Adesida, R. Nuzzo, J. Rogers, Transfer printing by kinetic control of adhesion to an elastomeric stamp, Nature Materials 5 (2005) 33-38.

[198] M. Lipson, Guiding, modulating, and emitting light on silicon-challenges and opportunities, Journal of Lightwave Technology 23 (2005) 4222.

[199] D. Kwong, J. Covey, A. Hosseini, Y. Zhang, X. Xu, R.T. Chen, Ultralow-loss polycrystalline silicon waveguides and high uniformity 1x12 MMI fanout for 3D photonic integration, Optics Express 20 (2012) 21722-21728.

[200] W. Suh, S. Fan, All-pass transmission or flattop reflection filters using a single photonic crystal slab, Applied Physics Letters 84 (2004) 4905.

[201] H. Wu, W. Mo, J. Hou, D. Gao, R. Hao, H. Jiang, R. Guo, W. Wu, Z. Zhou, A high performance polarization independent reflector based on a multilayered configuration grating structure, Journal of Optics 12 (2010) 045703.

[202] V. Lousse, W. Suh, O. Kilic, S. Kim, O. Solgaard, S. Fan, Angular and polarization properties of a photonic crystal slab mirror, Optics Express 12 (2004) 1575-1582.

[203] M. Notomi, H. Taniyama, S. Mitsugi, E. Kuramochi, Optomechanical wavelength and energy conversion in high-Q double-layer cavities of photonic crystal slabs, Physical Review Letters 97 (2006) 023903.

[204] Y.-G. Roh, T. Tanabe, A. Shinya, H. Taniyama, E. Kuramochi, S. Matsuo, T. Sato, M. Notomi, Strong optomechanical interaction in a bilayer photonic crystal, Physical Review B 81 (2010) 121101.

[205] Y. Shuai, D. Zhao, Z. Tian, J.-H. Seo, D.V. Plant, Z. Ma, S. Fan, W. Zhou, Double-layer Fano resonance photonic crystal filters, Optics Express 21 (2013) 24582-24589.

[206] J.A. Rogers, M.G. Lagally, R.G. Nuzzo, Synthesis, assembly and applications of semiconductor nanomembranes, Nature 477 (2011) 45-53.

[207] K. Zhang, J.H. Seo, W. Zhou, Z. Ma, Fast flexible electronics using transferrable silicon nanomembranes (Topical Review), Journal of Physics D: Applied Physics 45 (2012) 143001.

[208] J. Rogers, M. Lagally, R. Nuzzo, Synthesis, assembly and applications of semiconductor nanomembranes, Nature 477 (2011) 45-53.

[209] G.T. Reed, G. Mashanovich, F.Y. Gardes, D.J. Thomson, Silicon optical modulators, Nat Photon 4 (2010) 518-526.

[210] R.A. Soref, B.R. Bennett, Electrooptical effects in silicon, Quantum Electronics, IEEE Journal of 23 (1987) 123-129.

[211] G. Cocorullo, I. Rendina, in: Electronics letters, (Institution of Engineering and Technology, 1992).

[212] D. Rezzonico, M. Jazbinsek, A. Guarino, O.-P. Kwon, P. Günter, Electro-optic Charon polymeric microring modulators, Opt. Express 16 (2008) 613-627.

[213] Y. Enami, C. Derose, D. Mathine, C. Loychik, C. Greenlee, R. Norwood, T. Kim, J. Luo, Y. Tian, A.-Y. Jen, Hybrid polymer/sol–gel waveguide modulators with exceptionally large electro–optic coefficients, Nature Photonics 1 (2007) 180-185.

[214] E.M. McKenna, A.S. Lin, A.R. Mickelson, R. Dinu, D. Jin, Comparison of r< sub> 33</sub> values for AJ404 films prepared with parallel plate and corona poling, JOSA B 24 (2007) 2888-2892.

[215] Q. Xu, B. Schmidt, S. Pradhan, M. Lipson, Micrometre-scale silicon electro-optic modulator, Nature 435 (2005) 325-327.

[216] Y. Hu, X. Xiao, H. Xu, X. Li, K. Xiong, Z. Li, T. Chu, Y. Yu, J. Yu, High-speed silicon modulator based on cascaded microring resonators, Optics Express 20 (2012) 15079-15085.

[217] M.Y. Liu, S.Y. Chou, High-modulation-depth and short-cavity-length silicon Fabry–Perot modulator with two grating Bragg reflectors, Applied Physics Letters 68 (1996) 170-172.

[218] B. Schmidt, Q. Xu, J. Shakya, M. Lipson, in: Lasers and Electro-Optics Society, 2006. LEOS 2006. 19th Annual Meeting of the IEEE, (2006).

[219] R.A. Soref, B.R. Bennett, in: Cambridge Symposium-Fiber/LASE'86, (International Society for Optics and Photonics, 1987).

[220] J. Lorenzo, R. Soref, 1.3 μm electro-optic silicon switch, Applied Physics Letters 51 (1987) 6-8.

[221] L. Friedman, R.A. Soref, J.P. Lorenzo, Silicon double-injection electro-optic modulator with junction gate control, Journal of applied physics 63 (1988) 1831-1839.

[222] G. Treyz, Silicon Mach-Zehnder waveguide interferometers operating at 1.3 mu m, Electronics letters 27 (1991) 118-120.

[223] G. Treyz, P. May, J.M. Halbout, Silicon Mach–Zehnder waveguide interferometers based on the plasma dispersion effect, Applied Physics Letters 59 (1991) 771-773.

[224] S. Jackson, P. Hewitt, G. Reed, C. Tang, A. Evans, J. Clark, C. Aveyard, F. Namavar, A novel optical phase modulator design suitable for phased arrays, Journal of Lightwave Technology 16 (1998) 2016.

[225] S. Jackson, G. Reed, C. Tang, A. Evans, J. Clark, C. Aveyard, F. Namavar, Optical beamsteering using integrated optical modulators, Lightwave Technology, Journal of 15 (1997) 2259-2263.

[226] U. Fischer, B. Schuppert, K. Petermann, Integrated optical switches in silicon based on SiGe-waveguides, Photonics Technology Letters, IEEE 5 (1993) 785-787.

[227] C. Tang, G. Reed, A. Walton, A. Rickman, Low-loss, single-model optical phase modulator in SIMOX material, Lightwave Technology, Journal of 12 (1994) 1394-1400.

[228] C. Tang, G. Reed, A. Walton, A. Rickman, in: MATERIALS RESEARCH SOCIETY SYMPOSIUM PROCEEDINGS, (Cambridge Univ Press, 1993).

[229] C. Tang, G. Reed, Highly efficient optical phase modulator in SOI waveguides, Electronics letters 31 (1995) 451-452.

[230] A. Cutolo, M. Iodice, P. Spirito, L. Zeni, Silicon electro-optic modulator based on a three terminal device integrated in a low-loss single-mode SOI waveguide, Lightwave Technology, Journal of 15 (1997) 505-518.

[231] A. Cutolo, M. Iodice, A. Irace, P. Spirito, L. Zeni, An electrically controlled Bragg reflector integrated in a rib silicon on insulator waveguide, Applied Physics Letters 71 (1997) 199-201.

[232] A. Sciuto, S. Libertino, A. Alessandria, S. Coffa, G. Coppola, Design, Fabrication, and Testing of anIntegrated Si-Based Light Modulator, Journal of Lightwave Technology 21 (2003) 228.

[233] P. Hewitt, G. Reed, Improving the response of optical phase modulators in SOI by computer simulation, Lightwave Technology, Journal of 18 (2000) 443-450.

[234] P.D. Hewitt, G.T. Reed, in: Optoelectronics' 99-Integrated Optoelectronic Devices, (International Society for Optics and Photonics, 1999).

[235] I. Day, S. Roberts, R. O'carroll, A. Knights, P. Sharp, G. Hopper, B. Luff, M. Asghari, in: Optical Fiber Communication Conference and Exhibit, 2002. OFC 2002, (IEEE, 2002).

[236] P. Dainesi, A. Kung, M. Chabloz, A. Lagos, P. Fluckiger, A. Ionescu, P. Fazan, M. Declerq, P. Renaud, P. Robert, CMOS compatible fully integrated Mach-Zehnder interferometer in SOI technology, Photonics Technology Letters, IEEE 12 (2000) 660-662.

[237] C.E. Png, S.P. Chan, S.T. Lim, G.T. Reed, Optical phase modulators for MHz and GHz modulation in silicon-on-insulator (SOI), Journal of Lightwave Technology 22 (2004) 1573.

[238] C.A. Barrios, V. Almeida, R. Panepucci, M. Lipson, Electrooptic modulation of silicon-on-insulator submicrometer-size waveguide devices, Journal of Lightwave Technology 21 (2003) 2332.

[239] A. Liu, R. Jones, L. Liao, D. Samara-Rubio, D. Rubin, O. Cohen, R. Nicolaescu, M. Paniccia, A high-speed silicon optical modulator based on a metal–oxide–semiconductor capacitor, Nature 427 (2004) 615-618.

[240] L. Liao, D. Samara-Rubio, M. Morse, A. Liu, D. Hodge, D. Rubin, U.D. Keil, T. Franck, High speed silicon Mach-Zehnder modulator, Opt. Express 13 (2005) 3129-3135.

[241] K. Kajikawa, T. Tabei, H. Sunami, An Infrared Silicon Optical Modulator of Metal--Oxide--Semiconductor Capacitor Based on Accumulation-Carrier Absorption, Japanese Journal of Applied Physics 48 (2009) 04C107.

[242] F. Gardes, G. Reed, N. Emerson, C. Png, A sub-micron depletion-type photonic modulator in silicon on insulator, Optics Express 13 (2005) 8845-8854.

[243] L. Liao, A. Liu, D. Rubin, J. Basak, Y. Chetrit, H. Nguyen, R. Cohen, N. Izhaky, M. Paniccia, 40 Gbit/s silicon optical modulator for high-speed applications, Electronics letters 43 (2007) 1196-1197.

[244] A. Liu, L. Liao, D. Rubin, H. Nguyen, B. Ciftcioglu, Y. Chetrit, N. Izhaky, M. Paniccia, High-speed optical modulation based on carrier depletion in a silicon waveguide, Opt. Express 15 (2007) 660-668.

[245] F. Gardes, A. Brimont, P. Sanchis, G. Rasigade, D. Marris-Morini, L. O'Faolain, F. Dong, J. Fedeli, P. Dumon, L. Vivien, in: Group IV Photonics, 2009. GFP'09. 6th IEEE International Conference on, (IEEE, 2009).

[246] P. Dong, S. Liao, D. Feng, H. Liang, D. Zheng, R. Shafiiha, C.-C. Kung, W. Qian, G. Li, X. Zheng, Low V< sub> pp</sub>, ultralow-energy, compact, high-speed silicon electro-optic modulator, Optics Express 17 (2009) 22484-22490.

[247] J.-B. You, M. Park, J.-W. Park, G. Kim, 12.5 Gbps optical modulation of silicon racetrack resonator based on carrier-depletion in asymmetric pn diode, Optics Express 16 (2008) 18340-18344.

[248] D.J. Thomson, F.Y. Gardes, J.M. Fedeli, S. Zlatanovic, H. Youfang, B.P.P. Kuo, E. Myslivets, N. Alic, S. Radic, G.Z. Mashanovich, G.T. Reed, 50-Gb/s Silicon Optical Modulator, Photonics Technology Letters, IEEE 24 (2012) 234-236.

[249] P. Dong, S. Liao, D. Feng, H. Liang, D. Zheng, R. Shafiiha, C.-C. Kung, W. Qian, G. Li, X. Zheng, A.V. Krishnamoorthy, M. Asghari, Low Vpp, ultralow-energy, compact, high-speed silicon electro-optic modulator, Optics Express 17 (2009) 22484-22490.

[250] J. Liu, M. Beals, A. Pomerene, S. Bernardis, R. Sun, J. Cheng, L.C. Kimerling, J. Michel, Waveguide-integrated, ultralow-energy GeSi electro-absorption modulators, Nature Photonics 2 (2008) 433-437.

[251] D. Miller, Device requirements for optical interconnects to silicon chips, Proceedings of the IEEE 97 (2009) 1166-1185.

[252] M.R. Watts, D.C. Trotter, R.W. Young, A.L. Lentine, in: Group IV Photonics, 2008 5th IEEE International Conference on, (IEEE, 2008).

[253] http://www.synopsys.com/tools/tcad/devicesimulation/pages/taurusmedici.aspx.

[254] V.N. Astratov, I.S. Culshaw, R.M. Stevenson, D.M. Whittaker, M.S. Skolnick, T.F. Krauss, R.M. De La Rue, Resonant coupling of near-infrared radiation to photonic band structure waveguides, Journal of Lightwave Technology 17 (1999) 2050.

[255] T. Ochiai, K. Sakoda, Dispersion relation and optical transmittance of a hexagonal photonic crystal slab, Physical Review B 63 (2001) 125107.

[256] Y. Shuai, D. Zhao, Z. Tian, J.-H. Seo, R. Jacobson, D.V. Plant, M.G. Lagally, S. Fan, Z. Ma, W. Zhou, Stacked Fano Resonance Photonic Crystal Nanomembrane High-Q Filters.

[257] M. Soljacic, S.G. Johnson, S. Fan, M. Ibanescu, E. Ippen, J.D. Joannopoulos, Photonic-crystal slow-light enhancement of nonlinear phase sensitivity, Journal of the Optical Society of America B 19 (2002) 2052-2059.

[258] Y. Jiang, W. Jiang, L. Gu, X. Chen, R.T. Chen, 80-micron interaction length silicon photonic crystal waveguide modulator, Applied Physics Letters 87 (2005) -.

[259] L. Gu, W. Jiang, X. Chen, L. Wang, R.T. Chen, High speed silicon photonic crystal waveguide modulator for low voltage operation, Applied Physics Letters 90 (2007) -.

[260] T. Tanabe, K. Nishiguchi, E. Kuramochi, M. Notomi, Low power and fast electro-optic silicon modulator with lateral p-i-n embedded photonic crystal nanocavity, Optics Express 17 (2009) 22505-22513.

[261] X. Chen, Y.-S. Chen, Y. Zhao, W. Jiang, R.T. Chen, Capacitor-embedded 0.54 pJ/bit silicon-slot photonic crystal waveguide modulator, Optics Letters 34 (2009) 602-604.

[262] H. Taniyama, M. Notomi, E. Kuramochi, T. Yamamoto, Y. Yoshikawa, Y. Torii, T. Kuga, Strong radiation force induced in two-dimensional photonic crystal slab cavities, Physical Review B 78 (2008) 165129.

[263] A.W. Rodriguez, A.P. McCauley, P.-C. Hui, D. Woolf, E. Iwase, F. Capasso, M. Loncar, S.G. Johnson, Bonding, antibonding and tunable optical forces in asymmetric membranes, Optics Express 19 (2011) 2225-2241.

Biographical Information

Yi-Chen Shuai received his Ph.D. degree at University of Texas at Arlington (U.S.A.) in 2013. He got his Bachelor's degree in Southeast University (P.R.C.) and Master degree in SCNU (P.R.C.).

He received Dr. N.M. Stelmakh Outstanding Student Research Award, Department of Electrical Engineering, UT Arlington, in 2013 and Graduate Dean Doctoral Fellowship, UT Arlington (2009/2010/2011/2012), as well as STEM fellowship, Department of Electrical Engineering, UT Arlington (2008 to present). He also received Student Travel Grant from AFOSR CONTACT program (3-times: 2010/2011/2012). He is student member of Optical Society of America (OSA); Institute of Electrical and Electronics Engineers (IEEE); American Physical Society (APS) and Society of Photo-optical Instrumentation Engineers (SPIE).